# Sustainable management of muddy tidal flats

## A case study of the Jiangsu coast, China

Kuai, Y.

**DOI**
10.4233/uuid:dc707afb-791d-4c72-ad59-2cebbdc60c52

**Publication date**
2025

**Document Version**
Final published version

**Citation (APA)**
Kuai, Y. (2025). *Sustainable management of muddy tidal flats: A case study of the Jiangsu coast, China*. [Dissertation (TU Delft), Delft University of Technology]. https://doi.org/10.4233/uuid:dc707afb-791d-4c72-ad59-2cebbdc60c52

# SUSTAINABLE MANAGEMENT OF MUDDY TIDAL FLATS:

## A CASE STUDY OF THE JIANGSU COAST, CHINA

Yu Kuai 蒯宇

# SUSTAINABLE MANAGEMENT OF MUDDY TIDAL FLATS: A CASE STUDY OF THE JIANGSU COAST, CHINA

Yu Kuai

# SUSTAINABLE MANAGEMENT OF MUDDY TIDAL FLATS: A CASE STUDY OF THE JIANGSU COAST, CHINA

**Dissertation**

for the purpose of obtaining the degree of doctor
at Delft University of Technology
by the authority of the Rector Magnificus Prof.dr.ir. T.H.J.J. van der Hagen
chair of the Board for Doctorates
to be defended publicly on
Monday, 22 September 2025 at 12:30 o'clock

by

**Yu Kuai**

Master of Science in Harbor, Coastal and Offshore Engineering,
Hohai University, China
born in Jiangsu, China

This dissertation has been approved by the promotors.

Composition of the doctoral committee:

| | |
|---|---|
| Rector Magnificus, | chairperson |
| Prof.dr.ir. Z.B. Wang | Delft University of Technology, promotor |
| Prof.dr.ir. S.G.J. Aarninkhof | Delft University of Technology, promotor |
| | |
| *Independent members:* | |
| Dr.ir. B.C. van Prooijen | Delft University of Technology |
| Dr. D.S. van Maren | Delft University of Technology |
| Prof.dr. J.H. Slinger | Delft University of Technology |
| Prof.dr. P. Hoekstra | Utrecht University |
| Prof.dr. Z. Zhou | Hohai University |
| Prof.dr.ir. A.J.H.M. Reniers | Delft University of Technology, reserve member |



The research is financed by the China Scholarship Council (CSC).

*Keywords:* muddy tidal flat, reclamation, coastal morphology, beach profile, sediment grain size

*Printed by:* Ridderprint



ISBN 978-94-6518-079-3

An electronic version of this dissertation is available at
http://repository.tudelft.nl/.

*Wave on wave, tide after tide, grain by grain;*
*Pure gold emerges when the dross is shed away.*
千淘万漉虽辛苦，吹尽狂沙始到金。

Yuxi Liu, 822

# CONTENTS

# SUMMARY

Tidal flats play a critical role in coastal systems. They serve as essential buffers that protect inland communities from flooding by storm surges, contribute significantly to the maintenance of coastal biodiversity, and function as crucial sites for carbon sequestration. Moreover, they are indispensable for land reclamation projects, supporting economic activities such as agriculture and aquaculture. However, rapid coastal economic development and assertive human interventions have intensified conflicts of interest between socio-economic demands and the preservation of these fragile ecosystems. This increasing tension underscores the necessity for a detailed understanding of tidal flat evolution and the complex interplay between natural processes and anthropogenic activities.

This research aims to deepen our understanding of unvegetated tidal flat morphodynamics by examining both natural processes and the impacts of human interventions. The insights gained will provide valuable theoretical guidance for the sustainable and effective management of tidal flat resources in the future. To achieve this, the study focuses on tidal flats along the Jiangsu Coast in China as a case study. Because it is a typical example famous for its extensive and diverse tidal flat systems. At the same time, it has a long history of coastal land reclamations. A multi-faceted approach is adopted, combining field dataset analysis, a process-based Delft3D model, and a hybrid DET-ESTMORF model, which together provide a robust foundation for theoretical insights in sustainable coastal management.

Based on a unique field measurement data along the Jiangsu Coast, the morphology and sediment characteristics of the unvegetated intertidal flats along this coast are analysed. Both cross-shore and alongshore variations are observed. In the cross-shore direction, sediments exhibit a pronounced coarsening from the landward to the seaward side, indicating tide-dominated forcing. In the alongshore direction, the coast is divided into two parts depending on its morphological state. The northern coast, which is predominantly eroding, exhibits steeper intertidal slopes and a complex mix of sediment types, ranging from extremely fine to coarse de-

posits. The variation in sediment composition is attributed to natural processes such as self-weight consolidation and surface armouring. In the accreting southern coast, while tidal flat slopes are generally becoming milder towards the south, the corresponding bed surface sediment grain size is becoming coarser southward. This relationship between slope and sediment grain size in the southern coast is opposite to the findings on other muddy tidal flats.

In order to investigate the mechanism behind the region-specific alongshore pattern of the southern Jiangsu Coast, we formulate a conceptual model with special focus on describing the alongshore variations in hydrodynamics and shoreline evolution. Subsequently, a highly schematized Delft3D numerical model is employed in diagnostic mode. By integrating these approaches, the sediment provenance is found to be the sole factor capable of explaining the observed pattern.

Apart from natural processes, anthropogenic activities can also induce significant changes in tidal flat morphology. Available information on the tidal flat morphological responses to human interventions is limited based on the single-time measurements data. We therefore evaluate the resilience of tidal flats to anthropogenic disturbances (specifically, upper flat enclosure reclamation) using an extended DET-ESTMORF model. A series of sensitivity tests under various environmental conditions is conducted with this model. Our findings indicate that the concave or convex shape of tidal flat profiles is primarily governed by dominant hydrodynamic forces (whether tidal or wave-driven), while other variables modulate the profile slope. For a tidal flat to revert to its pre-reclamation configuration, it must exhibit continuous seaward progradation under natural conditions. Such restoration typically occurs in environments with abundant sediment supply, subdued wave activity, and the absence of cross-shore constraints imposed by shore-parallel tidal channels.

Overall, the insights derived from this study enhance our understanding of the interactions between natural hydrodynamic processes, sediment dynamics, morphology change and human-induced alterations. The findings highlight the importance of continuous monitoring and the adoption of adaptive management strategies to ensure that coastal development preserves the ecological integrity and long-term stability of tidal flat systems.

# SAMENVATTING

Getijdengebieden spelen een cruciale rol in kustsystemen. Ze fungeren als essentiële buffers die binnenlandse gemeenschappen beschermen tegen overstromingen door stormvloeden, dragen aanzienlijk bij aan het behoud van de biodiversiteit in kustgebieden en zijn van groot belang voor koolstofopslag. Bovendien zijn ze onmisbaar voor landaanwinningsprojecten en ondersteunen ze economische activiteiten zoals landbouw en aquacultuur. Echter, de snelle economische ontwikkeling van kustgebieden en ingrijpende menselijke interventies hebben de belangenconflicten tussen sociaaleconomische eisen en het behoud van deze kwetsbare ecosystemen verergerd. Deze toenemende spanning benadrukt de noodzaak van een gedetailleerd inzicht in de evolutie van getijdengebieden en de complexe wisselwerking tussen natuurlijke processen en menselijke activiteiten.

Dit onderzoek is gericht op het verdiepen van ons begrip van de morfodynamiek van onbegroeide getijdenplaten door zowel natuurlijke processen als de effecten van menselijke ingrepen te bestuderen. De verkregen inzichten zullen waardevolle theoretische richtlijnen bieden voor het duurzame en effectieve beheer van getijdenplaatbronnen in de toekomst. Om dit te bereiken, richt de studie zich op de getijdenplaten langs de Jiangsu-kust in China als casestudy, omdat dit een typisch voorbeeld is dat beroemd is om zijn uitgebreide en diverse getijdenplaten. Tegelijkertijd heeft het een lange geschiedenis van kustlandaanwinning. Er wordt een veelzijdige benadering gehanteerd, waarbij veldgegevensanalyse, een procesgebaseerd Delft3D-model en een hybride DET-ESTMORF-model worden gecombineerd, die samen een robuuste basis vormen voor theoretische inzichten in duurzaam kustbeheer.

Op basis van unieke veldmeetinformatie langs de Jiangsu-kust worden de morfologie en sedimentkenmerken van de onbegroeide intergetijdenplaten langs deze kust geanalyseerd. Zowel in dwarsrichting als in langsrichting worden variaties waargenomen. In dwarsrichting vertonen sedimenten een duidelijke grover wordende trend van landwaarts naar zeewaarts, wat wijst op door getijden gedomineerde krach-

ten. In langsrichting is de kust verdeeld in twee delen op basis van de morfologische toestand. De noordelijke kust, die overwegend aan het eroderen is, vertoont steilere intergetijdenhellingen en een complexe mengeling van sedimenttypes, variërend van uiterst fijn tot grof. De variatie in sedimentopbouw wordt toegeschreven aan natuurlijke processen zoals consolidatie door eigen gewicht en oppervlakverharding. In de aangroeiende zuidelijke kust worden de getijdenplaathellingen naar het zuiden toe geleidelijk vlakker, terwijl de korrelgrootte van het oppervlaktesediment grover wordt. Deze relatie tussen helling en korrelgrootte in de zuidelijke kust is tegengesteld aan bevindingen op andere slibgetijdenplaten.

Om het mechanisme achter het regio-specifieke langsrichtingpatroon van de zuidelijke Jiangsu-kust te onderzoeken, wordt een conceptueel model opgesteld met een speciale focus op de beschrijving van langsrichtingsvariaties in hydrodynamiek en kustlijnontwikkeling. Vervolgens wordt een sterk geschematiseerd Delft3D-numeriek model gebruikt in diagnostische modus. Door deze benaderingen te integreren, wordt vastgesteld dat de herkomst van sediment de enige factor is die het waargenomen patroon kan verklaren.

Naast natuurlijke processen kunnen menselijke activiteiten ook aanzienlijke veranderingen in de morfologie van getijdengebieden teweegbrengen. De beschikbare informatie over de morfologische respons van getijdengebieden op menselijke ingrepen is beperkt, omdat deze voornamelijk is gebaseerd op eenmalige metingen. Daarom evalueren we de veerkracht van getijdengebieden tegen menselijke verstoringen (specifiek, bovenflats en inpoldering) met behulp van een uitgebreid DET-ESTMORF-model. Een reeks gevoeligheidstesten onder verschillende omgevingscondities wordt uitgevoerd met dit model. Onze bevindingen geven aan dat de concaaf of convex gevormde profielen van getijdengebieden primair worden bepaald door de dominante hydrodynamische krachten (getijden- of golfgedreven), terwijl andere variabelen de hellingshoek van het profiel beïnvloeden. Voor een getijdengebied om terug te keren naar de configuratie van vóór de inpoldering, moet er een continue zeewaartse uitbreiding plaatsvinden onder natuurlijke omstandigheden. Dergelijk herstel treedt voornamelijk op in omgevingen met een overvloedige sedimenttoevoer, beperkte golfactiviteit en zonder dwarskustbeperkingen veroorzaakt door kust-parallelle getijdengeulen.

Al met al verbeteren de inzichten uit deze studie ons begrip van de interac-

ties tussen natuurlijke hydrodynamische processen, sedimentdynamiek, morfologische veranderingen en door de mens veroorzaakte aanpassingen. De resultaten onderstrepen het belang van voortdurende monitoring en de implementatie van adaptieve beheersstrategieën om ervoor te zorgen dat kustontwikkeling de ecologische integriteit en de langetermijnstabiliteit van getijdengebieden behoudt.

# 1

# INTRODUCTION

1

## 1.1. TIDAL FLATS

### 1.1.1. IMPORTANCE OF TIDAL FLATS

TIDAL flats are valuable natural resources that play an important role in human development from multiple dimensions. From the coastal safety perspective, tidal flats play a critical role in protecting inland areas from flooding and property damage. They act as natural buffers against storm surges and coastal erosion, absorbing and dissipating wave energy (Reed et al., 2018; Stark et al., 2015). From the economic perspective, tidal flats can provide space and materials for various aquaculture activities (Murray et al., 2019). These activities support local economies and provide livelihoods for coastal communities. From the ecological perspective, tidal flats are vital habitats for a wide range of species. They provide a living environment and breeding grounds for numerous vegetation species, migratory birds and other invertebrates (Horn et al., 2020; Tian et al., 2008). The biodiversity supported by tidal flats can contribute to the overall health and balance of coastal ecosystems. In addition, tidal flats also play a significant role in carbon sequestration as well as nutrient cycling. The sediments in these areas can trap and store carbon, which can mitigate the negative effects of climate change (Gong et al., 2023; Ouyang and Lee, 2020). As coastal wetlands, they are part of the blue carbon ecosystem, which sequesters carbon dioxide at a much higher rate than terrestrial ecosystems (Rosli et al., 2017). Due to the positive roles tidal flats play across so many dimensions, it is essential that we thoroughly understand their evolution patterns in order to engage in sustainable development and utilization.

### 1.1.2. DEFINITION AND CHARACTERISTICS OF TIDAL FLATS

TIDAL flats are distributed worldwide on low-sloping coastlines, tide-dominated estuaries and deltas, and low-energy tidal embayments (Figure 1.1). They occupy at least 127921 $km^2$ (2014-2016) of the Earth's surface area (Murray et al., 2019). They are sandwiched between marine, freshwater and land environments, and characterized by regular alternations of exposure and flooding by tides. The formation of the tidal flats needs two basic conditions (Klein, 1985): 1) sufficient supply of fine-grained sediments. 2) tidal currents dominant over other hydrodynamic forces such as wave impacts. These two conditions determine the sediments provenance

(such as river runoff, seabed erosion, and cliff recession), as well as whether these sediments can be deposited on the tidal flat (Gao, 2019). Tidal flats can develop on open coasts with significant wave exposure, provided tidal action remains the dominant force. However, when wave energy exceeds tidal influence, fine sediments are transported offshore, inhibiting tidal flat formation (King, 1972). In such conditions, and in the absence of abundant sediment supply, the coastline typically evolves into sandy or gravelly beaches rather than tidal flats (Gao, 2019).

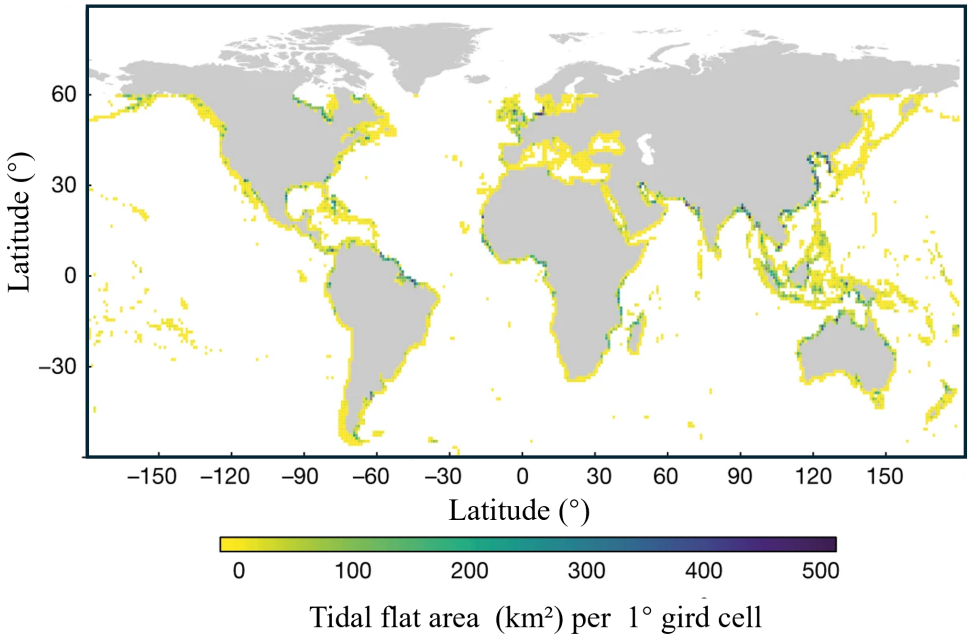


Figure 1.1: Global distribution pattern of tidal flats (2014-2016) based on Landsat satellite images within 1-km of the coastline (modified from Murray et al., 2019).

Tidal flats can develop in both sheltered environments like lagoons, or embayments, and completely exposed environment like estuaries, or coastal plains. In exposed environments, the wave exposure increases from open-mouth estuaries, deltas, to coastal plains. Tidal flats developed in these three areas all can be referred as open-coast tidal flats (Fan et al., 2013). This thesis chooses the open coast tidal flats as the environment of interest, and specifically focuses on the morphological evolution of tidal flats on coastal plains.

According to the relationship between the bed elevation and characteristic tidal

water levels, a tidal flat can be divided into three parts (Figure 1.2) (Amos, 1995): (1) supratidal flat, which is located above the spring tide high water and is only inundated under extreme conditions (e.g., storm surge events); (2) intertidal flat, which is located between the spring tide high and low water and is inundated periodically during spring–neap tidal cycles; and (3) subtidal zone, which is below the spring tide low water and is rarely exposed in air. Most studies on tidal flats have merely focused on the intertidal zone (Fivash et al., 2023; Hanssen et al., 2022; Zhou et al., 2022; de Vet et al., 2020; Maan et al., 2015). These authors usually prefer to use the term "tidal flat" to represent the intertidal part, and we adopt it as well in this thesis.

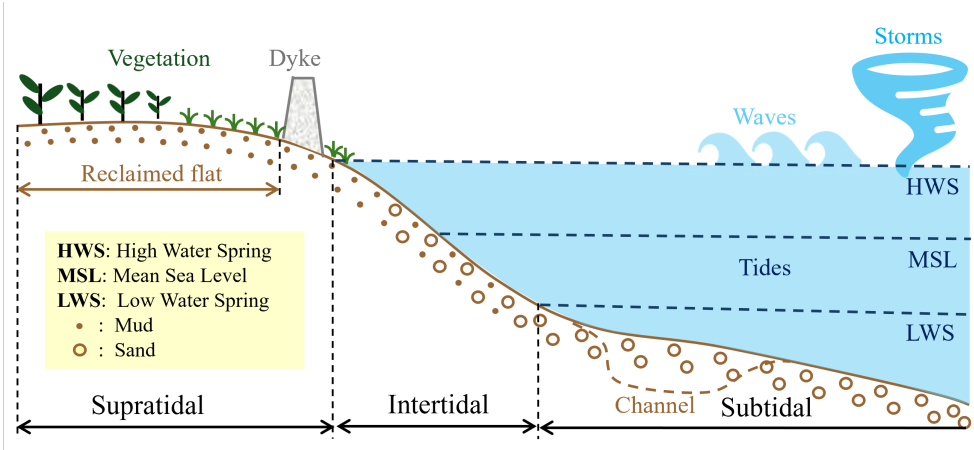


Figure 1.2: A open coast tidal flat profile and its zonation. Main natural forces and anthropogenic activities on the tidal flat are marked on the profile.

## 1.2. NATURAL FORCES AND ANTHROPOGENIC ACTIVITIES ON OPEN COAST TIDAL FLATS

THE evolution of the open coast tidal flats are driven by the dynamic interplay between natural forces and anthropogenic activities. To investigate the evolution patterns of the tidal flat, it is necessary to find out the primary forces acting on this area.

### 1.2.1. NATURAL FORCES

THE open-coast tidal flats are generally characterized by strong tidal action, and high exposure to waves as well as seasonal storms (Figure 1.2).

Tide is the dominant forcing on the tidal flat. Tidal range is usually adopted as an indicator to classify a coast (Davies, 1964). The coast with mean tidal range smaller than 2 m is recognized as a microtidal coast (Davies, 1964). On this type of coast, tide-driven cross-shore currents are very weak unless the tidal flat is extremely mild in slope. The coast with mean tidal range in between 2 m and 4 m is recognized as a mesotidal coast, while the one with mean tidal range larger than 4 m is recognized as a macrotidal coast (Davies, 1964). In environments with a relatively large tidal range, tidal currents also tend to be stronger as compared to them on the microtidal coast. Apart from the tidal range, the magnitude of tidal current can also be influenced by the tidal cycle. Given the same geometry setting and tidal range, semidiurnal tides will generate stronger tidal currents as compared to the diurnal ones (Archer, 1995; Gao and Collins, 1994). On an open coast, tidal flats are more likely to form in environments with larger tidal ranges (Gao, 2019).

On open coasts, the relative importance of tide and waves rather than the absolute tidal range that determines the coastal character. The relative tidal range (RTR), defined as the ratio of the mean spring tidal range to the wave height just before breaking, is used to evaluate the dominant forcing (Davis and Hayes, 1984). An RTR below 3 indicates that wave action prevails, resulting in surf zone breaking and the offshore transport of fine-grained sediments (Christensen et al., 2001). In the absence of an adequate supply of fine sediments, this process ultimately favours the formation of sandy or gravelly beaches rather than tidal flats. The other way around, if there is sufficient fine-grain sediment supply, the accumulated sediment can gradually flat out the intertidal regions. As a consequence, the wave energy is more likely to be dissipated during onshore propagation, and there will be less wave breaking. The mild slope favours stronger cross-shore tidal currents, and the tidal action is enhanced then. Eventually tides dominate over waves again, and a tidal flat can therefore form. Despite tides play a dominant role in the formation of tidal flat, waves are also important in terms of the sediment transport and the tidal flat shape (Fan et al., 2013; Friedrichs, 2011). The tide-wave interactions can stimulate the sediment motion initialization and trigger more bed materials into suspension

(Wang et al., 2022; Zhou et al., 2015). From the morphology perspective, tides tends to generate a convex-up tidal flat profile, while waves can modify the profile towards a more concave-up shape (Friedrichs, 2011).

In addition to the persistent influence of tides and waves, seasonal storm events can significantly impact tidal flats. Although they usually last only few days or weeks (when several storms land sequentially), they can dramatically change the tidal flat environment in such a short time (de Vet et al., 2020; Kim, 2003). During a typhoon event, storm surges as well as strong waves turn out to be the dominant forcing on the tidal flat temporarily. They can cause erosion over the middle–lower parts of the tidal flat, and great sedimentation over the upper part (Xie et al., 2021; Gong et al., 2019b; Andersen and Pejrup, 2001). After a storm, tides play a crucial role in restoring tidal flats by redistributing sediments that have been eroded and displaced. The regular tidal flow brings in new sediments from nearby areas, gradually filling in eroded sections and levelling the surface (Zhang et al., 1999). This thesis focuses on the long-term evolution of tidal flats on a decadal scale, emphasizing average annual changes. As a result, we consider only the persistent effects of tides and waves, excluding the seasonal impacts of storms.

### 1.2.2. ANTHROPOGENIC ACTIVITIES

THE evolution of tidal flats is influenced not only by natural hydrodynamic forces but also by various anthropogenic processes operating across different temporal and spatial scales. Typical examples are unban expansion (Xu and Liu, 2022), harbour construction (Muller et al., 2020a) and fish farming (Choi, 2019). Since the industrial revolution (post-AD 1780), human intervention has gradually become one of the most significant factors shaping the coastal morphology (Brown et al., 2017). Among these interventions, land reclamation plays a prominent role, often occurring alongside other anthropogenic activities on tidal flats. Reclamation projects have pronouncedly altered the coastline globally, as well as impacted local tidal flats environment (Sengupta et al., 2018). These activities consequently lead to various coastal issues, such as the rapid loss of tidal flats and associated ecosystems (Wu et al., 2018).

Coastal reclamation typically involves converting tidal flats or shallow seas into usable land by extending the coastline seaward. One of the prevailing reclamation

methods is the upper-flat enclosure (Xu et al., 2022; Zhong and Hu, 2021). This method is widely implemented in high-elevation coastal regions, where dikes or seawalls can be constructed near the mean high waterline and subsequently extended seawards. This method allows for the complete conversion of land behind the dikes into usable areas and has been employed for centuries to exploit coastal wetlands (Sengupta et al., 2023; Martín-Antón et al., 2016). The enclosure of upper tidal flats leads to an immediate reduction in the local tidal prism, and promotes sedimentation in front of the dyke toe (Chen et al., 2021; Wang et al., 2012a). Studies has revealed that coastal land reclamation can alter its local tidal dynamics as well as wave actions (Zhang et al., 2023; Zhang et al., 2021; Gao et al., 2014; Byun et al., 2004). The bed surface sediment distribution pattern and tidal flat morphology can change as the consequence of the variation in cross-shore hydrodynamic gradient (Chen et al., 2018; Flemming and Nyandwi, 1994).

The Jiangsu coastal tidal flats are an ideal research subject due to their extensive and diverse tidal flat systems, which have been significantly impacted by both natural processes and human activities, particularly large-scale reclamation projects. This region's complex hydrodynamic conditions, sediment supply, and ecological significance provide a rich context for understanding the effects of reclamation on tidal flat evolution. The availability of the unique coastal survey data covering the entire Jiangsu coast (Zhang, 2012) makes the tidal flats in this region an ideal subject for research as well.

## 1.3. GENERAL INFORMATION OF THE JIANGSU COAST, CHINA

THE following is a brief introduction to the Jiangsu coastal environment and the reclamation history of Jiangsu coastal tidal flats.

### 1.3.1. OVERVIEW OF THE JIANGSU COASTAL TIDAL FLATS ENVIRONMENT

THE Jiangsu Coast is situated on the eastern China, and adjacent to the South Yellow Sea (Figure 1.3). This coast starts from the Xiuzhen Estuary in the north, and extends all the way to the Yangtze River in the south (Ren, 1986a). This coast has been regarded as a typical examples of open coast tidal flats. The total alongshore length of the coastline is approximately 954 km. In the cross-shore direction, the

average tidal flat width is around 8 km, and the widest section can reach up to 36 km (Yang et al., 1997).

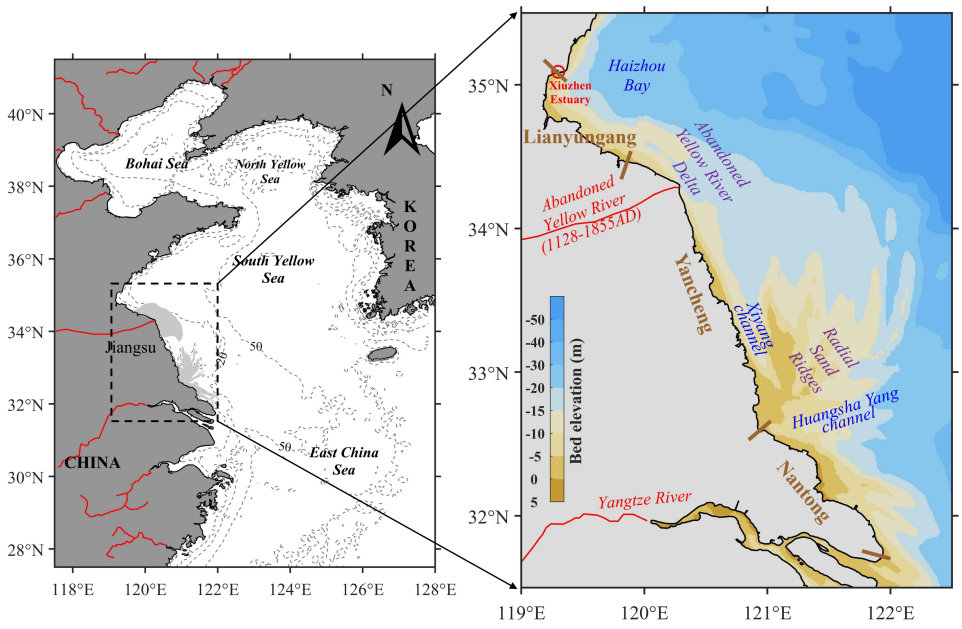


Figure 1.3: Location and bathymetry of the Jiangsu Coast, indicates the locations of different units and channels. The coastline of three cities (i.e. Lianyungang, Yancheng and Nantong) is marked in-between brown lines on the right panel.

There are two distinct geomorphological units developing on the Jiangsu Coast, viz the Abandoned Yellow River Delta on the north part, and Radial Sand Ridges on the central part of the coastline. The Yellow River discharged into the South Yellow Sea during 1128-1855 AD. During this period, the fine sediment carried by the Yellow River accumulated on the northern coast, and gradually formed the Abandoned Yellow River Delta nowadays (Liu et al., 2013; Su et al., 2017a). After 1855, the Yellow River shifted its lower reach into the Bohai Sea. As a result, the Abandoned Yellow River Delta has been under continuous erosion since then. The erosion initially took place only around the Abandoned Yellow River Delta, and gradually extends southwards (Zhou et al., 2020; Xing et al., 2016). The formation of the Radial Sand Ridges are considered to be induced by the radial tidal current pattern existed 7000 years ago (Tao et al., 2019; Zhu and Chen, 2005). These offshore ridges can protect

the adjacent tidal flat from the exposure to offshore waves. Thus, the Jiangsu coast is generally divided into two parts, viz the erosional open coast on the north and the accretional sheltered coast on the south. There are also several small rivers discharging into the sea through the Jiangsu Coast. However, most of them are channelized with small discharges.

The tides and waves on tidal flats exhibit pronounced alongshore variations along the Jiangsu Coast. Generally, the Jiangsu Coast is dominated by semi-diurnal tide, and the tidal range is larger in the central part of the coast as compared to the other parts (Ren, 1986a). The mean tidal current velocity is weak in the Abandoned Yellow River Delta zone (0.6-1 m/s) and gets stronger in the Radial Sand Ridges zone (Yao, 2016). There are several large tidal channels in the Radial Sand Ridges zone, such as Xiyang channel and Huangsha Yang Channel. The maximum tidal current velocity in these channels can exceed 2 m/s (Xu et al., 2016; Xing et al., 2012). Both swells and local wind waves are important on the northern open coast. Due to the sheltering effect of the Radial Sand Ridges, only the local wind waves can play a role on the central Jiangsu Coast (Yu and Yang, 2010; Wang and David, 1987).

### 1.3.2. THE COASTAL LAND RECLAMATION HISTORY OF THE JIANGSU COAST

THE anthropogenic activities on the tidal flats along the Jiangsu Coast has experienced three main stages, namely reclamation for salt production, reclamation for agriculture and aquaculture, and fast multi-objective reclamation (Liu et al., 2019).

**Salt production Reclamation phase**

The salt-making industry in the Jiangsu coastal region dates back to the Spring and Autumn Period (approximately 770–476 BC), with a certain scale of sea salt production already in place (Tang, 1997). With the improvement of the decocted salt production technology, Jiangsu saltworks constantly migrated seaward with the rapid coastal accretion (Bao and Gao, 2016). Until late 19th century, with the impact of socio-economic conditions, the low production efficiency of decocted salt in the south coast began to decline gradually, while solar salt production in the north coast started to develop rapidly (Bao, 2016). The history of the salt production along Jiangsu coast indicated the human adaption to the nature process and the rational

use of the tidal flat. However, anthropogenic influence to the tidal flat ecosystem was limited during this phase (Liu et al., 2019)

**Agricultural and Aquaculture Reclamation Phase**

From the early 20th century, the salt production could not satisfy the livings for the increasing population. In the year of 1901, the agriculture company funded by Zhang Qian started to make tidal flat reclamations for large scale agriculture, for example the cotton planting. From 1980's to 2000s the reclamation in the tidal flat of Jiangsu coastal plain was mostly used as shrimp ponds and fish ponds, and aquaculture quickly developed (Liu et al., 2019).

**Fast multi-objective reclamation Phase**

Since the early 21st century, with China's rapid economic development, especially in the coastal areas with port construction, industrial development zones, and new coastal district developments, reclamation activities have become more frequent and extensive (Xu et al., 2022). According to the Landsat data, Xu et al. (2022) investigated the spatial and temporal patterns of coastal reclamation in Jiangsu Province from 1984 to 2019, and revealed significant variations among its three coastal cities: Yancheng, Nantong, and Lianyungang (location can be referred to Figure 1.3).

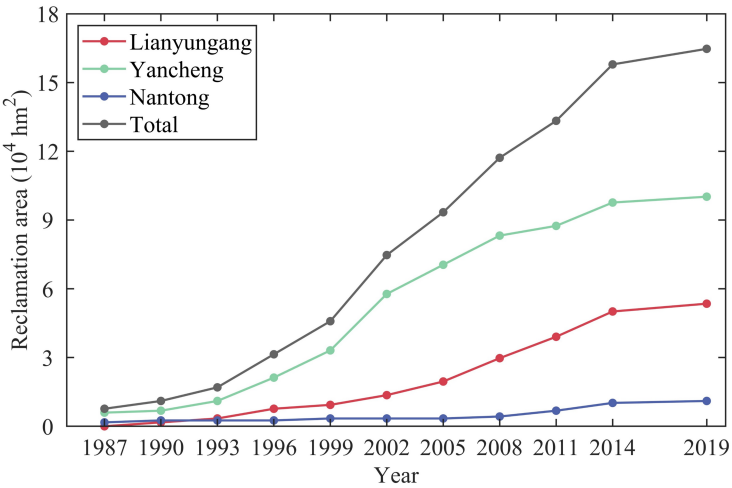


Figure 1.4: Cumulative coastal reclamation areas across three cities in Jiangsu Province from 1987 to 2019 (modified from Xu et al., 2022).

As it can be seen from Figure 1.4, over this period, Jiangsu's total reclaimed area

reached 166,100 hectares, with Yancheng contributing the most (101,100 hectares, 61%), followed by Nantong (54,200 hectares, 33%) and Lianyungang (10,700 hectares, 6%). The rate of reclamation accelerated after 1993, reaching two peaks. The first peak is between 1999 and 2002 when 29,600 hectares were reclaimed. The other peak is recorded between 2011 and 2014, and 24,300 hectares were reclaimed during this period. Post-2014, the reclamation pace slowed due to stricter regulations, averaging 1,500 hectares per year after 2014.

Starting from 2016, China's control over reclamation has been gradually strengthened and the reclamation policy has become stricter. On July 25, 2018, the State Council issued the "Notice on Strengthening Coastal Wetland Protection and Strictly Controlling Reclamation", cancelling local annual reclamation plan quota. The policy shows that China has made up its mind to strictly rectify the reclamation (Miao and Xue, 2021).

Jiangsu Coast's experience in tidal flat reclamation offers valuable insights into sustainable coastal management and land use optimization. The large-scale reclamation projects that once expanded arable land and supported economic development have also led to significant ecological impacts. It seems that there is a conflict between the social-economic and environmental interests when utilizing the tidal flat resources. This deteriorating contradiction creates an increasing pressure on the management of the tidal flat resources and associated ecological environment. It reflects the need for a scientific foundation for sustainable coastal resource utilization and protection. From the morphological perspective, it is important to know how coastal environments can accommodate these human interventions while minimizing the loss (or even promoting the growth) of tidal flat. This challenge prompts an urgent need to thoroughly investigate the evolution patterns of coastal tidal flats. Robust insight in these patterns is needed to be able to distinguish the effects of human interventions from natural morphodynamics, and to assess the implications for future coastal development and management.

## 1.4. AIM AND QUESTIONS

THE aim of this study is to strengthen the geomorphological knowledge base necessary for mitigating the impacts of coastal economic development on tidal flat resources. By enhancing the understanding of tidal flat dynamics along the

Jiangsu Coast, this research can offer theoretical guidance for the sustainable utilization of tidal flat resources in the future. This aim is pursued by addressing the following specific research questions, which form the core of this dissertation:

(1) **What are the slopes of cross-shore intertidal flat profiles and the surficial sediment grain size distributions patterns along the Jiangsu Coast?**

(2) **What physical mechanisms are driving the formation of these observed patterns?**

(3) **What is the resilience of tidal flats in response to anthropogenic interventions under different natural environmental conditions?**

## 1.5. METHODOLOGY

To address the research questions outlined above, this study employs a multi-method approach that integrates observational data analysis, comparative regional assessment, and numerical modelling.

**M1** To thoroughly understand the mechanisms driving the evolution of open coast tidal flats, it is essential to first examine the geomorphological characteristics of tidal flats under different hydrodynamic regimes. The Jiangsu Coast exhibits significant spatial variation in both hydrodynamic forcing and shoreline changes. Our analysis begins with a systematic examination of existing morphological datasets covering the entire Jiangsu coastal zone. These data provide the foundation for identifying spatial patterns in tidal flat morphology and surficial sediment distribution under varying environmental conditions.

**M2** The observed features are compared with those from other tidal flat systems worldwide. By evaluating similarities and differences, particularly in relation to known hydrodynamic regimes and sediment transport settings, we can hypothesize the primary mechanisms responsible for the formation of regional patterns on the Jiangsu Coast.

**M3** These hypotheses are tested using numerical models. A simplified, diagnostic-mode Delft3D model is applied to examine how gradients in hydrodynamic forcing and variations in sediment provenance influence profile development. For longer-

term morphological evolution, especially under anthropogenic interventions, an extended version of the DET-ESTMORF model is employed. Sensitivity analyses are conducted under different hydrodynamic and sediment supply scenarios to evaluate the capacity of tidal flats to recover post-reclamation.

By combining these methods, this study provides an integrated understanding of both the natural evolution and human-impacted dynamics of open-coast tidal flats. This framework supports the identification of key environmental factors that enhance tidal flat resilience and guides future sustainable coastal management strategies.

## 1.6. CONTRIBUTION OF THE RESEARCH

DESPITE this study is rooted in a single geographic region, the conclusions are of broader relevance through comparisons with other tidal flat systems and through the use of generalized, physics-based modelling approaches.

First of all, the Jiangsu Coast offers a uniquely diverse setting, encompassing both erosional and accretional shorelines and exhibiting various hydrodynamic conditions and sediment provenance. Combined with its long history of human interventions, the coast provides a valuable natural laboratory for understanding the complex mechanisms driving tidal flat evolution. The observed spatial variability across different sections of the coast enables a comprehensive examination of the controls on tidal flat morphology. Comparative analyses with other global tidal flats further enhance the transferability of the insights derived from Jiangsu.

This study aims to capture the general relationships between tidal flat morphology and its controlling factors, such as hydrodynamic forcing, sediment supply, and anthropogenic disturbances. The adoption of schematized, physics-based models allows the findings to be abstracted beyond local boundary conditions, offering a conceptual framework applicable to other open-coast muddy environments. Nevertheless, it is important to acknowledge the conclusions are robust within the modelled parameter range, they should be applied to other systems with attention to local environmental contexts.

The scientific contribution of this thesis lies in its effort to bridge large-scale coastal morphology observations with idealized modelling to reveal the first-order controls on tidal flat evolution and resilience. It contributes both to theoretical un-

1

derstanding and practical guidance for sustainable reclamation planning. The established simplified one-dimensional model also serves as a foundational framework for future research on the complex morphological responses of tidal flats under climate change and ecological impacts.

## 1.7. THESIS OUTLINE

THIS This thesis focuses on the morphological evolution of the tidal flat on the Jiangsu Coast, China under natural conditions and with anthropogenic activities. It consists of five chapters (Figure 1.5), and the organisation is as follows:

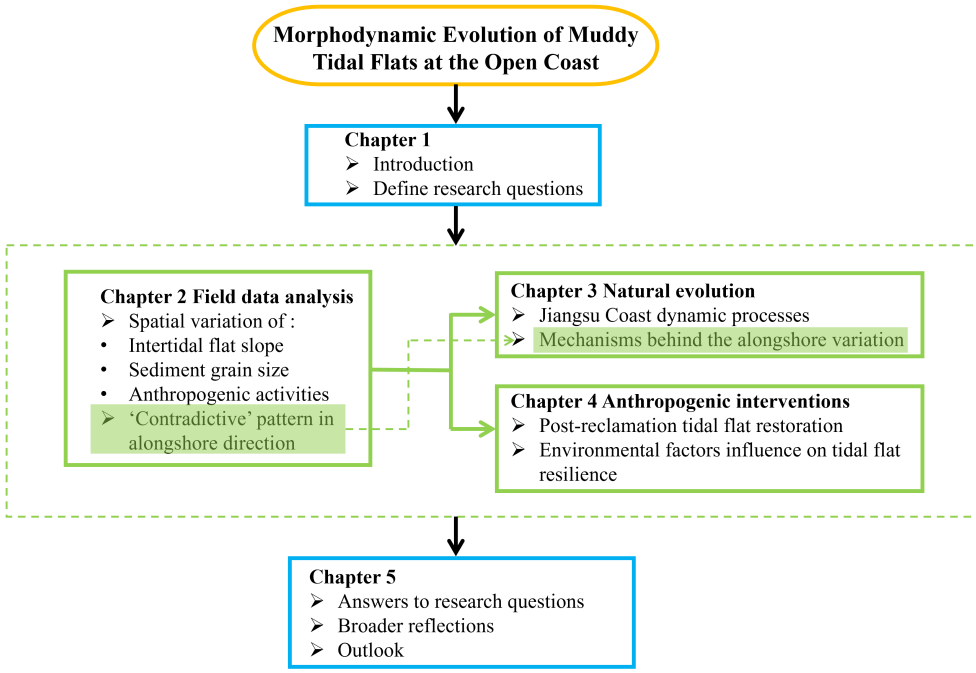


Figure 1.5: A overview of the content and outline of the thesis.

Chapter 2: Based on a high spatial-resolution dataset of morphological measurements along the Jiangsu Coast, the morphology and sediment characteristics of the unvegetated tidal flats along the coast are analysed. Furthermore, a preliminary hypothesis and explanation for the physical mechanism of some seemingly unexpected patterns are proposed.

Chapter 3: In order to make a robust explanation for the unexpected patterns

found in Chapter 2, an hypothesis is made based on a conceptual model of the hydrodynamics and shoreline evolution on this coast. A numerical model is applied in a diagnostic mode to verify the hypothesis.

Chapter 4: The morphological response of the tidal flat to reclamations (upper part enclosure) is investigated by the application of a numerical model. The influence of environmental factors on tidal flat resilience is analysed by a series of sensitivity test.

Finally, Chapter 5 summarises the overall conclusions of the thesis and further synthesizes into general findings. An outlook on future research is provided as well.

# 2

# SEDIMENT CHARACTERISTICS AND INTERTIDAL BEACH SLOPES ALONG THE JIANGSU COAST, CHINA

This chapter is published as Kuai, Y., Tao, J., Zhou, Z., Aarninkhof, S., and Wang, Z.B. (2021). Sediment characteristics and intertidal beach slopes along the Jiangsu Coast, China. *Journal of Marine Science and Engineering* 9 (3): 347.

**ABSTRACT** Tidal flats play an important role in promoting coastal biodiversity, defense against flooding, land reclamation and recreation. Many coastal tidal flats, especially the tide-dominant ones, are muddy. However, the number of studies on the profile shape and surficial sediment distribution of muddy tidal flats is small compared to sandy beaches. Based on high spatial-resolution measurements along the tide-dominant Jiangsu Coast, China, we analyzed the morphology and sediment characteristics of the unvegetated intertidal flats along the Jiangsu Coast. The Jiangsu Coast can be divided into an eroding north part (north coast) and an accreting south part (south coast). The beach slope of the north coast shows a southward flattening trend, apart from some outliers related to rocky parts of the coastline. We found alternating very fine and coarse sediment (depending on the local clay content) for different locations along the north coast, which can be explained from consolidation and armoring-induced erosion resistance. In the south coast, we found gradual coarsening of bed surface sediment and gradual flattening of beach slopes to the south. This seemingly unexpected pattern is explained by the flood-dominant current causing landward sediment transport, larger tidal range in the south part, sheltering effect of the Radial Sand Ridges, and contribution of different sediment sources, viz. the Abandoned Yellow River Delta and the Radial Sand Ridges. In the cross-shore direction, the sediment grain size decreases landward. Waves are only of secondary importance for the sediment dynamics at the unvegetated tidal flats along the Jiangsu Coast.

## 2.1. INTRODUCTION



LOCATED at the boundary between land and sea, tidal flats are under the joint control of both terrestrial and marine processes, while they play a vitally important role in promoting coastal biodiversity, protecting coastal regions from flooding, and providing potential land resources and recreation. Nowadays, in the progress of coastal resource development, many human activities (e.g. ports construction, reclamation) are conducted on tidal flats, like the Tongzhou Bay port on the Jiangsu Coast, China (Muller et al., 2020b), the Maasvlakte reclamation in the Netherlands (van der Spek and Elias, 2021). Therefore, tidal flat evolution has been a key research topic in the field of coastal engineering.

Many studies have been carried out on the characteristics of sandy, wave-dominated beach profiles (Karunarathna et al., 2016; Medina et al., 1994; Work and Dean, 1992; Dean, 1991). Sandy beaches with coarse materials tend to be steeper (Bujan et al., 2019; Firoozfar et al., 2014). Coarser sands have larger angle of repose than finer ones. Also, due to their higher permeability and roughness, coarser materials tend to be more stable in dynamic conditions (Bujan et al., 2019). However, because of difficulties in field observation, the number of studies on the profile shape and sediment distribution of the muddy and silt-muddy tidal flats is far less than for sandy beaches. It is found that, accreting tidal flats tend to have a convex-up shore-normal profile, while eroding tidal flats tend to have a concave-up one (Kirby, 2000; Lee and Mehta, 1997). The intertidal flats in muddy environments are more convex-up than those in sandy environments (Zhou et al., 2015).

Silt-muddy tidal flats are shallow areas characterized by fine cohesive sediment including clay (<0.004 mm), silt (0.004-0.062 mm) and very fine sand (0.062-0.125 mm) supplied from adjacent rivers, estuaries and coasts. They are found worldwide under a variety of climatic, hydrodynamic and sedimentological conditions, such as the East Coast of China (Gong et al., 2012), the Northwest Coast of America (Mariotti and Fagherazzi, 2012), the Severn Estuary of the UK (Carling et al., 2009) and the Wadden Sea in the Netherlands (Kleinhans et al., 2009). Based on the different dynamic conditions and terrains, silt-muddy tidal flats can be divided into open coast, embayment and estuarine tidal flats, among which the open coast tidal flat can be well developed because of complex dynamics and less restrictions for sediments transport routes. Figure 2.1 shows a characteristic cross-shore sediment

zonation pattern for a well-developed silt-muddy tidal flat.

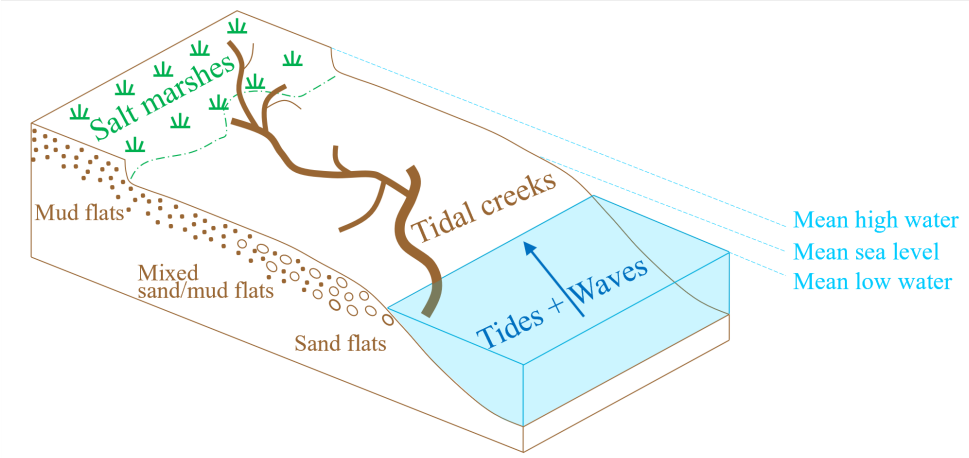


Figure 2.1: A profile view of sediment zonation (modified from Zhou et al., 2015).

Although silt-muddy tidal flats exist worldwide broadly, they are of different characteristics for several reasons. First of all, the sediment transport itself is a complex and multi-dimensional process that closely relates to the interactions involving various external forcing agents (e.g. tide, wave, wind and storm surge) (Soulsby, 1997; Van Rijn, 1993). In addition, the difference in sediment compositions (e.g. clay, silt, and very fine sand) and biological activities have apparent impacts on the processes like sediments erosion, mixing, deposition and bed consolidation (Winterwerp and Van Kesteren, 2004). Furthermore, changing environments (e.g. sea level rise, sediment supply) and human activities in different regions can also lead to different tidal flat morphologies (Coco et al., 2013). Thorough understanding of nearshore morphodynamic processes including the link between hydrodynamic forcing, surficial sediment distribution and beach profile change is of crucial importance for the assessment of coastal safety and natural values, as well as the impact of human interventions in the coastal zone.

Jiangsu Coast, China, is such a typical open coast with extended silty-muddy tidal flats. It represents great economic and environmental value for the country; it not only provides shelters for the littoral flora and fauna, land resources for agriculture and aquaculture, but also protects the safety of coastal cities. The goal of this study is to increase our insight in the morphological characteristics of the un-

vegetated intertidal flats along the Jiangsu Coast. On the basis of high-resolution bed surface sediment grain size and cross-shore profile elevation data from a large-scale coastal investigation, we analyzed the beach profile evolution and sediment distribution patterns along this coast.



## 2.2. AREA DESCRIPTION

THE Jiangsu Coast (Figure 2.2c) is situated between the Yangtze River and the Xiuzhen River Estuary (Ren, 1986a). Tidal flats along the Jiangsu Coastline are characterized by (1) its large width (with a mean width of 8 km), (2) abundant sediment supply from the two large rivers (from the Yangtze River during the end of the late Pleistocene and from the Yellow River from 1128-1855 AD), and (3) silt dominant sediments (Wang and Ke, 1997). It has been regarded generally as a typical example of open coast tidal flats (Ren, 1986b). From the embankment to mean low water, four distinctive zones can normally be found which are grass flat (freshwater or brackish water wetland), Suaeda salsa flat (saltmarsh), mud flat and silt or sand flat, respectively (Wang and Ke, 1997).

Two distinct geomorphological units can be recognized in the north and south parts of the Jiangsu Coast respectively, i.e. the Abandoned Yellow River Delta (AYRD) and the fan-shaped Radial Sand Ridges (RSRs) (Gao, 2009; Li et al., 2001; Zhang, 1984). During 1128–1855 AD, the Yellow River flowed into the South Yellow Sea at the north part of the Jiangsu Coast causing abundant fine sediment supply into the coastal areas, and gradually forming the (now) Abandoned Yellow River Delta (Gao, 2009). The paleo-Yangtze River also brought a large amount of sandy sediments to the RSRs, during the end of the late Pleistocene (Wang et al., 1999). These two large sediment sources led to a rapid tidal-flat formation. After 1855, The Yellow River shifted its lower reach to the Bohai Sea (Zhou et al., 2014). As the Yangtze River Estuary moved southward as well (Gao, 2009). The suspended sediments in the coastal areas are since then mainly generated by bed erosion, instead of fluvial supply, and the whole coastal areas can be treated as a quasi-enclosed sediment system (Zhang et al., 2002; Milliman et al., 1985). As a result, severe coastal erosion took place around the AYRD due to the cutoff of sediment supply (Figure 2.2c).

After 1970s, some shoreline protection projects were built at the AYRD, which decreased the shoreline regression rate. While the shallow part of the coastal pro-

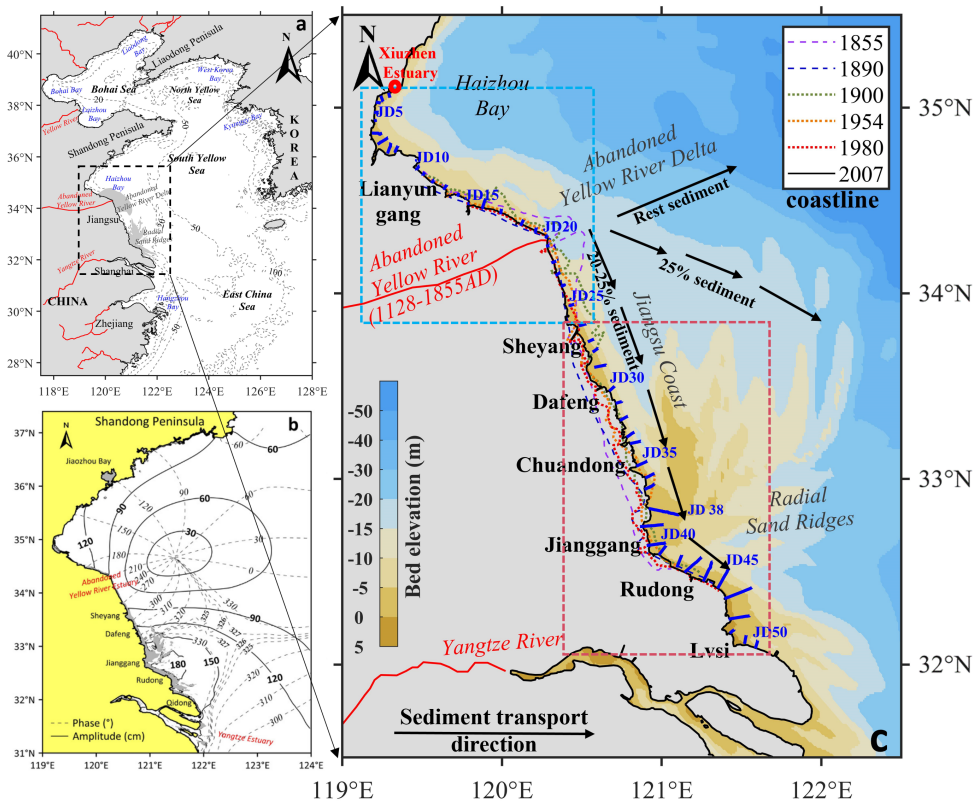


Figure 2.2: Map of the Bohai Sea, Yellow Sea and East China Sea (a). Subplot (b) shows the co-tidal charts of the $M_2$ constituent for the southern Yellow Sea. Amplitude is shown in cm, and phase in degrees (from Xu et al., 2016). Subplot (c) indicates the Jiangsu Coastline evolution from 1855 to 2007, transport pattern of the sediment eroded from the Abandoned Yellow River Delta and the location of measured profiles. The locations of the Abandoned Yellow River Delta and the Radial Sand Ridges are labelled in (a), and the historical shoreline location in (c) is collected from Su et al. 2017b, in which there is a detailed description of the shoreline data.

file remained in place, erosion of the deeper part continued resulting in a steepening of the cross-shore slope. Sheltered by enormous offshore ridges and fed by sediments supply derived from the eroding AYRD and these ridges, the coast between Sheyang and Lvsi is still accreting, most notably at the supratidal flats. The mudflats from Sheyang to Jianggang are the widest and fastest accretionary mudflats in China (Zhang, 1992). Meanwhile, due to decreasing sediment supply from the AYRD and erosion of the outer edges of the radial sand ridges (thus decreas-

ing the length of sheltered coastline), the eroding section near Sheyang is gradually expanding southwards (Zhang, 1984).

The semi-diurnal tide is of major importance for the tidal flats along the Jiangsu Coast. The tidal wave first enters the southern Yellow Sea and part of it is reflected by the Shandong Peninsula, forming an anticlockwise rotational tidal wave system. The rotational wave and the progressive wave from the southern Yellow Sea converge near Jianggang (Figure 2.2b). The convergence of these two tidal waves leads to the formation of an approximately standing tidal wave and the radial tidal current field in this area (Xu et al., 2016; Yao, 2016; Xing et al., 2012). The mean tidal range along the Jiangsu Coast is about 2-4 m (see Figure 2.3, Ren, 1986b). The tide there is flood dominant, which is of great importance to net sediment transport (Wang et al., 2012b; Zhang, 1992).

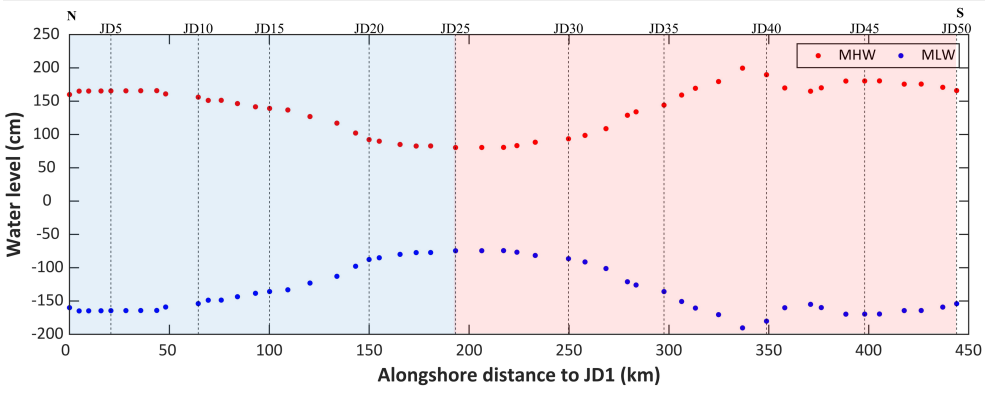


Figure 2.3: Interpolated MHW and MLW at each profile (the vertical dash lines indicate the location of every fifth profile; N denotes North and S denotes South and these are the same for the following figures).

The waves along the Jiangsu coastline are influenced primarily by the monsoon climate, characterized by a mixture of swells and locally generated wind waves with the latter being dominant. Waves from the north prevail in this region over the year and the probability of wave height smaller than 1 m is about 85% (Ren, 1986b). Due to the wave energy attenuation on the wide and shallow tidal flats, the effect of wave action on changing the coastal morphology is much weaker than the tidal action (Wang et al., 2012b; Ren, 1986b).

Classified by the mean grain size ($M_Z$) and the sand ($-1 \sim 4\Phi$, $\Phi = -\log_2 d$, $d$ is

grain size in mm), silt (4 ~ 8Φ), and clay (> 8Φ) proportion, the tidal flat sediments at the Jiangsu Coast are mainly composed of 5 types of sediment, named fine sand ($M_Z$ 2–4Φ, sand 70–90%), sandy silt ($M_Z$ 3–5Φ, sand 30–40%, silt >50%, clay <10%), silt ($M_Z$ 5–6Φ, sand 15–20%, silt 65–75%, clay <10%), clayed silt ($M_Z$ 5.5–6.5Φ, sand 5–10%, silt >60%, clay 20–25%), and clay ($M_Z$ 7.5–8Φ, sand <17%, silt 20–25%, clay 45–70%), respectively. The distribution of surface sediment on intertidal flats shows a seaward coarsening trend (Wang and Ke, 1997).

## 2.3. MATERIAL AND METHOD

### 2.3.1. DATA SOURCE

DATA of cross-shore beach profile bathymetry and grain size distribution of sediment samples are from a comprehensive field survey on coastal zone of Jiangsu province, which has been reported in Zhang 2012. To the authors' knowledge, this is the latest field survey dataset with such a large spatial scale on the Jiangsu Coast. The large-scale investigations were performed between 2006 and 2008. 50 cross-shore profiles starting from Xiuzhen estuary to Lvsi (Figure 2.2c) were defined along the Jiangsu Coast. The bed elevation was measured along these 50 profiles and 173 bed surface sediment samples were taken along only 36 of these profiles. For the bed elevation, the intertidal part was measured in 2007 by Real Time Kinematic (RTK) instrument (with a cross-shore interval of ~ 70 m), and subtidal part was measured in 2008 by vessel measurement (with a cross-shore interval of ~ 10 m). The samples were collected from the same layer (approximately the top ~ 10 cm of the bottom) in 2006 and 2007, and only the top (1-2 cm) of the samples are adopted for sediment gradation analysis. For the sediment samples on the same profile, the distance between adjacent sample points is around 500 m. Because the south part of the Jiangsu Coast has wider intertidal flats than the north part, more sample points were taken on the south profiles. In addition, the Landsat 7 ETM satellite images were used to check for detailed information, such as locations of the tidal creeks and human interventions in the past 20 years. The satellite images are downloaded from the United States Geographical Survey website (USGS, http://www.usgs.gov, accessed on 14 January 2020).

### 2.3.2. DATA PROCESSING

IN Figure 2.2c, two dash line rectangles were marked to divide the whole coastline into two parts, based on the shoreline evolution condition (erosion or accretion). The blue one (JD1-25, hereafter referred to as north part/ north coast) contains the Haizhou Bay and the AYRD. Haizhou Bay is the only zone of the Jiangsu Coast having rock coast with typical sandy sediment. The coastline around the AYRD is under severe erosion since 1855 when the Yellow River switched its course. During the large-scale investigation (2006-2008), the shoreline erosion in this part was already at a much slower rate. The red one (JD26-50, hereafter referred to as south part/ south coast) is under continuous accretion. This part is the most typical silty beach along the Jiangsu Coast. The alongshore distance is measured the between the landward ends of the adjacent profiles.



In order to compare the profile shapes, the intertidal flat slope was determined. We estimate the intertidal flat slope ($slope = \tan\alpha$, see Figure 2.4) from the width of the intertidal beach, as determined from the locations of the mean high water (MHW) and mean low water (MLW) beach contours. The MHW and MLW levels are determined from the historical Yellow Sea mean tidal range distribution data after Ren, 1986, assuming Mean Sea Level (MSL) is half-way between MHW and MLW (see Figure 2.3). The elevations thus obtained can be used to determine the MHW and MLW locations at each profile.

This approach is obscured by potential presence of old/new dykes at the shoreward end of the profile and presence of tidal channels at the seaward end of the profile, which hamper consistent identification of the MHW and MLW contour locations. A systematic approach was followed to overcome these difficulties at either end of the beach profile, in order to enable quantitative beach slope estimates along the Jiangsu Coast. This approach (Baseline Method) is explained here:

At the shoreward end of the profile, old dykes and newly built dykes are occasionally located below MHW. Instead of calculating the intertidal beach slope from the MHW level, at influenced profiles (e.g. 17, 33, and 35) we choose the most seaward dyke toe and associated beach elevation to be the start point (see Figure 2.4).

At the seaward end of the profile, as we link the measured profile data (Figure 2.6) to the satellite images (Figure 2.5), we can find that in the region of the RSRs, the intertidal flat is cut through by tidal creeks of different sizes at many places, and

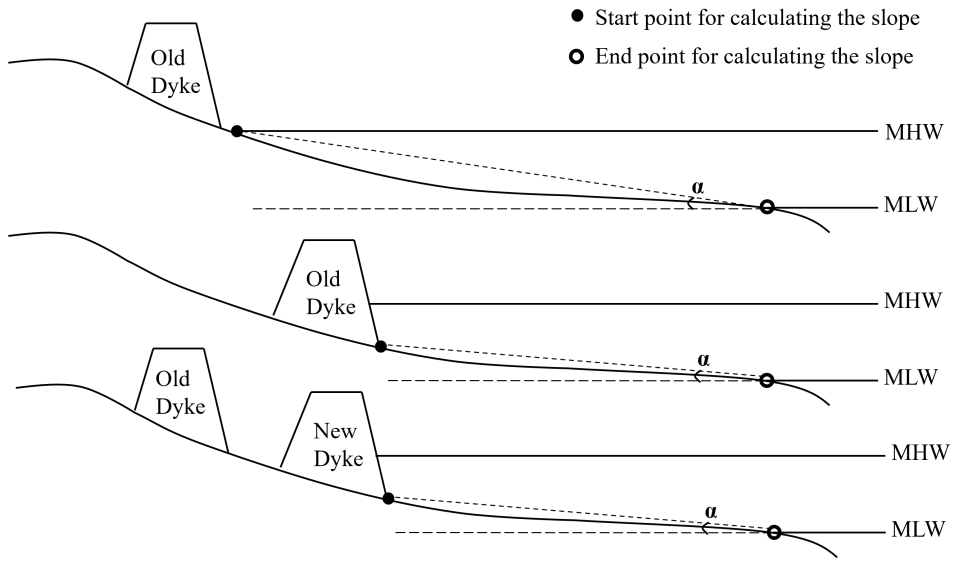


Figure 2.4: Scheme of calculating the intertidal flat slope.

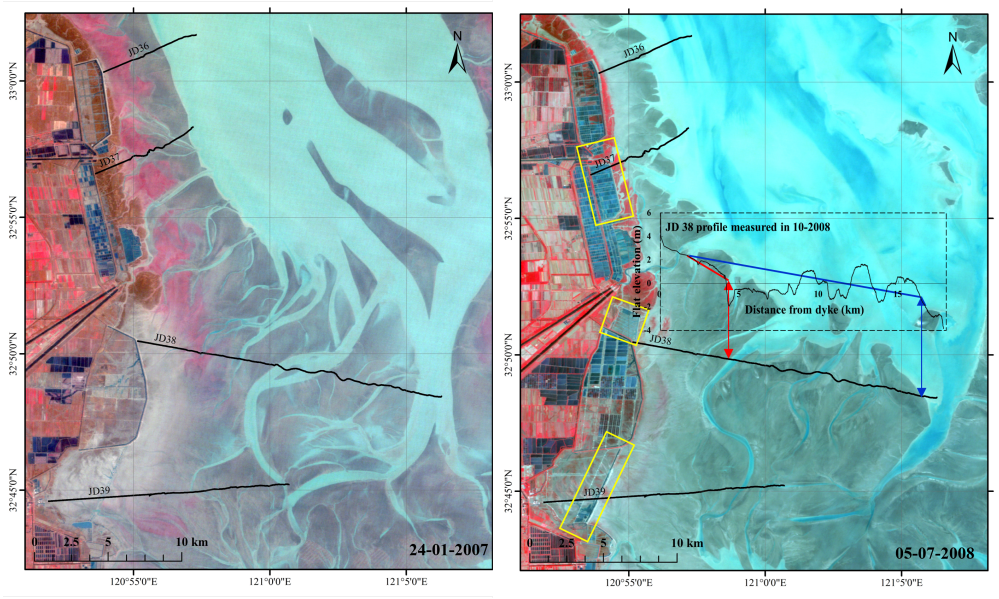


Figure 2.5: Satellite image of the JD 36 to 39 from Landsat 7 ETM on 24$^{th}$ January, 2007 (**left panel**) and 5$^{th}$ July, 2008 (**right panel**). The yellow box indicates the human interventions taking place between these two image times. The dash black box indicates the measured profile JD38 in October, 2008, and the red and blue lines in the dash box are associated with two beach slope calculation methods.

these tidal creeks change their locations continuously. Here, we took profile JD38 (see Figure 2.2c) for example. As we see in Figure 2.5, the profile JD38 shows strong fluctuations. It is not easy to define the seaward end point for intertidal beach slope calculation on this profile, because there are several positions of which the elevation is equal to MLW. For the previous approach, we simply took the most seaward one as the end point, as the blue arrow shows in Figure 2.5. However, as some tidal creeks could be rather wide and deep, we cannot take the whole profile as a continuous one, because this could make the beach slope definition criterion differ among profiles. Hence, for these profiles (e.g. 38, 39, 43 ~ 50) cut through by a large (wider than 100 m or deeper than 1 m) tidal creek, we defined the end point as the landward bank (the point where cross-shore slope changes abruptly) of the tidal creek, as the red arrow shows in Figure 2.5.



Thus, in this Baseline Method, for the profiles not affected (Figure 2.7 black dots) by the dykes or large tidal creeks, we calculate the beach slope from MHW to MLW beach contours; for the affected ones (Figure 2.7 black circles), we calculate their slopes using the approach introduced above. In this study, we used the Baseline Method to calculate each intertidal beach slope.

To ensure the consistency of the approach among different profiles, all sediment samples are included in the analysis, although same of them are located behind the new dykes. At each sample point, we take the mean sediment grain size ($M_Z$ according to the Folk and Ward 1957 definitions as the representative grain size (see equation 2.1). Then we plotted the mean sediment grain size with reference to the cross-shore location to have a clear view of sediment grain size distribution pattern. Sediment types are classified according to the scheme proposed by Shepard 1954, in which sand, silt, and clay are defined as sediment with grain size of $-1 \sim 4\Phi$, $4 \sim 8\Phi$, and $> 8\Phi$, respectively.

In order to further seek into the alongshore distribution pattern of sediment characteristics, more sediment characteristic parameters (sorting ($\sigma_I$), and skewness ($Sk_I$)) were calculated based on Folk and Ward 1957 definitions (see equation 2.2 and 2.3):

$$M_Z = \frac{\Phi_{16} + \Phi_{50} + \Phi_{84}}{3} \tag{2.1}$$

$$\sigma_I = \frac{\Phi_{84} - \Phi_{16}}{4} + \frac{\Phi_{95} - \Phi_5}{6.6} \tag{2.2}$$

$$Sk_I = \frac{\Phi_{84} + \Phi_{16} - 2\Phi_{50}}{2(\Phi_{84} - \Phi_{16})} + \frac{\Phi_{95} + \Phi_5 - 2\Phi_{50}}{2(\Phi_{95} - \Phi_5)} \tag{2.3}$$



where $\Phi_{84}$, $\Phi_{16}$, $\Phi_{50}$, $\Phi_{95}$, $\Phi_{75}$, $\Phi_{25}$ and $\Phi_5$ represent the $\Phi$ values at 84, 16, 50, 95, 75, 25 and 5 percentiles in a cumulative frequency curve (i.e. horizontal axis: sediment grain size in phi; vertical axis: percentage of sediment coarser than a certain size by weight). The verbal classification scales for sorting and Skewness are shown in Table 4.1 and Table 4.2, respectively.

Table 2.1: Classification scale for sorting

| $\sigma_I$ **Values** | **Sorting verbal scale** |
|---|---|
| $< 0.350$ | very well sorted |
| $0.35 \sim 0.500$ | well sorted |
| $0.5 \sim 0.710$ | moderately well sorted |
| $0.71 \sim 1.00$ | moderately sorted |
| $1.00 \sim 2.00$ | poorly sorted |
| $2.00 \sim 4.00$ | very poorly sorted |
| $> 4.00$ | extremely poorly sorted |

Table 2.2: Classification scale for skewness

| $Sk_I$ **Values** | **Skewness verbal scale** | **Graphically skewed to** |
|---|---|---|
| $-1.00 \sim -0.30$ | strongly negative skewed | strong coarse tail |
| $-0.30 \sim -0.10$ | negative skewed | coarse tail |
| $-0.10 \sim 0.10$ | near symmetrical | symmetrical |
| $0.10 \sim 0.30$ | positive skewed | fine tail |
| $0.30 \sim 1.00$ | strongly positive skewed | strong fine tail |

Because of continuous reclamations along the Jiangsu Coast, some dykes were newly built, which made it impossible to do the analysis of bed slope and sediment grain size from the same horizontal reference. Using Landsat 7 ETM satellite images, we checked the human activities processes on each profile from 1988 to 2008, and derived the time between measurement and nearest reclamation at each profile. The bed levels in front of and behind the newly built dykes were compared to find out whether these dykes influence intertidal beach evolution.

## 2.4. RESULTS

### 2.4.1. CROSS-SHORE INTERTIDAL BEACH SHAPE



THE measured 50 cross-shore profiles are shown in Figure 2.6 (note that the horizontal axis scales are different between the first three and the other two panels). As the measurements started from the top of old dykes, a sharp decrease in bed elevation in the seaward direction can be observed at the beginning of each profile. Some abnormal peaks can also be noticed on the upper part of the profiles; according to the investigation report (Zhang, 2012), the large peaks are newly built dykes and small ones are abandoned stones and fences of small fishponds. Generally, the south part of Jiangsu Coast has wider and flatter tidal flats with a width that may exceed 10 km. However, the south profiles also tend to be more fluctuating, and that is because of the existence of shore-parallel tidal channels and creeks, especially in the RSRs region (see Figure 2.5).

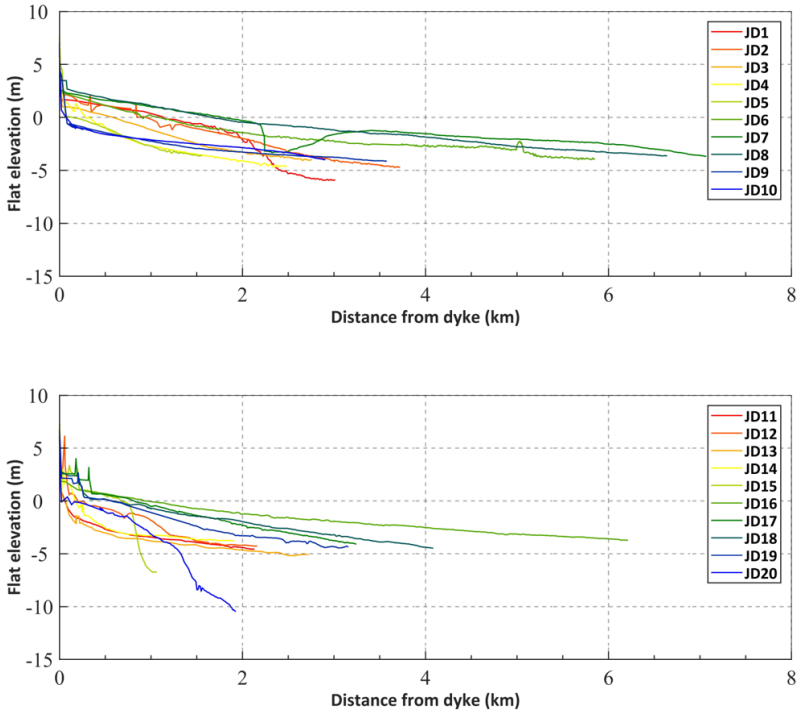


Figure 2.6: Measured bed elevation of the 50 profiles.

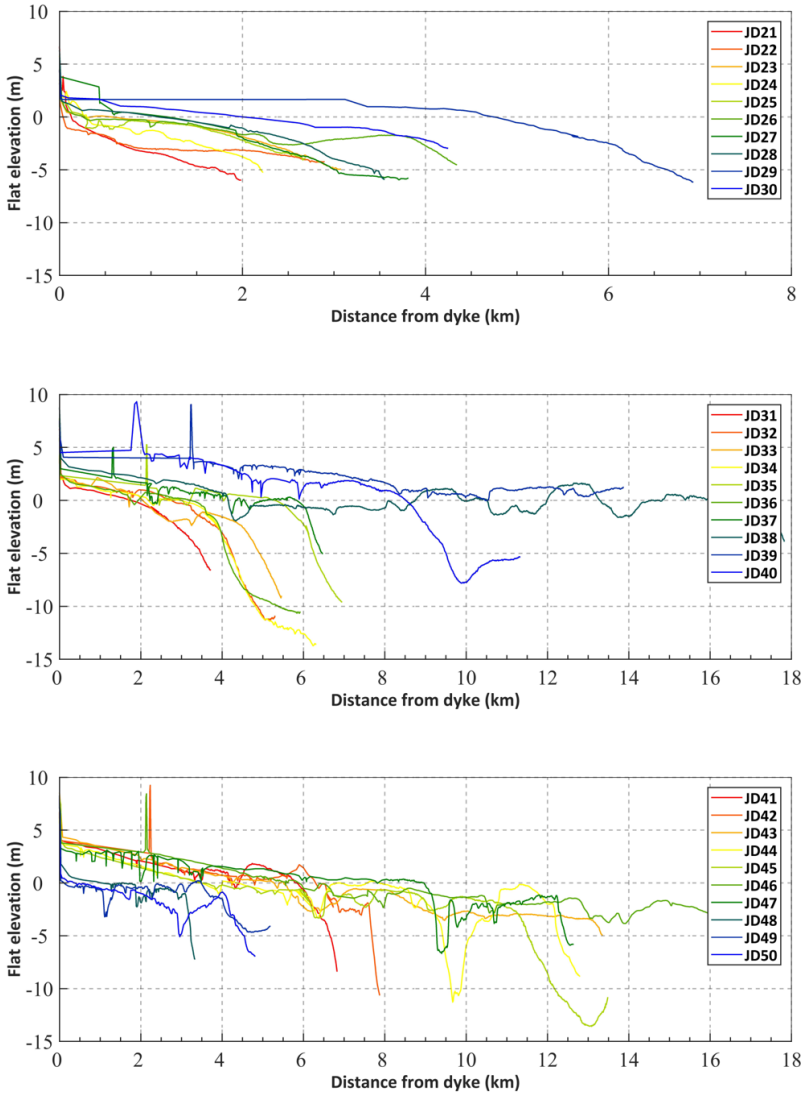


Figure 2.6: Measured bed elevation (continued).

Figure 2.7 depicts the intertidal flat slopes of the 50 cross-shore sections. Generally, cross-shore slope decreases from north to south along the Jiangsu Coast, see Figure 2.7b for the 0–5‰ part. At the eroding north coast, intertidal flat slope is several times larger than on the accretionary south part. Also, the slope distribution fluctuates a lot in the north part. JD9 has very small value, because the measure-

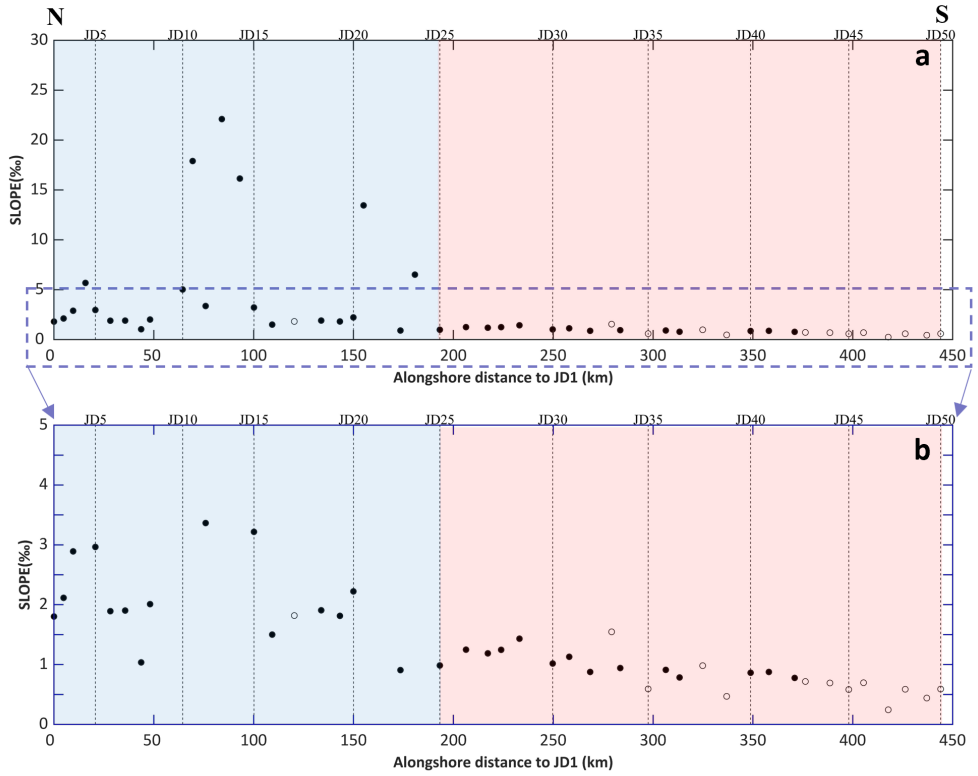


Figure 2.7: Calculated intertidal flat slopes of the 50 profiles based on Baseline Method. (b) is a zoom in of the 0–5‰ part on (a). Black dots represent profiles not affected by dykes or large tidal creeks, black circles are associated with profiles which are affected.

ment took place near small estuary, where riverine supplied sediments can prevent severe erosion. The very large values (>15‰) between JD10 and JD15 are because of the existence of rocky coastline. Apart from these local outliers, the slope decreases from north to south in the eroding north part. At the south part, the slope is basically below 1‰ and the southward flattening trend can be more apparent than it in the north part.

### 2.4.2. SEDIMENT GRAIN SIZE DISTRIBUTION

MEAN grain size ($M_Z$) averaged over sample points on the intertidal part of each profile are shown in Figure 2.8. The sediment grain size shows a notably southward coarsening pattern ($\Phi$ value decreases) in the south part. In the

north part, it shows much variability. A southward fining pattern can be clearly observed only in the small part from profile 20 to profile 25. Compared to the surrounding zone, the bed surface sediment on profile 20, at the top of AYRD, is quite coarse (Figure 2.8). This is understandable, as the top of the AYRD is under heaviest erosion.

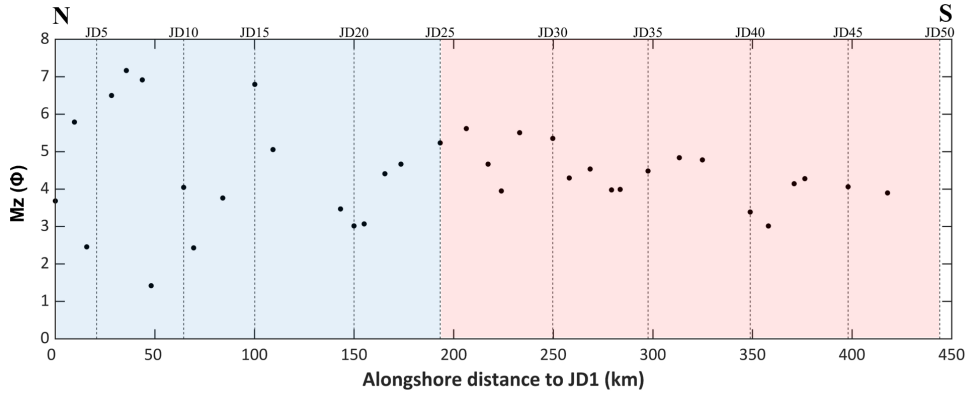


Figure 2.8: Averaged (through profile) bed surface mean sediment grain size of each profile.

Figure 2.9 shows the spatial (alongshore and cross-shore) variation of the sediment characteristic parameters. As can be seen in the figure, most sample points are located on the intertidal flats except only very few points in the south part (Figure 2.9 first panel).

In the cross-shore direction, the grain size generally decreases in the landwards direction. This is a common pattern for tide dominated coasts (Wang and Ke, 1997). However, in the alongshore direction, we cannot directly tell if north part of Jiangsu Coast has finer sediment than the south part, because both dark red dots (very fine sediment) and dark blue dots (very coarse sediment) can be found. The sediment type in the north Jiangsu Coast can be sometimes sand dominant or clay dominant, while in the south part, it is basically silt dominant. As the Jiangsu coastal areas can be treated as a quasi-enclosed sediment system nowadays, the sedimentation in the south Jiangsu Coast partly comes from the eroded fine sediments in the north part. However, it is noted the extremely fine sediments are hardly found in the south part.

For most profiles the bed surface sediment becomes from sand dominant to silt dominant landward (Figure 2.9 panel 4–6). Only in the very north zone (blue zone)

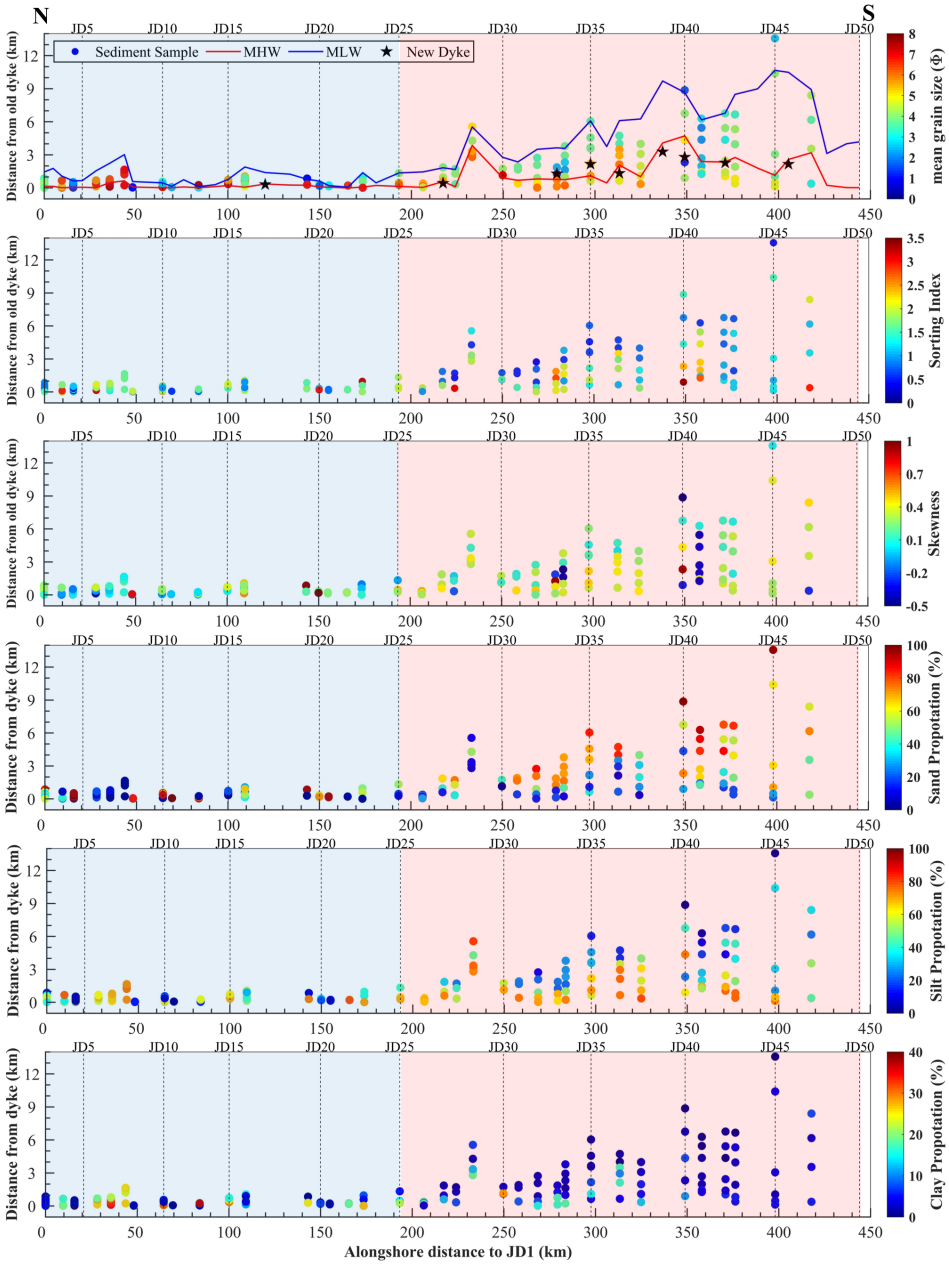


Figure 2.9: Bed surface sediment characteristic parameters distribution related to distance from old dyke (location of MHW, MLW, and new dykes are marked in the first panel).

the clay content can reach a relatively high proportion (note that the color bar limitation for clay proportion is from 0% to 40%, not 100%). In the south part, the sand proportion increases southward around MLW, and the clay proportion decreases southward around MHW. The silt content remains almost uniform.

The sorting is getting better seaward, which means the sediments in the sand dominant part are better sorted, while they are quite mixed in the shallower and silt dominant part. This sorting distribution is also consistent with the observation that in this tide-dominated environment, the upper part of the intertidal beach is less dynamic than the lower part (Le Hir et al., 2000). The Skewness distribution shows that the sediment is fine-skewed for most of the samples, and it becomes more fine-skewed landward. This indicates that the upper part of the intertidal flat tends to have excess fine materials, consistent with the landward fining pattern.

In the cross-shore direction of the Jiangsu Coast, sediment tends to be finer landward. This is opposite to wave-dominated sandy beaches, where the coarsest sediment is near shoreline. Comparing the alongshore intertidal beach slope variation and sediment grain size variation, an interesting phenomenon has been observed at the accretionary south part of the Jiangsu Coast. While tidal flat slopes are becoming milder towards the south, the corresponding bed surface sediment grain size is becoming coarser southward. This seems to be opposite to wave-dominated sandy beaches, where milder wave conditions tend to be associated with finer sediments. Another seemingly unexpected phenomenon is that sediments at some of the profiles in the eroding north part are much finer than in the accreting south. These seemingly unexpected phenomena are further discussed in the discussion section.

### 2.4.3. HUMAN INTERVENTIONS

THE time difference between the profile measurement and the most recent reclamation at each location is shown in Figure 2.10. Recent reclamations mostly took place in the south part, where the construction time is very close to the measurement time. Earlier reclamations usually took place above the MHW, whereas more recent reclamations gradually extend to deeper areas (especially at the tidal flats shielded by the RSRs, see profile 33 and 35 in Figure 2.9 first panel and Figure 2.11). We need to compare the bed elevation in front of and behind these dykes to

find out how dyke construction has affected the bed level changes.

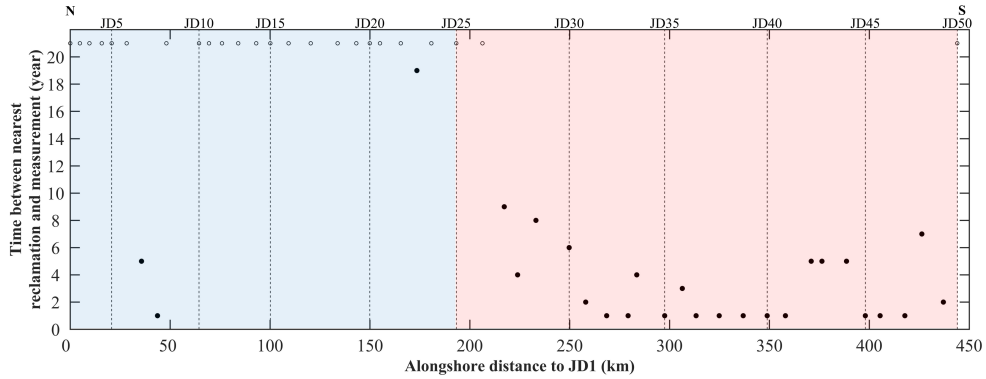


Figure 2.10: Time between measurement and nearest reclamation at each profile (circles means time larger than 20 years).

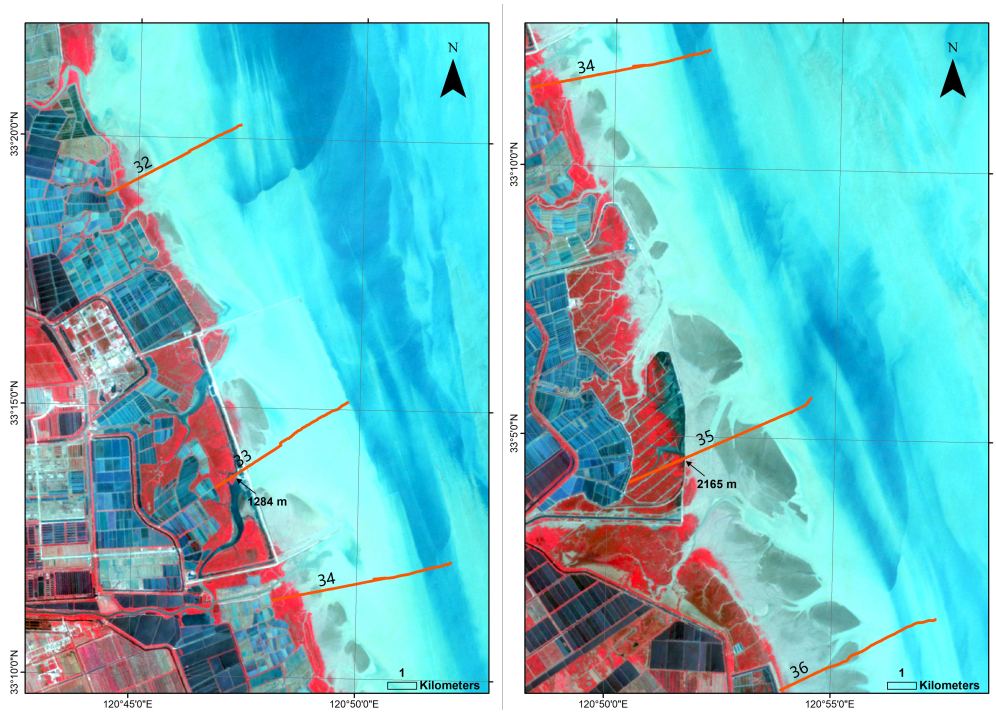


Figure 2.11: Satellite images of the JD 33 and 35 from Landsat 7 ETM on 5$^{th}$ July, 2008 (arrows indicate the location of new dykes on each profile and distance to the old dykes).

Figure 2.9 (first panel) shows that only for profiles JD17 (at the eroding part),

JD33 and 35 (at the accreting part), dykes are located on the intertidal zone. Zooming in around the new dykes of these three profiles (Figure 2.6) we can easily compare the bed elevation in front of and behind these dykes (Figure 2.12). The bed elevations remain almost the same in front of and behind the dykes in JD33 and 35. At JD17, the dyke was built 20 years ago, so we can treat it as an old dyke, and the lower bed elevation in front of it suggests strong erosion.

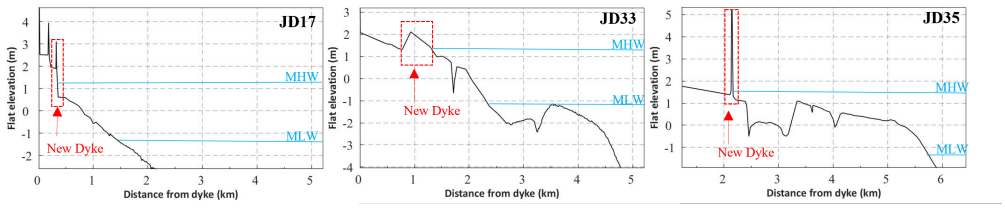


Figure 2.12: Zoom in on the bed elevation in front of and behind the newly built dykes (note that the scales of the threes panels are not uniform).

In summary, we conclude that:

- Intertidal beach slopes are larger in the eroding north part of the Jiangsu Coast than in the accreting south part. Apart from some outliers that relate to rocky parts of the coastline, beach slopes show a southward flattening trend in both the north and south part of the coastline, albeit more obvious in the accreting south part.

- In the cross-shore direction, the bed surface sediment grain size decreases landward, and the sorting is getting better seaward. In the alongshore direction, the sediment grain size distribution pattern is more complex, with explicitly the following two features: In the eroding north part, both extremely fine sediment dominant profiles and coarse sands dominant profiles can be found. In the accreting south part, sediment grain size shows a southward increasing pattern.

- Human interventions continuously took place along the Jiangsu Coast. The most recent dykes in the north Jiangsu Coast were built more than 20 years before the time of measurement. While in the south part, new dykes were built more recently, most within one year time before the measurement.

## 2.5. DISCUSSION

### 2.5.1. RELIABILITY OF THE RESULTS



THE way we defined the beach slope cannot guarantee all results are calculated under the same reference, because at some profiles MHW is above the elevation of the dyke toe, while at some other profiles large alongshore direction tidal creeks could cut the profiles into separate parts. This was resolved through application of the Baseline Method; however, this could influence the alongshore intertidal beach slope distribution pattern we found. In order to check if slope definition boundaries influence the observed variation pattern, intertidal beach slopes were recalculated on the basis of different contour levels, namely from -1 m to 1 m (Sensitivity scenario 1) and -0.5 m to 0.5 m (Sensitivity scenario 2) respectively, as the mean sea level is around 0 m. Sensitivity scenario 2 thus provides a zoom in with respect to scenario 1. These two scenarios with narrowed vertical ranges can avoid the dykes and some of the tidal creeks influences.

Figure 2.13 shows the results of alongshore beach slope distribution calculated with different upper and lower boundaries. For most profiles, results are similar to each other, with only minor difference (less than 1‰) in magnitude. They all show a southward slope decreasing trend and this trend is more notable in the south part. With all these boundaries, the beach slope along the north part is quite fluctuating, because the beach type is variable in this part. However, there are still some profiles having large variations among these scenarios. Figure 2.14 indicates the standard deviation of the beach slopes calculated with three different boundaries. It is based on three data points only and serves as an indication to highlight variability in results. Apparently, for the north part more variability can be noticed. While in the south part, the variations are relatively small. Therefore, in the north part, the estimated beach slopes are more sensitive to the chosen upper and lower boundaries of the intertidal profile as used in the analysis. The above comparison result means the beach slope definition boundaries do have an impact on the detailed slope distribution, but do not change the key-findings on the beach slope southward flattering pattern.

In the Figure 2.15, the beach profiles were divided into two parts (divided at 0 m, about the mean sea level) in order to see the profile shape (concave-up or

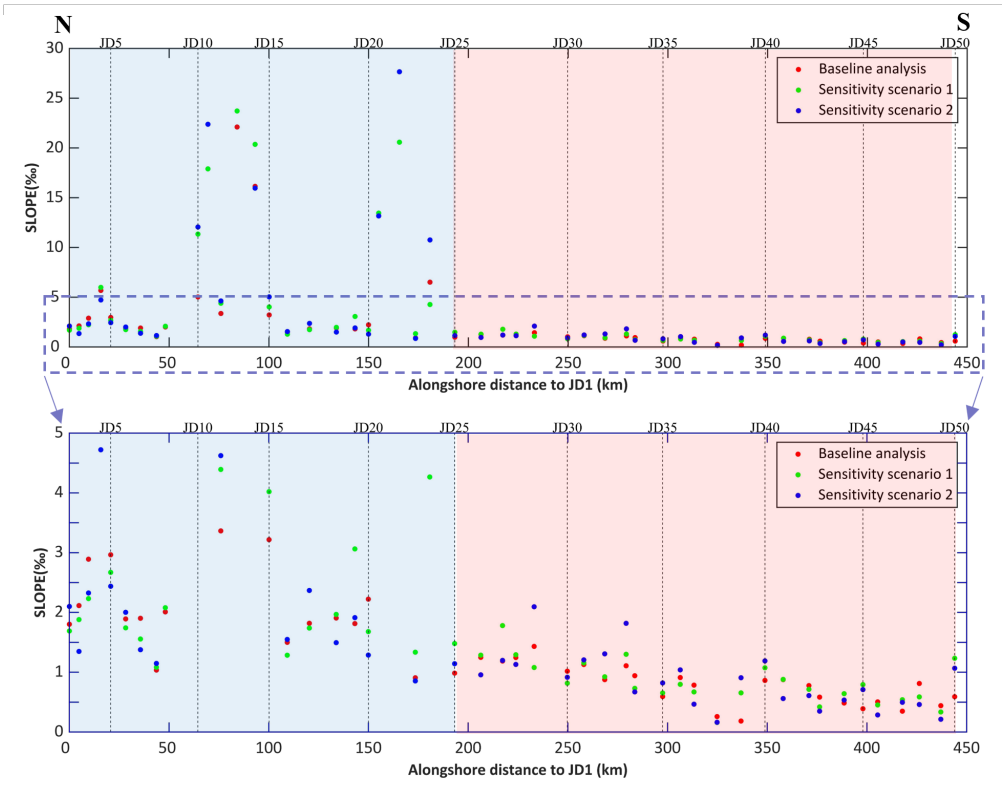


Figure 2.13: Intertidal beach slopes of the 50 profiles calculated with different boundaries.

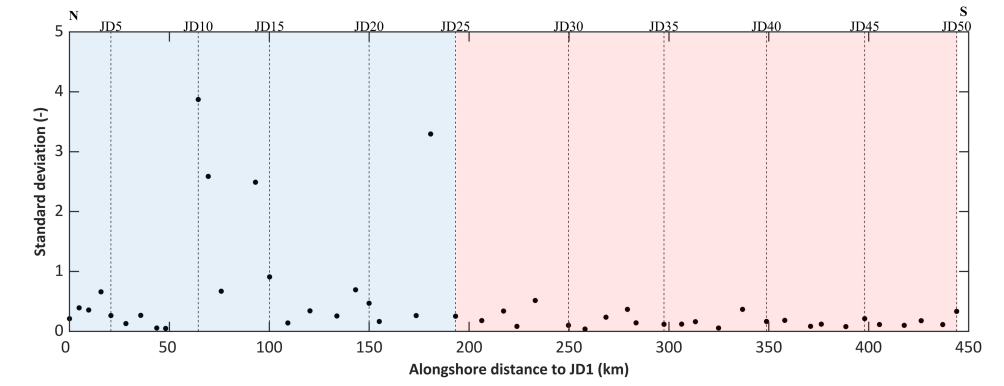


Figure 2.14: Standard deviation of three intertidal beach slopes calculated with different boundaries.

convex-up). JD20 is located on the top of AYRD (see figure 2.1c), which is under the greatest erosion. From JD20 to JD50, the beach profiles changes from concave-up

to convex-up, which is consistent with shoreline condition (eroding profiles tend to be concave-up while accretionary ones tend to be convex-up). As the tidal range increases southward, the beach profile tends to be more convex-up towards the south. This pattern was also found at the tidal flats in South San Francisco Bay (Bearman et al., 2010).

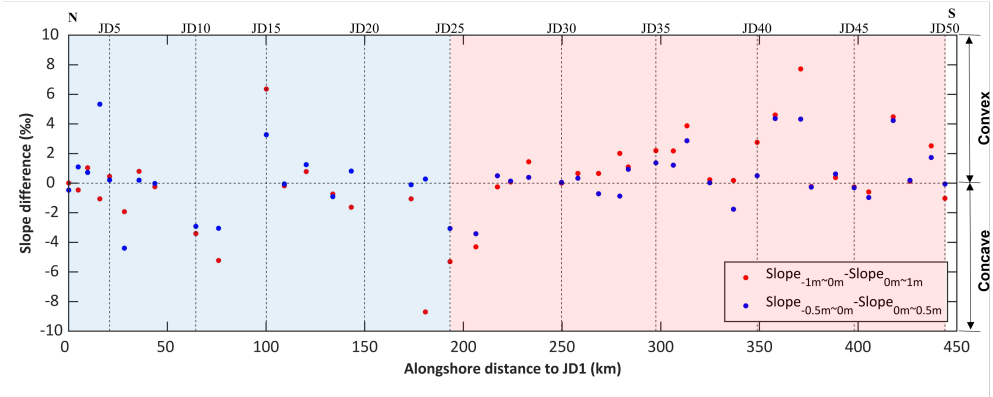


Figure 2.15: Upper and lower intertidal beach slope difference of the 50 profiles calculated with different boundaries.

From this sensitivity analysis, we conclude that the southward flattening beach slope pattern found in this study is not affected by the specific definitions used to derive beach slopes from the field data, nor from the quality of the data itself.

### 2.5.2. EXTREMELY FINE OR COARSE SEDIMENT IN THE NORTH COAST

IN the north part, extremely fine (clay component dominant) or extremely coarse (sand component dominant) sediment are present (Figure 2.9). This fluctuating pattern can be explained by the occurrence of two erosion resistance mechanisms, namely self-weight consolidation and armoring of the beach surface.

Cohesive fine sediment is an important component of the silt-muddy tidal flat and its self-weight consolidation processes (Winterwerp and Van Kesteren, 2004) play a significant role on the tidal flat morphological evolution (Whitehouse et al., 2000a). Consolidation makes the bed material less erodible. Figure 2.9 shows that the grain size of fine sediment in the north Jiangsu Coast can be less than 8Φ, which is in the range of clay. During the long-time formation of the AYRD, the cohesive sediments settled on the delta got enough time to get well consolidated and formed

an erosion resistant layer. Thus, although the north Jiangsu Coast is under erosion, the eroding system ends up at the erosion resistant layer and the upper layer silts are transported southward. This erosion resistance due to consolidation effects has resulted in the presence of fine-sediment hotspots along the north Jiangsu Coast. This mechanism explains the seemingly unexpected phenomenon that sediments at some profiles in the eroding north part can be finer than in the accreting part of the coast.

When the profiles have sufficient coarse sediment available, armoring of the bed surface by suspension of the fines also becomes an important factor limiting erodibility. As it can be seen from Figure 2.9, the bed surface sediment can also be coarse at some profiles, which is the contribution of the sand armoring effect. When the clay content is quite little, the finer components are easier eroded than the coarse ones. Under normal hydrodynamic conditions, the silt components were taken away, and the sand components still remained on the bed, which make the bed surface sediment be coarser – hence more resistant against erosion.

These two erosion resistance mechanisms can explain why the sediments in the eroding north part can be extremely fine or coarse, depending on the local clay content. Also, it indicates that silt is the main components transported southward.

### 2.5.3. ALONGSHORE VARIATION OF INTERTIDAL BEACH SLOPE AND SEDIMENT GRAIN SIZE

THE development of the tidal flat along the Jiangsu Coast is facilitated by three most essential conditions, namely a low-energy environment, sufficient sediment supply and a medium to large tidal range (Allen, 2000; Ren et al., 1984). In addition to the hydrodynamics and sediment sources, human interventions can also influence the beach evolution. These three factors are discussed in the following in order to explain the seemingly strange relation between the grain size and beach slope variations along the coast: southward coarsening and flattening.

#### 2.5.3.1. HYDRODYNAMICS

Tide force is the main driver influencing the sediment erosion and transport processes along the Jiangsu Coast. The tidal range is much larger in the south part than in the north (Figure 2.2b and Figure 2.3). Larger tidal range favors wider flats (Wang and Zhu, 1994). Tidal motion, especially the alongshore tidal current, is consid-

ered to be the main force causing sediment erosion and transport along the Jiangsu Coast. Wang et al. 2019b found that in a wave-absence systems, bed profile and mud content on the upper flat are independent of the alongshore tidal current magnitude. In contrast, the strong alongshore currents can erode mud on the lower flat and promote landward sand transport from the subtidal area to the lower flat, forming a sandy flat. In-situ measurements near Jianggang showed that the mean flood current speed was about 1.4 times of the ebb current speed, and the mean suspended sediment concentration during floods was 1.25 times of that during ebbs (Ren, 1986a; Zhang, 1986). Thus, in the south part, coarser sediments in the subtidal area provided by RSRs tends to be easier transported to the shoreline, and the landward transport process made the sediment on the whole profile coarser. This tide-induced mechanism explains why the southward coarsening pattern is more apparent in the accreting part (i.e. JD25 to JD50).

The wave height is generally lower than 1 m in the RSRs area (Yang et al., 2014), because the RSRs form a natural barrier for the shoreline, dissipating a large amount of wave energy. This provides the sheltered flats in the south part favorable conditions to develop to flatter beach profiles. On wave-dominated beaches, as waves are further dissipated towards the shore line, the maximum dynamics are found near the shoreline and decrease to deeper water. Therefore, the coarsest sediments are found near the shoreline and the sorting is better near the shoreline as well (Gunaratna et al., 2019; Prodger et al., 2017). At the Jiangsu Coast, these three patterns were observed to be opposite, which further indicates that this is a tide-dominated coastline and waves are of secondary importance.

#### 2.5.3.2. SEDIMENT SOURCES

Both in-situ measurements and model simulations proved that the major sediment source for the modern Jiangsu mudflat are the RSRs and AYRD (Zhang et al., 2013; Fu and Zhu, 1986; Ren, 1986a). The width of intertidal zone at equilibrium is positively related to sediment supply, which means higher sediment supply leads to wider and flatter tidal flats (Liu et al., 2011). The southward beach flattening tendency coincides with the shoreline evolution state that the north part of the Jiangsu Coast is eroding while the south part is accreting (Figure 2.2c). This means that the north part is losing sediment forming a sediment source for the south part. The south part can receive sediment supply not only from the eroded north part but

also from the outside RSRs. The large-scale sediment budget the Jiangsu Coast according to model simulations (Yao, 2016) shows that tidal flats south to Jianggang receive more sediment from the RSRs than from AYRD. Towards the south, the intertidal flat has thus more potential sediment supply and can become wider and flatter.

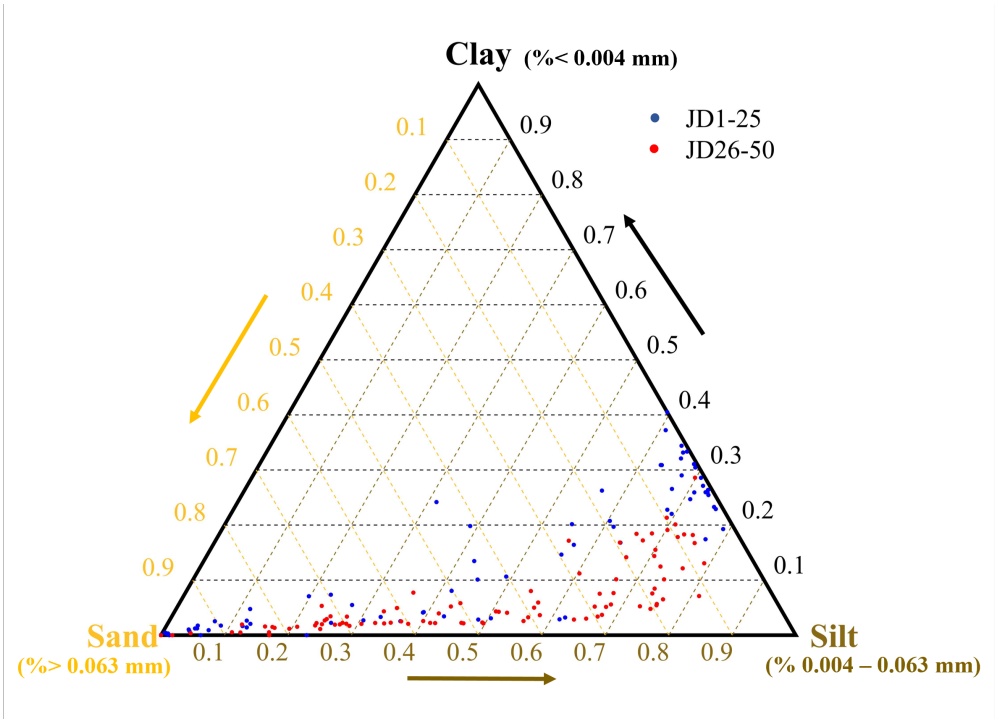


Figure 2.16: Sand-Silt-Clay triangle with two different color scatters, and colors representing different zones.

For the southward coarsening pattern, we consider different sediment sources would also be a main reason contributing to this. In order to further analyze sediment composition in different zones, we plotted the sand-silt-clay triangle (Figure 2.16). Usually, sediment from the same source tends to show a straight band in this triangle (with constant silt-clay ratio) (Van Ledden et al., 2004). For our case, samples at JD26–50 have a turning point around the silt content between 60–80%. This indicates that the sediments in the south part come from different sources. The alongshore sediment mineralogical composition difference further proves that the sediments on the Jiangsu Coast are from different sources (Wang et al., 2017;

Yang et al., 2002). The sediments in the AYRD mainly came from the Yellow River, and sediments from the Paleo-Yangtze River contributed to the formation of the RSRs. Nowadays both the AYRD and RSRs supply sediments to the south Jiangsu tidal flat. The RSRs provided sediments are coarser than the AYRD provided ones. As the south part tends to receive more sediment from the RSRs, the bed surface sediment tends to be coarser.

Studies on the relationship between beach profile and sediment grain size for sandy beaches are all under the premise of equilibrium state (Bujan et al., 2019; Karunarathna et al., 2016; Medina et al., 1994; Work and Dean, 1992; Dean, 1991), although equilibrium concept in coastal environment can be questioned (Zhou et al., 2017). Besides, this conclusion is driven based on a large dataset from different beaches, and we do not know if it also works for different profiles in the same beach. As the century-long erosion of AYRD and RSRs, their sediment supply is reducing (Zhang et al., 2002), which means the evolution of the Jiangsu tidal flats has not been at an equilibrium state. As we only have one time large scale data, we cannot tell the temporal change of the relationship. Will this relationship change as the Jiangsu Coast further evolves and will sediment from different resources further redistribute? We still need numerical models to help us explore the change of this relationship as sediment supply reduces.

#### 2.5.3.3. HUMAN INTERVENTIONS

Apart from natural processes, the beach slope and sediment grain size patterns we found could also be caused by human interventions.

According to previous studies (e.g. Wang et al., 2012a), in an accretionary system affected by land reclamations, the intertidal flat will become narrower and steeper, and the surficial sediment tended to become finer on the mid-upper intertidal flat but coarser on the lower intertidal flat. However, the reclamations taking place in intertidal beaches are mostly located in the south part of the coast (see Figure 2.9 first panel). The observed southward flattening pattern is thus not in accordance with earlier findings by Wang et al. 2012a. Meanwhile, we cannot find the accretion (see Figure 2.12) and finer sediment (Figure 2.9 first panel) near the dyke toe on the reclamation influenced profiles. The bed elevation in front of and behind the new dykes are almost the same (see Figure 2.12, JD 33 and 35). This is mainly because the time of this reclamation are so close to the measurement (Figure 2.10), so that

morphology have not responded to the human interventions yet. From Figure 2.5 we can also see it clearly that the human interventions took place between 2007 and 2008, only several months before the measurement, which means there is limited time for the tidal flat to respond. It partly explains why we find that there is no obvious difference in bed elevation and sediment grain size between in front of and behind the dykes.

In conclusion, the influence of human interventions on the morphological and sedimentological characteristics of the Jiangsu Coast cannot be determined from this dataset, as it was collected too shortly after the implementation of large-scale land reclamation schemes. In order to check the influence of human interventions, more field survey needs to be carried on the temporal variation of tidal flat morphology.

## 2.6. CONCLUSIONS

JIANGSU Coast is a typical tide-dominant open coast with extensive intertidal flats. This study investigates the intertidal beach slopes and surficial sediment grain size distribution pattern, using the high spatial-resolution field data from a large-scale coastal zone investigation. We analyzed the morphology and sediment characteristics of the Jiangsu Coast and found the following features:

1. Intertidal beach slopes are larger in the north eroding part than in the accreting south part. A clear southward flattening pattern can be observed in the accreting south part.

2. The bed surface sediment grain size decreases landward in the cross-shore direction. In the alongshore direction, sediment grain size shows a southward increasing pattern in the south part.

3. Both extremely fine sediment dominant profiles and coarse sands dominant profiles can be found in the north part.

4. Human intervention took place continuously along the Jiangsu Coast. However, its influence on the morphological and sedimentological characteristics of the Jiangsu Coast cannot be determined from this one-time investigation dataset, as it was collected too soon after the implementation of large-scale

land reclamation schemes. More field surveys are needed to further study the tidal flat response to human interventions.



The extremely fine or coarse sediments in the north coast can be explained by two erosion resistance mechanisms, viz. consolidation effect and armoring effect. The southward flattening and coarsening pattern is due to the following factors: flood-dominant current causing landward sediment transport, larger tidal range in the south part, sheltering effect of the RSRs, and contribution of different sediment sources namely AYRD and RSRs. Waves play a minor role in this behavior. Whether the relationship between intertidal beach slope and bed surface sediment size will change when Jiangsu Coast evolution reaches an equilibrium state still remains to be investigated.

# 3

# DIAGNOSTIC MODELLING OF THE SHORELINE VARIATION ALONG THE JIANGSU COAST, CHINA

This chapter is published as Y. Kuai, S.G.J. Aarninkhof and Z.B. Wang (2023). Diagnostic modeling of the shoreline variation along the Jiangsu Coast, China. *Geomorphology* 425, 108581.

**ABSTRACT** Intertidal flats are of great socio-economic and ecological importance in defending the coastal cities from flooding, providing resources for land reclamations and habits for wildlife. On the intertidal flats, milder profiles are usually featured with finer sediment. However, we find the opposite relationship between the alongshore variation in intertidal slope and sediment grain size on the intertidal flat along the Jiangsu Coast. With a conceptual figure of the hydrodynamics and shoreline evolution on this coast, we hypothesize that the unexpected pattern is caused by the alongshore gradient in hydrodynamic forcing. In order to test our hypothesis, we carry out a series of numerical model simulations in a highly schematized manner to investigate the real mechanism behind this unexpected pattern. Through the analysis, we find that only the southwards coarsening pattern is inconsistent with the shoreline evolution pattern. This inconsistency is not induced by alongshore hydrodynamic gradient, and can only be explained by different sediment provenances. We also find that the alongshore shoreline evolution pattern is not only determined by the alongshore gradient in hydrodynamic forcing, but also influenced by the alongshore variation in bed composition. In the erosion/sedimentation transition zone, the bed composition factor plays the major role.

## 3.1. INTRODUCTION

INTERTIDAL flats are normally formed in fine-sediment-rich environment, where tides dominate over wind waves (Gao, 2019; Friedrichs, 2011). The intertidal flats serve as a vital component in land- ocean interactions. They are of great socio-economic and ecological importance in defending the coastal cities from flooding, providing resources for land reclamations and habits for wildlife (Chen et al., 2021; Muller et al., 2020b; Reed et al., 2018). In order to comprehensively manage the coastal engineering and maintain the ecosystem in a more effective and sustainable way, it is crucial to understand the intertidal flat morphodynamics and physical processes.



Tide is considered to be the most dominant force in determining the existence of the intertidal flats (Pritchard et al., 2002; Le Hir et al., 2000). Tidal current can normally be split into a cross-shore component and an alongshore one, and the relative importance of these two components depends on the large-scale circulation around the flat (Le Hir et al., 2000). The cross-shore tidal current is often considered to be responsible for shaping the profile. Therefore, the intertidal flat is usually schematized into a one-dimensional cross-shore profile in previous studies to investigate its morphological and sedimentary characteristics (Zhou et al., 2015; Maan et al., 2015; Liu et al., 2011; Pritchard and Hogg, 2003; Pritchard et al., 2002; Roberts et al., 2000). The contribution of the other natural processes to the evolution of intertidal flats has also been studied, such as wind waves (Zhou et al., 2015; Green and Coco, 2007), and sediment supply (Zhou et al., 2015; Liu et al., 2011). By driving an one-dimensional model with different combinations of tidal range, wave climate and sediment supply, Liu et al. (2011) found that the width of equilibrium intertidal flat is positively related to tidal range with invariant sediment supply, and increasing sediment supply leads to wider intertidal flats. The intertidal flats in straight shorelines exhibit the convex-up shape in the tide-dominant environment and the concave-up shape in case of wave dominance, respectively (Roberts et al., 2000). The intertidal flat sedimentation zonation generally presents a shoreward fining pattern (Kuai et al., 2021; Whitehouse et al., 2000b; Alexander et al., 1991), and this zonation is influenced by the tidal currents, wind waves, sediment properties and sediment supply as well (Zhou et al., 2015).

However, the contribution of alongshore currents to the intertidal sediment trans-

port has also been addressed (Wang et al., 2019b; Gong et al., 2012; Wang, 2006). The alongshore currents enhance the bed shear stress and stimulate the re-suspension of surficial sediments. This alongshore gradient can also lead to the alongshore variation of the intertidal flat morphology and sedimentology.

In our previous field data study (Kuai et al., 2021), we found several morphological and sediment distributions patterns on the Jiangsu Coast, China (Figure 3.1a), a typical tide-dominated muddy open coast with significant alongshore tidal current.



1. In the cross-shore direction, sediment tends to be finer landward in the intertidal zone. The same phenomenon was found at many muddy environment, like the Skeffling mudflat inside the mouth of Humber estuary (Whitehouse et al., 2000b), the northern intertidal flat of the Seine estuary (Le Hir et al., 2000), and the central west coast of Korea (Alexander et al., 1991). This is opposite to wave-dominated sandy beaches where the coarsest sediment is near shoreline (Elfrink and Baldock, 2002).

2. In the alongshore direction:

   (a) The intertidal beach slope in the eroding northern coast is larger than that in the accreting southern coast, and the eroding profiles tend to be concave up and the accreting ones are more convex up. Similar pattern was also observed on the tidal flats in the northern coast of the Gulf of Tonkin, Vietnam (Tong et al., 2020). The tidal flats in the San Francisco Bay were also found to be concave up under erosion conditions, while convex up under sedimentation conditions (Bearman et al., 2010).

   (b) In the accreting southern coast, while tidal flat slopes are generally becoming milder towards the south, the corresponding bed surface sediment grain size is becoming coarser southward (Figure 3.2). This is opposite to the findings on other tidal flats where the milder tidal flats have finer bed materials, like the tidal flats in the San Francisco Bay (Bearman et al., 2010) and the mudflat on the eastern coast of the Ariaka Bay, Japan (Yamada and Kobayashi, 2004).

3. In the eroding northern coast, we found alternating patterns of very fine and coarse sediment (depending on the local clay content). The same pattern

was also found in the Mekong Delta (Gugliotta et al., 2019). This pattern was attributed to the occurrence of two different erosion resistant mechanisms, viz. self-weight consolidation and armoring effect (Figure 3.3), when the flat erodes to an erosion resistant layer (Kuai et al., 2021).



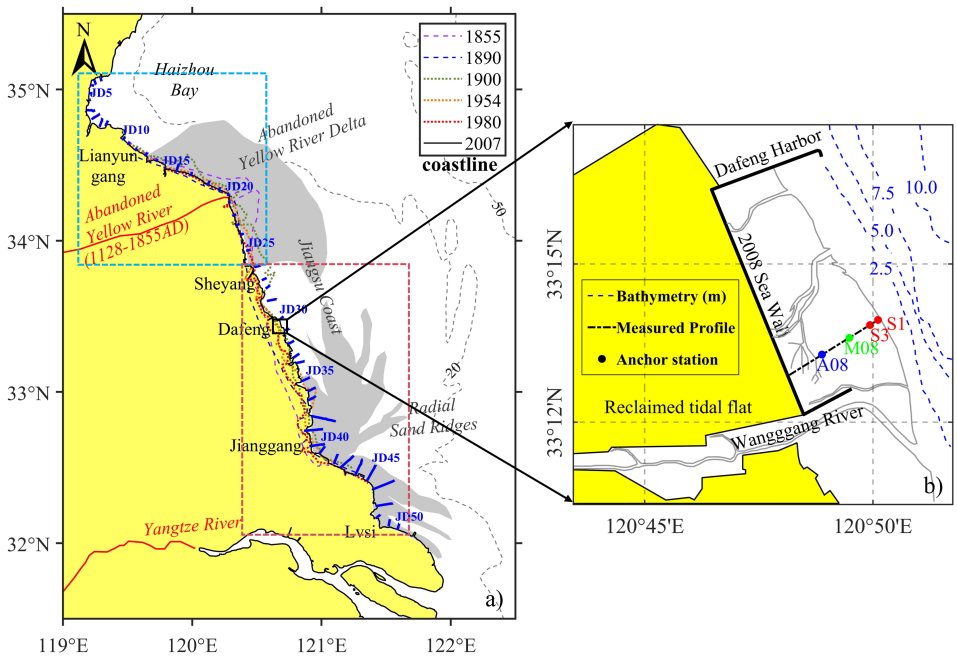


Figure 3.1: Overview of the Jiangsu Coast. a) Shoreline evolution of the Jiangsu Coast (adapted from Su et al. 2017b) and measured profiles location (marked with blue short solid lines). The blue and red dash rectangular indicate the eroding northern and accreting southern coast, respectively. b) The site of field measurements in Dafeng in 2008: A08, M08, and S1/S3 are anchor stations for hydrodynamic and sediment concentration measurements (adapted from Wang et al. 2012a)

The observed morphological and sediment distribution patterns on the Jiangsu Coast are similar to other tide-dominant muddy flats, except the relationship between alongshore beach slope variation and sediment grain size pattern, which is totally opposite to these flats. This paper is aimed to explain the mechanism behind the alongshore variation of beach slope and remarkable sediment grain size along the Jiangsu intertidal flats. To that end, we formulate a conceptual figure with special focus on describing the alongshore variations in hydrodynamics and shoreline evolution pattern. Based on the conceptual figure, a highly schematized Delft3D

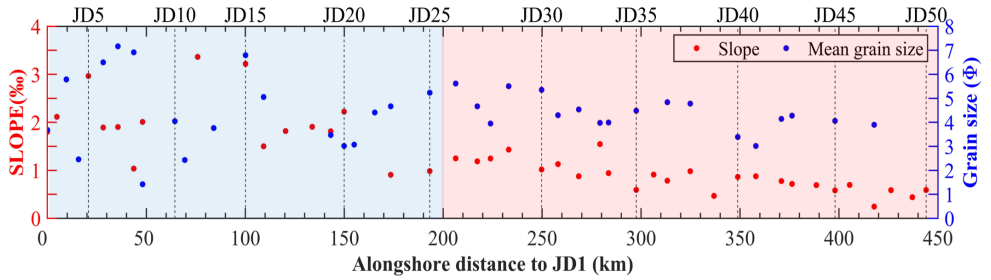


Figure 3.2: Alongshore distribution of intertidal beach slope and mean grain size of the surficial sediments. Blue and red shades indicate the eroding and accreting part of the coast as shown in Figure 3.1. Dash lines represent the location of every 5 measured profiles.

numerical model is set up, with which we investigate the sediment transport pattern at different alongshore transects driven by tides and waves. By comparing the sediment transport rates along different transects, we get the erosion/sedimentation pattern in-between these transects and validate that with the shoreline evolution history. With further analysis of simulated sediment transport pattern of different fractions, we deepen our insight into the mechanisms that can explain the observed alongshore distribution of sediment grain sizes at the intertidal beach.

## 3.2. METHODS

### 3.2.1. CONCEPTUAL FIGURE OF THE JIANGSU COAST

KUAI et al. (2021) provides a detailed overview of the hydrodynamics and morphology of the Jiangsu Coast. Based on those findings, we formulate a conceptual figure that breaks up the Jiangsu coast in four different sections, namely P1–P4, characterized by similar shoreline evolution and hydrodynamics (Figure 3.3). P1 is near the top of the Abandoned Yellow River Delta (AYRD), P2 is near the transition boundary between erosion and accretion shoreline, P3 is at the north part of the sheltered coast and P4 is near the central of the Radial Sand Ridges (RSRs). The northern Jiangsu coast is under erosion while the southern part is still accreting. Meanwhile the transition boundary between the two parts is gradually moving southwards (Zhang et al., 2002). The eroded fine sediment from the north part partly transports along the coastline towards the south and eventually settles there.

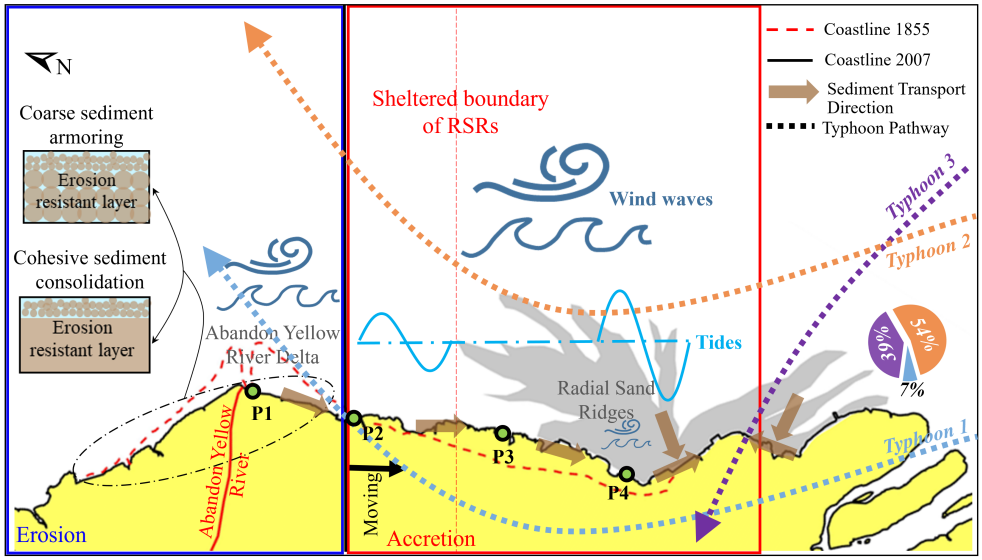


Figure 3.3: A conceptual figure of the Jiangsu Coast dynamic processes including shoreline evolution, general nearshore sediment transport direction of the Jiangsu coast, tidal amplitude distribution, wind waves sheltering conditions and ~50 years (1949–2007) typhoon pathways and frequency (pie chart).

Apart from the feeding from the northern coast, the intertidal beach on the southern coast also has great sediment exchange with the offshore RSRs. The tidal wave propagates parallel to the coastline in the nearshore zone. The mean tidal range increases from ~2 m at the AYRD to ~6 m near the center of the RSRs (Wang et al., 2019a). Due to the sheltering effect of the RSRs, the wave energy in the sheltered zone is smaller than that in the exposed area. Overall, according to the ~50 years meteorological record (from 1949 to 2007), there are 76 typhoons that influenced the Jiangsu Coast, of which only 5 (~7%) landed on the Jiangsu Coast or the Yangtze Estuary (Typhoon1 in Figure 3.3). On the one hand, the frequency of storm surges can be considered minor compared to the continuous sediment reworking by tidal currents and normal wind waves; On the other hand, they usually only last 1-2 days with a maximum significant wave height of ~2 m at the nearshore zone (Gong et al., 2019a) and the tidal flats are under a 'storm surges destroy - tidal currents restore' cycle (Gong et al., 2019b; Zhang et al., 1999). According to the existing model study (Pu et al., 2022), the net sediment transport caused by the northerly winds (representing winter storms) is comparable to that of the southerly winds (representing

typhoons). Therefore, although winter storms and typhoons can drive massive sediment transport in a short period, their contribution to annual sediment transport is limited. In this study, we focus on the annual evolution of the beach, and the temporal influence of storm surges is not investigated in line with other studies (Xu et al., 2016; Xing et al., 2012).



Based on this conceptual figure, we hypothesize that the observed alongshore variations in morphology and sedimentology (southward flattening of beach slopes, and coarsening of sediment grain size) can be explained by alongshore gradients in hydrodynamic forcing (variations in tidal amplitude, alongshore vertical tide phase variation, and wave sheltering in lee side of RSRs). We will test these hypotheses with a simple, 1D process-based model applied to a few characteristic, cross-shore transects along the Jiangsu coast.

### 3.2.2. NUMERICAL MODEL

In order to investigate the impact of alongshore variations in the hydrodynamic forcing, we carry out morphological simulations for different, representative parts of the coastline. We do so with a highly schematized model using the Delft3D software (Lesser et al., 2004), assuming hydrodynamic processes (tides, waves) to be uniform within a short distance alongshore (~10 km). Under this assumption, the coast is divided into several sections, namely P1–P4 in the conceptual figure (Figure 3.3), based on the local hydrodynamic conditions (in terms of tidal amplitude, alongshore vertical tidal phase variation and wave climate). Each section is schematized with a rectangular domain and an alongshore uniform initial bathymetry. These sections have different initial intertidal slope and the same initial bed sediment composition.

The model domain is 10 km in both cross-shore and alongshore directions (Figure 3.4). The grid size is 100 m in cross-shore direction and 400 m in alongshore direction. The initial bed elevation is set to be 2.5 m above Mean Sea Level (MSL) at the landward end of the model and linearly decreases to the seaward end based on the local intertidal beach slope. The threshold depths for drying / flooding and sediment transport computing are both set to be 0.05 m. A uniform Chezy coefficient of 65 $m^{1/2}s^{-1}$ is applied throughout the whole domain.

Three open boundaries are set, namely north, south and sea boundary. Since

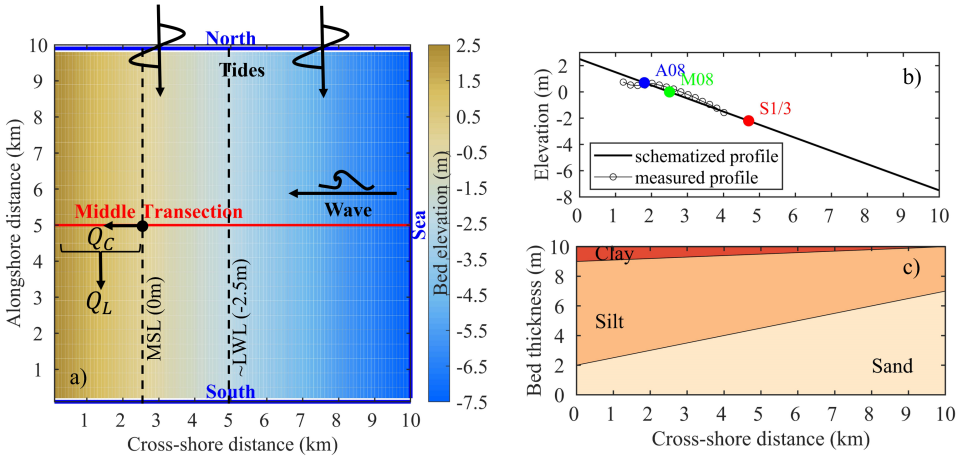


Figure 3.4: Numerical model scheme set up. a) Grid and initial bathymetry of the schematized model (Middle transection is chosen as the monitoring profile; Three open boundaries are marked with blue solid lines; The mean sea level is set to be 0 m in this model). b) Measured and schematized cross-shore profile, and the location of monitoring points. c) Initial bed composition of the Dafeng validation case based on the measured data from Wang et al. 2012a.

the purpose of the model is to compare the different transects, not to reproduce the accurate morphological evolution on each transect, we neglect the spring-neap variation in the tidal signal. we simplify the tidal signals into the $M_2$ harmonic (as it is the most dominant harmonic in this region) to represent the mean tidal amplitudes at different locations. The $M_4$ harmonic is also added in the model to represent tidal asymmetry. The $M_2$ and $M_4$ tides with a phase difference ($2\phi M_2 - \phi M_4$) of $-142°$ are prescribed at the lateral boundaries (North and South boundaries). Their amplitude and alongshore phase variation are set according to different local conditions. A Neumann boundary condition (Roelvink et al., 2004) viz. zero cross-shore water level gradient is imposed at the seaward boundary.

Due to refraction, waves tend to be more or less perpendicular to the coastline when approaching the shallow zone. In the model, the wave is assumed to normally incident along the sea boundary with stationary wave parameters which are determined by the local situations and represent the year-round wave condition. A stationary wind field of 5 m/s is set to maintain the wave energy when it propagates landwards. The wind wave is online coupled with the flow during the simulation. There are only two nearshore wave stations along the Jiangsu coast (i.e., Lianyu-

gang station and Lvsi station, see Figure 3.6e), which are insufficient to represent the wind/wave climate of the whole domain. Therefore, we consider the wave effect in a schematic manner, i.e., extracting the significant wave height for the schematized model from a large-scale model, which is driven by stationary wind and wave conditions.



Table 3.1: Sediment properties in the model setting ($\rho_D$ is the dry bed density, $T_{cr}$ is the critical bed shear stress for erosion, $W_0$ and $W_s$ are the fresh and saline settling velocity respectively, $M$ is the erosion parameter and $D_{50}$ is the medium grain diameter)

| **Sediment ID** | $\rho_D$ (kg/m$^3$) | $T_{cr}$ (Pa) | $W_0$ (mm/s) | $W_s$ (mm/s) | $M$ (kg/m$^2$/s) | $D_{50}$ ($\mu$m) |
|---|---|---|---|---|---|---|
| Clay | 1000 | 0.1 | 0.1 | 0.5 | 0.0002 | 0.5 |
| Silt | 1000 | 0.2 | 0.2 | 0.5 | 0.0002 | 25 |
| Sand | 1600 | – | – | – | – | 100 |

The bed material is schematized into three sediment fractions, namely clay, silt and sand. The clay and silt are treated as cohesive sediment and the sand is treated as non-cohesive sediment, and the sediment property parameters are listed in Table 4.1. The widely adopted Partheniades-Krone formulations (Partheniades, 1965) and Engelund-Hansen formulations (Engelund and Hansen, 1967) are used for cohesive and non-cohesive sediment respectively. Because there is no such measured data introducing the detailed Suspended Sediment Concentration (SSC) of each sediment fraction along a cross-shore profile at different alongshore locations, it is difficult to get the accurate SSC boundary conditions for different alongshore location. The general measured cross-shore SSC distribution pattern at the Jiangsu Coast shows that the SSC can reach more than 1 kg/m$^3$ on the tidal flat and decreases to less than 0.5 kg/m$^3$ at 20 km offshore (Wang et al., 2019b; Xu et al., 2016; Ren, 1986a). In our model, we set the boundary SSC the same value for different locations. On lateral boundaries, the SSC is set to decrease linearly from 1.25 kg/m$^3$ at the landward edge to 0.75 kg/m$^3$ at the seaward end. The ratio between SSC of clay and silt is 1:4. The initial bed is composed of 10 m well mixed sediments, and the detailed composition of each fraction adopts an existing filed data set collected on the intertidal flat in Dafeng (Wang et al., 2012a, Figure 3.1b). According to this observation data, from landward end to seaward end, the clay proportion is decreasing from 10% to 0%, the silt proportion is decreasing from 70% to 30%, while the sand proportion is increasing from 20% to 70% (Figure 3.4c).

In order to test the reliability of the simplified model scheme as regards to hy-

drodynamics and sediment transport processes, we compare model results to the existing field data set in Dafeng (Wang et al., 2012a). In the verification run, we drive the model with tide and wave signals measured in Dafeng. The $M_2$ and $M_4$ tides are set to be 2 m and 0.2 m in amplitude, and the significant wave height and wave period are set to be 0.3 m and 2.5 s, respectively. Then we compare the model results between different sections (P1–P4), and the hydrodynamic parameters for these sections are described in Section 3.2.4.



### 3.2.3. MODEL VERIFICATION

THE purpose of the model is to compare the sediment transport pattern between different transects. Therefore, the model needs to reproduce reliable sediment

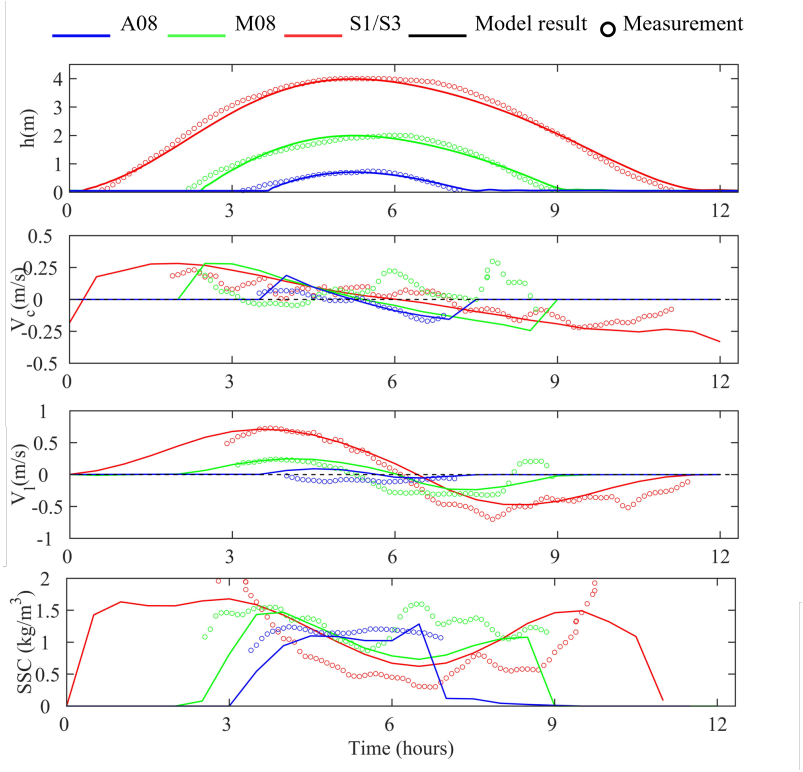


Figure 3.5: Measured (circles) and modelled (solid lines) time series of water depth, depth-averaged velocity, and suspended sediment concentration measured at the upper (A08, blue line), middle (M08, green line), and lower (S1/S3, red line) intertidal flat. $V_c$ and $V_l$ are the current velocity components across (offshore [ebb] "−" and onshore [flood] "+") and along (northward [ebb] "−" and southward [flood] "+") the intertidal flat, respectively.

transport processes. We compare the simulated time series of water depth, cross-shore and alongshore depth-averaged velocities and SSC with the measurement in Dafeng. Three observation points namely A08, M08 and S1/S3 are selected on the central profile of the model domain (Figure 3.4b), representing the upper, middle, and lower intertidal flat, respectively, which is consistent with the field measurement in Dafeng (Figure 3.1b).



The simulated variation of water depth agrees well with the measurement (Figure 3.5). Since the measured variations are rather noisy due to the shallow water depth, our model adopts a simplified initial bathymetry and takes only two tidal components into account. It is difficult to compare the exact temporal variations of cross-shore velocity ($V_c$), alongshore velocity ($V_l$) and SSC between the simulated and measured results in a strictly point-by-point manner. Despite the model is highly simplified, the measured and simulated magnitudes of $V_c$, $V_l$ and SSC match well with each other. As it can be seen from Figure 3.5, the simulated peak flood/ebb velocity magnitude, flood/ebb duration, and maximum SSC agree well with the measured data. The verification results demonstrate that such model is capable of reproducing reliable sediment transport processes.

### 3.2.4. HYDRODYNAMIC PARAMETERS

We couple the wind and wave to a well-validated Jiangsu Region tide model (Yao et al., 2018). The wind considered in the model is simplified with a NE–E direction and a speed of 4.5-–5 m/s, which is similar to the existing model study (Su et al., 2017b). The boundary wave force is set with a mean significant wave height of 1 m and mean period of 5 s to represent the yearly average situation, following the previous study (Chen et al., 2013).

The tidal amplitude, alongshore phase gradient and significant wave height at the seaward end of each measured profile (location see Figure 3.1) are extracted from the coupled Jiangsu Region tide and wave model results (Figure 3.7). As it can be seen from Figure 3.7, from JD 20 to JD40, the $M_2$ tidal amplitude shows an increasing pattern, while its alongshore phase gradient shows a decreasing trend. The significant wave height slightly increases from JD20 to JD30, and then dramatically decreases southwards due to the sheltering effect of the RSRs (Figure 3.7b). The wave is getting perpendicular to the shoreline when it is approaching the shallower

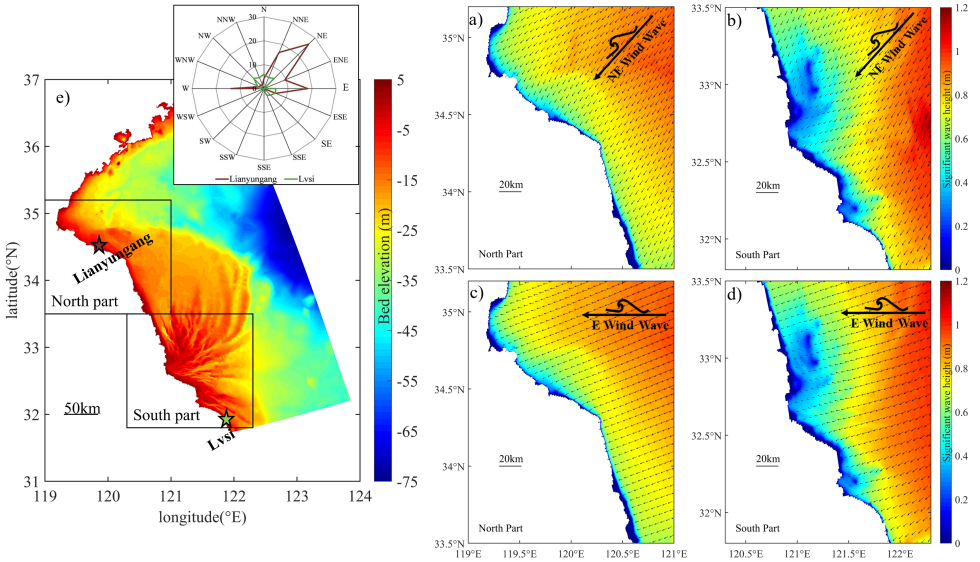


Figure 3.6: Simulated wave energy distribution with different incident wind wave directions. a) and b) represent the results of NE incident wind wave. c) and d) represent the results of E incident wind wave. The colors indicate the significant wave height, and the arrows denote the mean wave direction. e) indicates the bathymetry of the modelled domain, and the frequency distribution of wave directions at two stations: Lianyungang (in red) and Lvsi (in green). Different circles denote different levels of concurrency frequency.

Table 3.2: Tide, wave and initial slope conditions for different scenarios.

| Scenario ID | Tidal boundary | | Wave condition | | Profile condition |
|---|---|---|---|---|---|
| | Amplitude (m) | Phase difference (°) | Tp (s) | Hsig (m) | Slope (‰) |
| P1 | $M_2$: 0.83<br>$M_4$: 0.17 | $M_2$: 11.75<br>$M_4$: 9.68 | 3.0 | 0.52 | 2.0 |
| P2 | $M_2$: 1.15<br>$M_4$: 0.18 | $M_2$: 7.65<br>$M_4$: 11.90 | 2.9 | 0.58 | 1.2 |
| P3 | $M_2$: 1.74<br>$M_4$: 0.20 | $M_2$: 5.40<br>$M_4$: 11.26 | 2.7 | 0.40 | 1.0 |
| P4 | $M_2$: 1.92<br>$M_4$: 0.39 | $M_2$: 4.05<br>$M_4$: 16.11 | 2.0 | 0.18 | 0.9 |

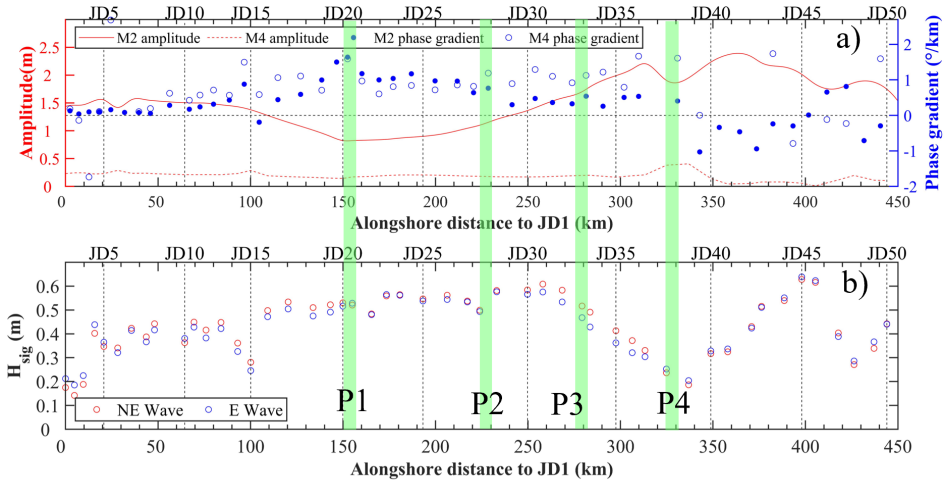


Figure 3.7: a) Alongshore distribution of $M_2$ and $M_4$ tide properties derived from the Fourier analysis of a large scale Jiangsu Coast tide model (Yao, 2016). The red lines indicate the amplitude and the blue dots and circles indicate the alongshore tidal phase gradient. b) Alongshore distribution of the significant wave height at seaward end of each measured profile. Red circles represent the result of NE wind waves and the blue circles represent the results of E wind waves. Green bars indicate the profile data adapted for scenario (namely P1–P4) simulations.

zone (Figure 3.6), which is consistent with the wave setting in our schematized model. The detailed hydrodynamic setting of the scenarios is shown in Table 4.2.

## 3.3. RESULTS

### 3.3.1. SIMULATED SEDIMENT TRANSPORT AND SHORELINE EVOLUTION PATTERN

WE calculate the net cross-shore ($Q_C$) and alongshore ($Q_L$) sediment transport rates during one $M_2$ tidal cycle after 30 tidal cycles (Figure 3.8). The $Q_C$ is the tidal averaged cross-shore sediment transport rate at a certain depth, which means the net cross-shore sediment transport tendency at a certain point during one $M_2$ tidal cycle. The $Q_L$ is the tidal averaged alongshore sediment transport rate integrated from a certain depth to the most landward point, which means the net alongshore sediment transport tendency above a certain point during one $M_2$ tidal cycle (Figure 3.4a). It can be seen from Figure 3.8 that the $Q_L$ is one order larger

than the $Q_C$ near the low water line (-2.5 m), while their magnitudes are similar at the mean sea level (0 m). This is mainly because the coast is an alongshore current dominant one, and the alongshore current is dominant over the cross-shore one in the lower intertidal flat. However, in the upper intertidal flat, the alongshore current is weak due to the limited water depth, and the current in two directions are of similar magnitude (see Figure 3.5). This is consistent with other research on alongshore tidal current dominated flat (Wang et al., 2019b; Gong et al., 2012; Wang, 2006). We also found that the sediment transport rate near the low water line is more than one order larger as compared to that at the mean sea level. This is because the alongshore tidal currents are much larger at deeper water and waves are only of secondary importance.



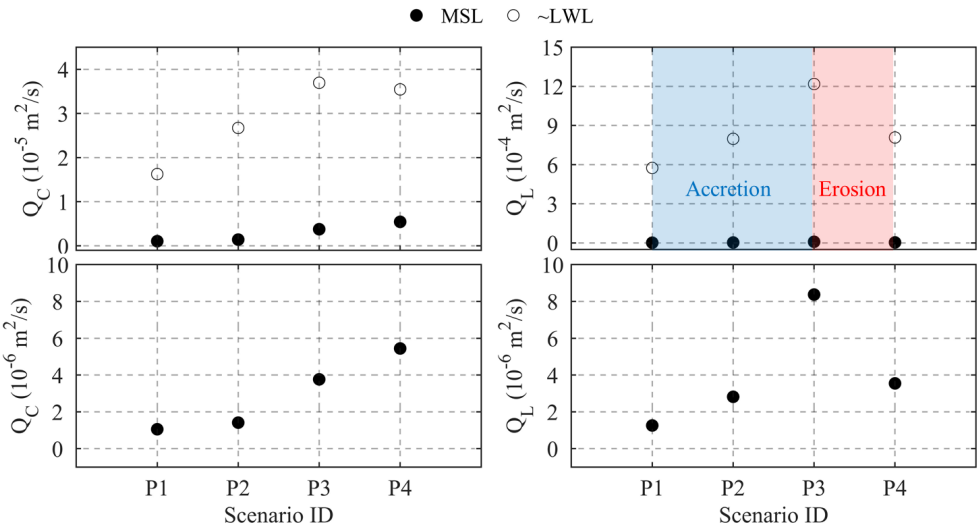


Figure 3.8: Simulated net suspended sediment transport rate during one $M_2$ tidal cycle, the left panels are the cross-shore component (positive value means onshore transport), and the right panels are the alongshore component (positive means southward transport). The lower two panels are zoom in on the upper panels in the range of $0 \sim 10 \times 10^{-6}\,m^2/s$. Black dots represent the results calculated at mean sea level (0 m in the model domain), and black circles represent the results calculated near the low water line (-2.5 m in the model domain).

The simulated net onshore sediment transport rate generally shows a southward increasing pattern, except for the slightly decreasing trend between P3 and P4 (Figure 3.8). This is because the tidal range increases towards the south in this tide-dominant environment. Although wave is only of secondary importance, the

sheltering effect of the RSRs makes the wave dynamic much weaker in P4 than it in P3 (Table 4.2). In P3, the enhanced bed shear stress by waves leads to more resuspension and hence larger sediment transport rate. The southward increasing net onshore transport pattern indicates that more sedimentation on the intertidal flat to the south by cross-shore sediment transport. However, its magnitude is much smaller compared to the alongshore sediment transport induced shoreline evolution.



The simulated net alongshore sediment transport rate shows an increasing trend from P1 to P3, and a decreasing trend from P3 to P4 (Figure 3.8). By looking at the gradient of the alongshore sediment transport between these four sections, we can get the shoreline evolution tendency in-between these sections. The coastline is experiencing severe erosion between P1 and P2, P2 and P3, and notable accretion between P3 and P4. This pattern is not fully consistent with the shoreline evolution history (Figure 3.3). In the conceptual figure, P2 is chosen near the erosion and deposition boundary of the coastline, which means the coastline between P2 and P3 should be experiencing mild sedimentation.

The inconsistency of the shoreline evolution condition between P2 and P3 proves that we cannot get the proper alongshore pattern of morphological changes by only taking the alongshore gradient in hydrodynamic forcing into account. We discuss the influence of initial bed composition setting on model results in Section 3.3.3.

### 3.3.2. SIMULATED TRANSPORT OF DIFFERENT SEDIMENT COMPOSITIONS

IN order to interpret the sediment grain size alongshore variation pattern, we further calculate the contribution of each sediment fraction to the total net cross-shore and alongshore transport. The transport proportions of each fraction are listed in Tables 3.3 and 3.4. By comparing the transport of each fraction between different sections, we investigate how the bed grain size evolves under the alongshore varying hydrodynamic forcing.

As it can be seen from the Tables 3.3 and 3.4, the net cross-shore transport rate proportion of each sediment fraction (clay, silt and sand) keeps more or less the same among different transects. The alongshore difference of the net cross-shore transport rate proportion is less than 0.5%. As a consequence, the cross-shore transport process is considered to be minor importance to the observed alongshore vari-

Table 3.3: Net sediment transport rate proportion of each fraction at 0 m.

| Mean sea level | Sediment ID | Transport rate proportion (%) | | | |
|---|---|---|---|---|---|
| | | P1 | P2 | P3 | P4 |
| Cross-shore | Clay | 19.55 | 19.62 | 19.55 | 19.37 |
| | Silt | 80.40 | 80.28 | 80.28 | 80.38 |
| | Sand | 0.05 | 0.10 | 0.17 | 0.25 |
| Alongshore | Clay | 23.38 | 22.45 | 21.50 | 17.90 |
| | Silt | 76.57 | 77.50 | 78.43 | 81.94 |
| | Sand | 0.06 | 0.05 | 0.06 | 0.16 |

Table 3.4: Net sediment transport rate proportion of each fraction at -2.5 m.

| Low water line | Sediment ID | Transport rate proportion (%) | | | |
|---|---|---|---|---|---|
| | | P1 | P2 | P3 | P4 |
| Cross-shore | Clay | 18.77 | 18.38 | 17.01 | 17.11 |
| | Silt | 80.59 | 81.02 | 82.21 | 81.78 |
| | Sand | 0.64 | 0.60 | 0.78 | 1.11 |
| Alongshore | Clay | 21.40 | 21.34 | 19.68 | 18.46 |
| | Silt | 78.16 | 78.30 | 79.95 | 80.93 |
| | Sand | 0.44 | 0.36 | 0.37 | 0.61 |

ation in sediment grain size.

In the alongshore direction, the alongshore variation of the relative contribution of these three sediment fractions shows similar pattern to the cross-shore transport. However, difference between transects is much larger, especially near the mean sea level. Towards the south, the relative contribution of the fine material (clay) to the net southward alongshore sediment transport is decreasing around 5%, while the relative contribution of the coarser materials (silt or sand) is increasing. This variation pattern suggests the north profiles tend to be coarser while the south ones tend to be finer, which is totally opposite to our observations.

With the same initial bed composition setting, we cannot derive the observed southward coarsening pattern under the alongshore hydrodynamic variation. Apparently, the hydrodynamics alongshore gradient are not the main mechanism leading to the alongshore sediment grain size distribution pattern on the Jiangsu Coast.

We further discuss the mechanism behind this phenomenon in Section 3.4.3

### 3.3.3. COMPARISON BETWEEN THE DIFFERENT INITIAL BED COMPOSITION SETTINGS

SINCE we consider the alongshore variations in morphology and sedimentology are determined by the alongshore gradient in hydrodynamic forcing, we applied the same initial bed sediment compositions for all the four sections in the previous simulations. It turns out that neither the derived shoreline evolution nor alongshore sediment grain size distribution pattern matches the measured ones. In order to arrive at a good match, we take the variation of initial bed material composition into consideration in the following simulations. In the previous field data study (Kuai et al., 2021), we have the bed sediment samples data about every 500 m along each measured profile (Figure 3.1). In the following simulation, we linearly interpolate the proportion of sand, silt and clay from landward end to seaward end in the model domain (Tables 3.5) according to this measured dataset.

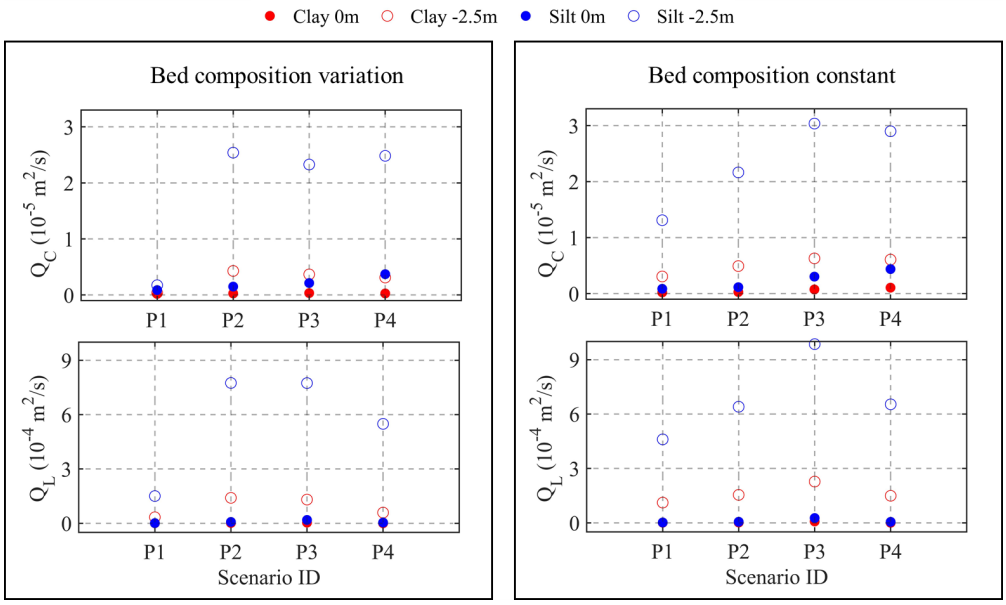


Figure 3.9: Modeled net suspended sediment transport rate during one tidal cycle. The left panel shows results with bed composition applying measured data, and the right panel shows results with the same bed composition for all profiles.

We compare the simulated net sediment transport rate between the initial vary-

Table 3.5: Initial bed compositions (according to field data) for different scenarios.

| Scenario ID | Bed fraction land to sea (%) | | |
|---|---|---|---|
| | Sand | Silt | Clay |
| P1 | 50–80 | 45–20 | 5–0 |
| P2 | 10–50 | 80–50 | 10–0 |
| P3 | 35–80 | 60–20 | 5–0 |
| P4 | 43–90 | 55–10 | 2–0 |



ing and constant bed composition runs. As the sand transport proportion is quite small compared to the clay and silt fraction (about 1–2 orders smaller than the other two fractions, see Tables 3.3 and 3.4), we only present the difference of the clay and silt transport rate between different transects (Figure 3.9). As it can be seen from the figure, the initial bed composition does have a great impact on the net sediment transport pattern. There is a remarkable difference of the relative net sediment transport magnitude between these two bed composition settings between the P2 and P3. By considering the bed composition variation, we get a slightly decreasing trend of the net alongshore sediment transport rate between P2 and P3, which matches well with the measured mild sedimentation condition in this part of the coast. In the bed composition variation run, the initial bed composition reflects the southward coarsening pattern between P2 and P4, which is more obvious between P2 and P3 (Table 3.5). Due to the increase in sand composition and decrease in silt and clay compositions from P2 to P3, the net total sediment transport rate decreases as well. Sand particles are more difficult to start into motion as compared to silt and clay, and silt and clay have a larger net transport rate due to the scour and settling lag effect.

The relative net sediment transport magnitudes between P1 and P2, P3 and P4 are similar in these two bed composition settings. Considering the bed composition variation, we find that cross-shore transport rate between P2 and P4 has minor difference, which further indicated that it is mainly alongshore gradient in alongshore sediment transport rate leading to the shoreline erosion/sedimentation evolution on this coast.

As a conclusion, the alongshore gradient in hydrodynamic forcing is not the

only mechanism forming the alongshore morphology variation, especially for the erosion/sedimentation (P2 and P3) transition part of the coast. The bed sediment composition is also a very important factor in determining the shoreline evolution condition. We can only derive the right shoreline evolution pattern by applying the bed composition variation in the simulation. It is very important to take the bed composition into consideration, if we want to reproduce large spatial scale shoreline evolution condition with numerical model.



## 3.4. DISCUSSIONS

### 3.4.1. SENSITIVITY TEST OF THE SSC BOUNDARY CONDITION

IN our models we apply the same SSC boundaries for different scenarios. In reality, the yearly mean SSC is different at different alongshore locations, and its cross-shore distribution and composition are varying as well. These are influenced by many factors, like the large-scale, non-equilibrium background sediment supply, local topography and hydrodynamics. In our study we only investigate the sediment transport pattern in the middle profile of the model, and make the model domain large enough to eliminate the influence from the boundary SSC condition. The adaptation length-scale of the SSC (viz. the influenced distance by the boundary) is typically defined as a function of the water depth times the flow velocity divided by the sediment settling velocity (Galappatti et al., 1986). For our model settings, the adaptation length-scale of the SSC is about 5 km near the low water line, and smaller in the intertidal zone. As a result, the 10 km horizontal length is considered large enough to minimize the boundary influence and computation time.

In order to test the sensitivity of the modelled net sediment transport rate to the SSC boundary condition, we set up two extra test scenarios. The first one is the High SSC case, which takes the same SSC boundary conditions as the measured data in Dafeng, i.e. the SSC is set to decrease linearly from 1.25 kg/m$^3$ at the landward edge to 0.75 kg/m$^3$ at the seaward end. The ratio between SSC of clay and silt is 1:4. The second one is the Low SSC case, in which the SSC is only half as compared to the High SSC case, i.e. the SSC is set to decrease linearly from 0.625 kg/m$^3$ at the landward edge to 0.375 kg/m$^3$ at the seaward end. The other model settings of these two cases are the same as the Dafeng case. After letting the model run for

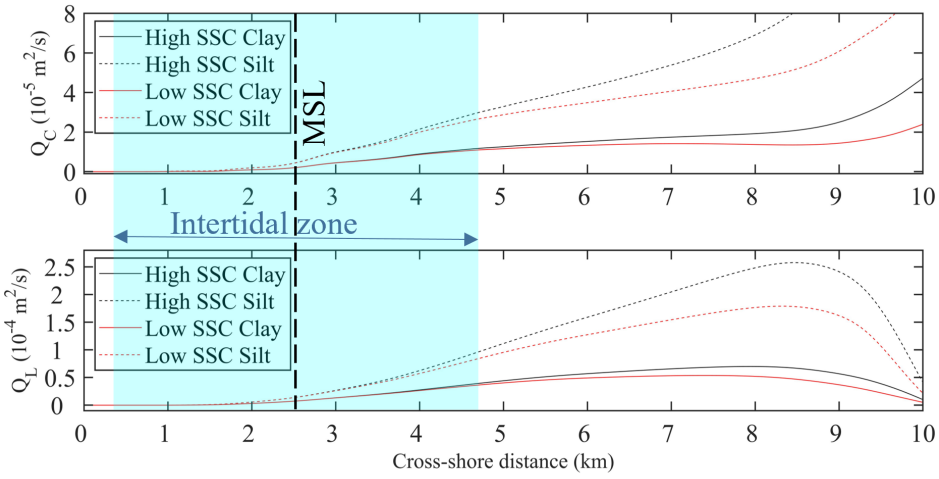


Figure 3.10: Sensitivity of the sediment transport rate to the SSC boundary conditions. Light blue shadow marks the intertidal location, vertical black dash line indicates the location of mean seal level.

30 $M_2$ tidal cycles (long enough to get the stable sediment transport in the whole model domain), we calculate the net sediment transport rate during one $M_2$ tidal cycle along the central profile in these two cases (Figure 3.10).

Table 3.6: Net sediment transport rate with different boundary SSC condition setting (Δ is the difference compared to the High SSC scenario)

| Scenario ID | **MSL** | | | | **LWL** | | | |
|---|---|---|---|---|---|---|---|---|
| | Cross-shore | | Alongshore | | Cross-shore | | Alongshore | |
| | $Q_C$ (m$^2$/s) | Δ (%) | $Q_L$ (m$^2$/s) | Δ (%) | $Q_C$ (m$^2$/s) | Δ (%) | $Q_L$ (m$^2$/s) | Δ (%) |
| **High SSC** | -5.63E-06 | 0.00 | -9.71E-05 | 0.00 | -4.53E-05 | 0.00 | -2.11E-03 | 0.00 |
| **Low SSC** | -5.59E-06 | -0.86 | -9.73E-05 | 0.18 | -4.03E-05 | -10.90 | -1.95E-03 | -7.43 |

Figure 3.10 shows that the difference in SSC boundary does influence the sediment transport rate in the offshore zones. However, its influence gradually becomes negligible when it comes to the intertidal zones (see also Table 3.6). The variation of net sediment transport rate is about 10% in the low water line, which is much smaller as compared to the fluctuations in the boundary SSC with a factor of 2. On the other hand, in this study we focus on the alongshore gradient of the net sediment transport rate, and this 10% difference is small as it compared to the alongshore difference in sediment transport rate. So we may consider the sediment

transport rate in the area of interest is not sensitive to the boundary SSC condition, as long as the model domain is large enough (in our case the 10 km), and interested area is far enough from the boundary. In other words, the variation of alongshore sediment transport rates as a result of changes in the hydrodynamic forcing, beach slope and bed composition are not affected by the assumed SSC at the model boundaries.



### 3.4.2. THE MECHANISM BEHIND THE SOUTHWARD COARSENING PATTERN

We hypothesized that the southward coarsening pattern could be caused by the alongshore hydrodynamic gradient. To prove this hypothesis, we calculated the net transport rate of different sediment fractions by setting constant bed composition at different profiles. From the simulated net sediment transport pattern with constant bed composition, we can find that the relative contribution of fine sediment to the net southwards transport is larger in the north as compared to the south. This behavior can be explain by the selective erosion, transport and deposition processes. When the eroded sediments from the northern coast are transporting southwards, the coarser fractions will gradually deposit alongshore first. The finer fractions can be transported a longer distance, and finally reach further southward. Our model proves that under the alongshore gradient in hydrodynamic forcing, the north part is getting coarser while the south part is getting finer, which means there must be another mechanism leading to the observed pattern.

By focusing on the formation of the Jiangsu Coast, we find that the sediment provenance is the main mechanism behind the southward coarsening pattern. Historically, the Jiangsu Coast was mainly fed by the sediment from two large rivers, i.e. the paleo-Yangtze River during the end of the late Pleistocene (Wang et al., 1999), and the Old Yellow River in the most recent period from 1128-1855 AD (Gao, 2009). The sediment supplied by the paleo-Yangtze River is found coarser as compared to the Old Yellow River (Wang et al., 2017; Yang et al., 2002). So, initially the sediment on the south part of the Jiangsu Coast was coarser than it in the north.

Nowadays, the suspended sediment along the Jiangsu Coast is mainly from the bed erosion, rather than fluvial supply (Zhou et al., 2014). According to a detailed sediment transport model study (Yao et al., 2018),the eroded sediment from the AYRD and offshore RSRs are currently the main sediment source for the nearshore

zone of the Jiangsu Coast. Although the sediment sources of the RSRs are debatable (Chen et al., 2013), some geological measurement results (e.g., Wang et al., 2012b; Yang et al., 2002) show that the RSRs have coarser materials as compared to the AYRD. From our model results, we find that the net onshore sediment transport rate near the low water line in the south profiles is larger as compared to that in the north profiles. This means the offshore RSRs continuously serve as a sediment source for the intertidal flat on the sheltered coast, and the southwards coarsening pattern can be maintained.



As a conclusion, our model proves that this southward coarsening pattern cannot be generated or maintained by the alongshore variation of the hydrodynamics, instead it is caused by the different sediment provenance, viz the Old Yellow River and paleo-Yangtze River in the history, and the AYRD and offshore RSRs in the present.

### 3.4.3. THE MECHANISM BEHIND THE SOUTHWARD FLATTENING PATTERN

BY looking at the conceptual figure of the Jiangsu Coast (Figure 3.3), we can notice that the northern Jiangsu coast is under erosion while the southern part is still accreting. Meanwhile the transition boundary between the two parts is gradually moving southwards. This provides the evidence that this coastline is gradually transiting from eroding to accreting from north (near the AYRD) to the south (near the central region of the RSRs). In our model, we try to reproduce the history of shoreline with originally spatial uniform sediment distribution. Due to morphological changes and redistribution of sediments, we cannot get the shoreline evolution in align with the existing data. Apparently, the sediment provenance difference is very important in the shoreline evolution.

The eroding in the north part (P1 to P2) is caused by both sediment supply shortage and alongshore gradient in hydrodynamics. Due to the northward shift of the Yellow River, there is sharp decrease in the fluvial sediment supply to the AYRD. Meanwhile, as there is no sheltering outside the AYRD, waves can continuously stir up the bed materials and flow will carry them towards the south. On the other hand, the tidal amplitude is increasing from the tip of the AYRD southwards, which leads to a larger transport capacity towards the south. As a consequence, the AYRD is gradually losing its sediments. The eroded fine sediment from the north part partly

transports southwards and eventually settles along the coastline.

In the erosion/sedimentation transition zone (around P2 to P3), despite the hydrodynamics is stronger to the south, the bed material is also coarser to the south due to sediment provenance difference. This means the bed sediments have more resistance to the hydrodynamic forcing, which leads to the slightly sedimentation in this zone. According to the conceptual figure, the coarser bed composition in this zone may come from the RSRs, which also serves as a sediment source for the accreting coastline.



When it comes to further south, this part of coastline (P3 to P4) is sheltered by the RSRs. The RSRs can largely shelter the coast from offshore waves, which provides the sediment a relative milder environment to settle down. As a consequence, this part is experiencing continuous sedimentation.

In the tide-dominated environment, it is a generic phenomenon that the eroding flats are steeper than the accreting ones. Given the shoreline evolution pattern from north to south, this southward flattening pattern is just consistent to the shoreline state. And our model shows that in order to get the reliable shoreline evolution simulation, it is very important to consider the spatial variation in bed sediment composition.

## 3.5. CONCLUSIONS

FROM previous field data study, we find a special relationship between alongshore beach slope variation and sediment grain size pattern on the intertidal flats along the Jiangsu Coast as compared to other tide-dominated muddy flats, i.e. the beach is getting milder southward while the sediment grain size is getting coarser. By formulating a conceptual figure focusing on the alongshore variation in hydrodynamic processes and shoreline evolution pattern, we consider the special phenomenon is related to the alongshore gradient in hydrodynamic forcing. After testing the hypothesis with a highly schematized 1D Delft3D numerical model, we have the following conclusions:

1. The southwards flattening pattern is consistent with the shoreline evolution pattern (i.e. erosion to accretion from north to south), and accreting coast tends to be milder.

2. The alongshore shoreline evolution pattern is not only determined by the alongshore gradient in hydrodynamic forcing, but also influenced by the alongshore variation in bed composition. In the erosion/sedimentation transition zone, the bed composition factor plays the major role.

3. The southwards coarsening pattern cannot be explained by the classical sediment transport processes under the alongshore hydrodynamic gradient. The only way to explain this phenomenon is different sediment provenances.

4. In order to make a reliable morphological simulation of the Jiangsu Coast, it is very important to take into account the effect of spatial variations in sediment composition.

# 4

# On tidal flat morphological restoration after coastal land reclamation

**ABSTRACT** Tidal flat resources play a crucial role in coastal disaster prevention and ecological conservation. However, human activities, such as reclamation, have led to the continuous reduction of these resources. To sustainably develop and protect tidal flat resources, it is essential to systematically understand the post-reclamation evolution characteristics of tidal flats. By establishing a one-dimensional DETESTMORF tidal flat profile model and incorporating the influence of alongshore currents in the bed shear stress calculation, we simulated the evolution of tidal flats before and after reclamation under different natural conditions. Further comparisons of the recovery capacity of the intertidal zone under various conditions allowed us to preliminarily identify the natural environmental characteristics conducive to the post-reclamation restoration of the intertidal zone. In this working in progress chapter, we find that the fundamental geometry of tidal flat profiles is determined by the dominant hydrodynamic forces (either tidal or wave forces), while other investigated variables influence the slope of the tidal flat. For a tidal flat to recover its pre-reclamation morphology, it needs to exhibit continuous seaward progradation under natural conditions, typically characterized by sufficient sediment supply, relatively low wave energy, and the absence of cross-shore constraints imposed by tidal channels parallel to the shoreline.

## 4.1. INTRODUCTION

TIDAL flats are the zones submerged during high tide but exposed during low tide (Gao, 2019). They have multiple functions in both coastal protection and ecological conservation. These areas act as natural buffers against storm surges and waves, which effectively reduces flooding risks and provides cost-effective alternatives to hard engineering structures (Schoutens et al., 2019). Beyond their role in coastal defence, tidal flat are crucial stopovers for migratory shorebirds (Studds et al., 2017), habitats for marine species (Horn et al., 2020), and natural filters for water quality as well (Teuchies et al., 2013). In the context of climate change, the fine-grained sediments in these area function as significant carbon sinks (Ouyang and Lee, 2020), which offers nature-based solutions to mitigate the global warming (Wang et al., 2023). As a consequence, conservation of the area and extent of tidal flats are of strategic importance for sustainable socioeconomic and ecological development in coastal regions.



The evolution of tidal flats is driven by natural processes as well as anthropogenic activities. Natural processes include hydrodynamics (Friedrichs, 2011; Le Hir et al., 2000), sediment dynamics (Zhou et al., 2015) and biological activity (Paarlberg et al., 2005), while anthropogenic activities involve land reclamation (Wu et al., 2024), aquaculture (Li et al., 2021), dredging (van Dijk et al., 2021), and so on. Human intervention started to significantly influence the global climate (Foley et al., 2013) as well as the coastal morphology (Brown et al., 2017) after the Industrial Revolution (post–AD 1780). Increasing human population and activities in the coastal regions have highly threatened the ecosystems there by declining the area of coastal tidal flats (Newton et al., 2020; Murray et al., 2019; Deegan et al., 2012; Waycott et al., 2009). Meanwhile, the sharp loss of coastal tidal flats induced has reduced the buffer zones against storms (Zhang et al., 2021) and the amount of mud capable of storing organic carbon(Bianchi et al., 2024). This will present a significant challenge to the sustainable development of coastal areas in addressing climate change (Sengupta et al., 2023).

Among all anthropogenic activities along the coast, the most prevalent one is coastal land reclamation (Newton et al., 2020), which refers to creating land for human use from coastal wetlands (Martín-Antón et al., 2016). A commonly adopted method for coastal land reclamation is upper-flat enclosure (Hereafter, the term

'reclamation' all refers to this method). This technique is typically applied in flats with sufficient elevation to facilitate the construction of dykes. It is most prevalent along sediment-rich coasts characterized by extensive tidal flats, such as those in Jiangsu Coast, China (Xu et al., 2022). When the seawall is built below the spring high water, the enclosure of upper tidal flats can reduce the local tidal prism, and ultimately promote sediment accumulation at the dyke toe (Wu et al., 2024; Wang et al., 2012a; Flemming and Nyandwi, 1994). The disturbed tidal flat profile will subsequently evolve toward a new equilibrium state, depending on the local hydrodynamic conditions and sediment supply (Zhong and Hu, 2021). Moreover, studies have shown that land reclamation can alter the conditions of local tidal dynamics (Chen et al., 2021; Gao et al., 2014; Tao et al., 2012) and wave actions (Zhang et al., 2023; Zhang et al., 2021). The variation in hydrodynamic gradients in the cross-shore direction further influences the sediment grain size distribution pattern along this direction (Chen et al., 2018; Flemming and Nyandwi, 1994). To achieve a balance between coastal economic development and resource conservation, it is essential to comprehensively understand the evolution characteristics of coastal tidal flats under various environmental conditions. There is a need for a systematic study investigating the post-reclamation morphological responses and recovery processes of tidal flats under varying combinations of environmental factors such as hydrodynamics, sediment supply, and sediment properties.

In this study, we extend the one-dimensional cross-shore DET-ESTMORF model by incorporating the influence of alongshore currents. In this model, the alongshore currents make contributions to the total bed shear stress and change its cross-shore gradient. Using this enhanced model, we simulate and compare the evolution of tidal flat profiles under natural conditions and post-reclamation scenarios in an open coast environment. The simulations examine various combinations of hydrodynamics, sediment supply, and sediment properties. Particular attention is given to changes in the slope and extent of the intertidal zone following reclamation. The specific research questions addressed in this study are as follows:

1. Can the tidal flat profile restore to its natural slope after a reclamation?

2. What are the key environmental features that are favourable for the post-reclamation tidal flat restoration?

## 4.2. METHODS

### 4.2.1. ORIGINAL DET-ESTMORF MODEL DESCRIPTION

THE DET-ESTMORF model is a hybrid-type morphological model that integrates morphological equilibrium relations with hydrodynamics and sediment transport (Hu et al., 2015). The basic theory of erosion/sedimentation in model is described as Figure 4.1. All the sediment transport in the DET-ESTMORF model is defined as in suspension form. In this model, tidal flats in equilibrium are assumed to have uniform Bed Shear Stress (BSS) $\tau_E$ and Suspended Sediment Concentration (SSC) $c_E$ across the entire profile. If the simulated local BSS $\tau$ is higher than $\tau_E$, then there is a tendency of erosion (blue lines in Figure 4.1). It means that the local hydrodynamic conditions can mobilize more sediment into suspension. Therefore, the local equilibrium SSC $c_e$ is higher than the overall level (i.e., $c_E$). If the simulated local SSC $c$ is lower than $c_e$, erosion happens (orange lines in Figure 4.1). The sedimentation situation is vice versa. In summary, the discrepancy between $\tau$ and $\tau_E$ triggers the tendency for morphological changes, but whether the erosion or sedimentation will actually take place or not is ultimately determined by the discrepancy between $c$ and $c_e$.



In our model study, it is assumed that the system outside the model domain is always in an equilibrium state, and the morphological evolution of the tidal flat within the model domain has no influence on the sediment availability outside. The sediment supply from the boundary can therefore be defined as a constant value $c_E$ for long-term morphological simulation. $\tau_E$ is defined as the equilibrium BSS which can maintain the constant $c_E$ over the whole submerged flat. Similar to the process-based models, in an equilibrium state, the mass of erosion balances out the mass sedimentation in the model domain, which can be describe as:

$$m_e\left(\frac{\tau_E}{\tau_{cr}}-1\right)=c_E w_s \tag{4.1}$$

where $m_e$ is the erosion coefficient, $\tau_{cr}$ is the critical BSS for erosion. The local equilibrium SSC $c_e$ is defined according to the ratio between the simulated local BSS $\tau_{90}$ and equilibrium $\tau_E$ as equation (4.2). The detailed description of $\tau_{90}$ will be introduced in next part.

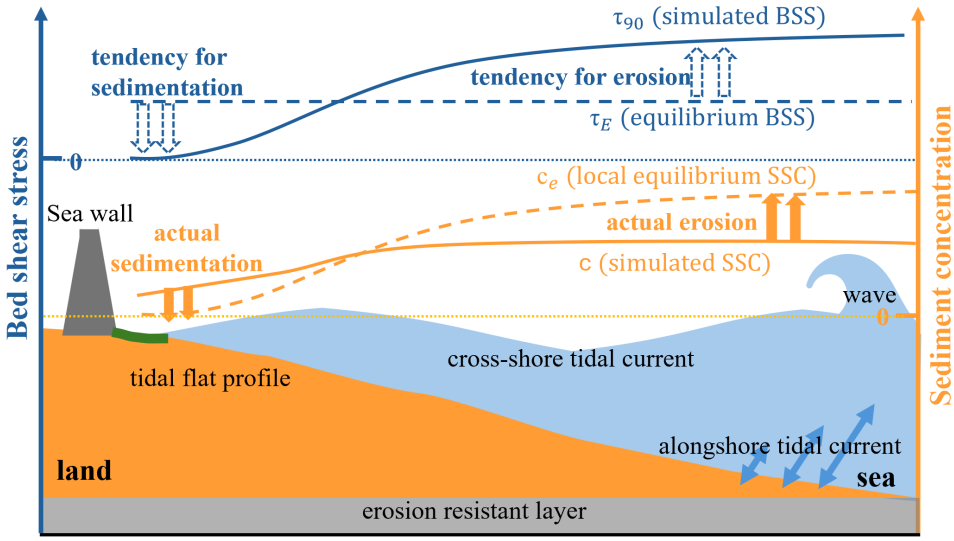


Figure 4.1: A schematization of the DET-ESRMORF cross-shore profile model (modified from Hu et al., 2015).Cross-shore and alongshore tidal currents and waves are the hydrodynamic forcings considered in this model. The blue and orange lines illustrate the cross-shore distributions of Bed Shear Stress (BSS) and Suspended Sediment Concentration (SSC), respectively. The solid lines present the simulated actual values, while the dash lines present the equilibrium values depending on the model input. An erosion resistant layer is implemented in the bed to avoid unrealistic erosion.

$$c_e = c_E \left( \frac{\tau_{90}}{\tau_E} \right)^n \tag{4.2}$$

The SSC is solved by the diffusion equation in a tide-averaged manner as:

$$\frac{\partial (hc)}{\partial t} = w_s (c_e - c) + \frac{\partial}{\partial x} \left( Dh \frac{\partial c}{\partial x} \right) \tag{4.3}$$

Where $h$ is the water depth, $t$ is the time, $w_s$ is the settling velocity, and $D$ is the tide-averaged diffusion coefficient, which can be estimated according to Wang et al. 2008.

$$D \propto \frac{u_s^2 h_s}{w_s} \tag{4.4}$$

Where $u_s$ and $h_s$ are the scales of mixing velocity and water depth, respectively. The bed elevation after each tidal cycle is calculated based on the discrepancy between simulated SSC and local equilibrium SSC as:

$$\frac{\partial z}{\partial t} = \frac{1}{(1-p)\,w_s}(c - c_e) \tag{4.5}$$

Where $z$ is the bed elevation and $p$ is the bed porosity.

Both tidal current and wave are driving forcing considered in the model study. The local BSS $\tau_{90}$ are therefore composed by two components: tidal current induced part and wave induced part.

#### 4.2.1.1. TIDAL CURRENT INDUCED BSS

In the original DET-ESTMORF model, only cross-shore current is taken into account, so the total current induced BSS is the same as the cross-shore current induced one. Assuming a pumping tide mode, the cross-shore tidal current velocity can be derived by the volume of water passing through an imaginary vertical plane parallel to the shore within an short time interval (see Figure 4.2).

$$u_c = \frac{\partial V}{\partial (t\,hB)} \tag{4.6}$$

where $u_c$ is the cross-shore tidal current velocity, $V$ is the water volume, $B$ is the longshore unit width of the flat.

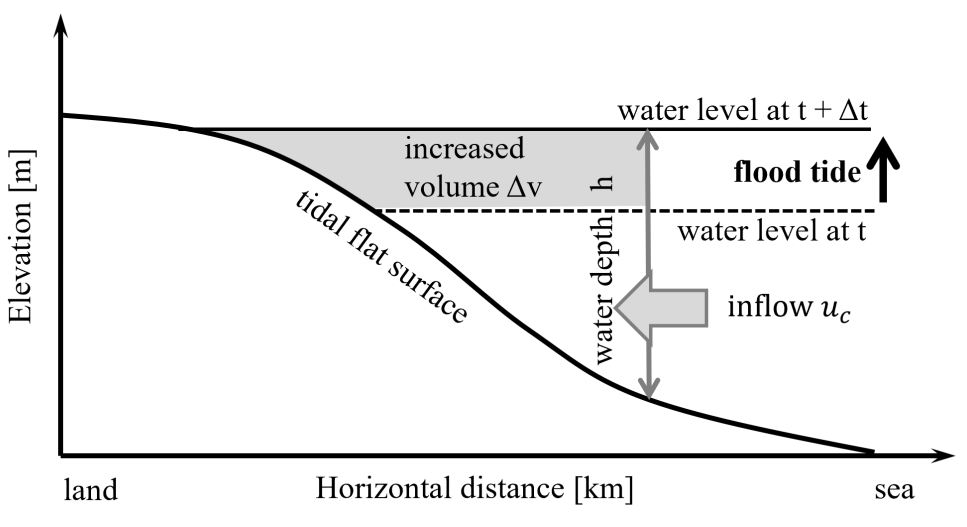


Figure 4.2: A schematization of the mass balance when calculating the cross-shore tidal current velocity $u_c$. The gray double arrows indicate the location of the reference cross-section, with the volume of flow entering the section over the time interval $\Delta t$ represented as $\Delta v$.

And then the cross-shore tidal current induced BSS $\tau_f$ can be derived as:

$$\tau_f = \tau_c = \frac{1}{2}\rho f_c u_c^2 \tag{4.7}$$

Where $\tau_c$ and $\tau_f$ are the cross-shore and total tidal current induced BSS respectively, and $f_c$ is the drag coefficient for currents.

#### 4.2.1.2. WAVE INDUCED BSS

In alignment with the settings previously employed in long-term tidal flat morphological simulations using DET-ESTMORF (Zhong and Hu, 2021), the wave height $H$ at the seaward boundary is Rayleigh distributed with a constant mean value. To derive the cross-shore distribution of $H$, a series of equations describing the dissipation of wave are solved. Meanwhile, the effect of wave breaking on local wave height is taken into account by relating the wave height to local water depth to a ratio $\gamma_b$. The wave energy E is dissipated due to bed friction, which can be described by the continuity equation for the wave energy flux (Christoffersen and Jonsson, 1985):

$$\frac{d(Ec_g)}{dx} = \frac{d}{dx}\left(\frac{1}{8}\rho g c_g H^2\right) = -D_w \tag{4.8}$$

$$H = \min(H, \gamma_b h) \tag{4.9}$$

Where $x$ is the cross-shore coordinate, $c_g$ is the group velocity given by the linear wave theory, and $D_w$ is the energy dissipation calculated according to Christoffersen, 1982 :

$$c_g = \sqrt{\frac{g}{k}\tanh(kh)}\left[\frac{1}{2} + \frac{kh}{\sinh(2kh)}\right] \tag{4.10}$$

$$D_w = \frac{2}{3\pi}\rho f_e U_\delta^3 \tag{4.11}$$

In which $k$ is the wave number, $f_e$ is the energy dissipation coefficient, and $U_\delta$ is the significant bottom orbital velocity:

$$U_\delta = \frac{\pi H}{T\sinh(kh)} \tag{4.12}$$

Then the wave-induced bed shear stress $\tau_w$ can be obtained as equation (4.13).

$$\tau_w = \frac{1}{4}\rho f_w U_\delta^2 \tag{4.13}$$

$$f_w = 1.39\left(\frac{A_\delta}{k_b}\right)^{-0.52} \tag{4.14}$$

$$A_\delta = U_\delta T \tag{4.15}$$

$$k_b = \frac{2\pi d_{50}}{12} \tag{4.16}$$



In which the wave friction factor $f_w$ is given by Soulsby, 1997. The bottom wave orbital semi-excursion $A_\delta$ and bed roughness $k_b$ can be derived as equation (4.15) and (4.16).

#### 4.2.1.3. TOTAL BSS

The BSS under combined wave and current action is calculated as Soulsby, 1995:

$$\tau_m = \tau_f\left[1 + 1.2\left(\frac{\tau_w}{\tau_w + \tau_f}\right)^2\right] \tag{4.17}$$

$$\tau_{\max} = \left[(\tau_m + \tau_w|\cos\theta|)^2 + (\tau_w|\sin\theta|)^2\right]^{1/2} \tag{4.18}$$

Where $\tau_m$ and $\tau_{\max}$ are the mean and maximum value during a wave cycle, respectively. $\theta$ is the angle between tidal current and wave incident direction. In our simulations, wave are defined to propagate perpendicular to the shoreline. We apply the $90^{\text{th}}$ percentile of the $\tau_{\max}$ in a tidal cycle to be the characteristic BSS to determine the local equilibrium SSC. This scale method has been proved to be valid when evaluate coastal morphology (Friedrichs, 2011).

### 4.2.2. MODEL EXTENSION

On open-coast tidal flats, when alongshore tidal currents are strong, they also play a role in shaping the geomorphology of the tidal flat, as observed on the tidal flats in the central Jiangsu coast (Wang et al., 2019b; Gong et al., 2012). On those open coast flat with shore parallel channels on the lower part of the flat, the

strong alongshore current can enhance the BSS. The cross-shore gradient in alongshore velocity can change the cross-shore BSS distribution pattern, which further changes the profile shape. Although only cross-shore processes are considered in the model, we take the alongshore tidal current into consideration when determining the current induced BSS.

#### 4.2.2.1. ALONGSHORE CURRENT INDUCED BSS

Assume the local longitudinal water surface slope is uniform across the whole tidal flat. In the alongshore direction, we can have the balance between the pressure gradient caused by alongshore water level variation and bed friction in a simplifying manner:

$$\rho g h s = \rho C_D \left(u_c^2 + u_l^2\right)^{1/2} u_l \tag{4.19}$$

$$C_D = \frac{g n^2}{h^{1/3}} \tag{4.20}$$

Where $u_l$ is the alongshore tidal current velocity, $\rho$ is the water density, $g$ is the gravitational acceleration, $s$ is the alongshore water level gradient, $C_D$ is the drag coefficient, and $n$ is the Manning coefficient.

Combining the previous two equations, if $u_l$ is not far less than $u_c$, we obtain the cross-shore distribution pattern of $u_l$ as a function of the local water depth:

$$u_l \propto h^{2/3} \tag{4.21}$$

Assuming a constant tidally averaged alongshore water discharge $Q_l$ in the model domain, the profile-averaged alongshore velocity $u_{l\_mean}$ depending on the submerged area $A$ at high water can be expressed as:

$$u_{l\_mean} = \frac{Q_l}{A} \tag{4.22}$$

The alongshore current also follows the periodic motion of the $M_2$ tidal constituent. Combining equations (4.21) and (4.22), with a pre-defined $u_{l\_mean}$ and the initial $A$, we can derive the alongshore current velocity $u_l$ over the entire flat during each tidal cycle.

And then the cross-shore tidal current-induced bed shear stress $\tau_l$ can then be calculated as:

$$\tau_l = \frac{1}{2}\rho f_c u_l^2 \tag{4.23}$$

#### 4.2.2.2. EXTENDED CURRENT INDUCED BSS

In this extended model, the tidal current-induced shear stress consists of two components: the cross-shore current and the alongshore current. Consequently, the updated expression for the total tidal current-induced shear stress is as follows:

$$\tau_f = \frac{1}{2}\rho f_c \left(u_c^2 + u_l^2\right) \tag{4.24}$$

#### 4.2.2.3. EROSION RESISTANT LAYER

In reality, once tidal channels are eroded to a certain depth, the increasing erosion resistance of the channel bed prevents further deepening(Choi et al., 2023; Zhu et al., 2019). However, the DET-ESTMORF model does not account for this physical process, whereby bed resistance to erosion increases with depth. Consequently, when alongshore currents are introduced, thus enhancing BSS, the model can produce an artifact, resulting in unbounded deepening of the channels. In order to prevent such an unrealistic erosion in offshore deep, an erosion resistant layer (see Figure 4.1) is implemented at the elevation of -15 m (the mean sea level is at 0 m). When erosion takes place in this layer, there will be no further erosion. Here, we employ the most simplified approach, using a constant depth resistant to erosion, to represent the resistance of the deep substrate to erosion. The magnitude of this parameter is, to some extent, influenced by the local physical properties of the bed, including sediment composition, consolidation, etc. In the model, the value of -15 m is an arbitrarily assigned uniform parameter, representing the assumption that the soil becomes sufficiently consolidated at this depth. A more rational determination of this value and a sensitivity analysis of the model results to this parameter will be discussed in detail in Section 4.4.1.

### 4.2.3. MODEL APPLICATION

We set up a one dimensional cross-shore model to simulate the tidal flat profile evolution under natural conditions as well as after the enclosure of the up-

per flat The simulations are composed of two phases: the natural evolution phase and the restoration after the implementation of a dyke. The first phase starts from a linear initial profile, resulting in a stable profile shape after a 20-year evolution. The second phase takes the final profile of the previous phase as the initial condition. A dyke will be placed on the intertidal part then. Behind the dyke, there is no hydrodynamic forcing and sediment transport. We make a subsequent simulation for another 20 years. To set up a comparison scenario, we simulate the geomorphological evolution of the tidal flat without a dyke for another 20 years as well.



#### 4.2.3.1. PHYSICAL PARAMETERS

The computational domain spans 15 km cross-shore with a grid resolution of 50 m. Based on a series of sensitivity tests, it is found the final profile shape is not influenced by initial slope (see detailed discussion in Section 4.4.3). In our models, the initial flat elevation is set to linearly decrease seawards from 2.5 m to -8 m with a slope of 7‰. The tide is represented by a harmonic signal, incorporating an $M_2$ tidal component. The wave is driven by the significant wave height specified at the seaward boundary. The SSC is supplied from the seaward boundary with a constant value. A detailed physical parameters setting is listed in Table 4.1.

Table 4.1: Constant values for model parameters

| Parameter | Physical description | Value | Reference |
|---|---|---|---|
| $m_e$ | Erosion coefficient (kg/(m$^2$/s)) | 0.00005 | Roberts et al., 2000 |
| $D$ | Tide-averaged diffusion coefficient (m$^2$/s) | 600 | Wang et al., 2008 |
| $n$ | Power in Equation (4.2) (-) | 2 | Wang et al., 2008 |
| $p$ | Bed porosity (-) | 0.4 | Liu et al., 2011 |
| $d_{50}$ | Sediment grain size (mm) | 0.075 | Liu et al., 2011 |
| $f_c$ | Drag coefficient for currents (-) | 0.002 | Roberts et al., 2000 |
| $\gamma_b$ | Depth ratio for wave breaking (-) | 0.5 | Roberts et al., 2000 |
| $f_e$ | Wave energy dissipation coefficient (-) | 0.055 | Le Hir et al., 2000 |
| $\rho$ | Water density (kg/m$^3$) | 1000 | - |

#### 4.2.3.2. SCENARIO SETTING

In order to investigate the tidal flat natural evolution and post-reclamation restoration under various environmental conditions, a series of simulations are designed

varying the hydrodynamic forcings, sediment properties, and dyke location (Table 4.2). S0 represents the standard scenario, characterized by tidal-dominated tidal flats. In this scenario, both wave and alongshore current effects are minimal, while external suspended sediment supply is abundant, ensuring continuous seaward accretion of the tidal flat. As a benchmark scenario, S0 facilitates comparison with other scenarios. Each of the other scenarios modifies a single parameter as compared to S0. If two scenario IDs are combined, it indicates simultaneous changes in the parameters corresponding to both scenarios. For instance, "AV+WH" represents simultaneous changes to the mean velocity of the alongshore current and the offshore significant wave height.



Table 4.2: Scenario parameters setting

| ID | Hydrodynamic Forcings | | | Sediment Properties | | | Dyke |
|---|---|---|---|---|---|---|---|
| | **TR** (m) | **MAV** (m/s) | **SWH** (m) | **ET** ($N/m^2$) | **SV** (mm/s) | **BC** ($kg/m^3$) | **DL** (m) |
| S0 | 4 | 0.1 | 0.1 | 0.2 | 0.5 | 0.1 | -1 |
| TR | 3 | 0.1 | 0.1 | 0.2 | 0.5 | 0.1 | -1 |
| AV | 4 | 0.5 | 0.1 | 0.2 | 0.5 | 0.1 | -1 |
| WH | 4 | 0.1 | 1.0 | 0.2 | 0.5 | 0.1 | -1 |
| ET | 4 | 0.1 | 0.1 | 0.1 | 0.5 | 0.1 | -1 |
| SV | 4 | 0.1 | 0.1 | 0.2 | 0.3 | 0.1 | -1 |
| BC | 4 | 0.1 | 0.1 | 0.2 | 0.5 | 0.05 | -1 |
| DL | 4 | 0.1 | 0.1 | 0.2 | 0.5 | 0.1 | 1 |

**TR**: Tidal Range, **MAV**: Mean Alongshore Velocity, **SWH**: Significant Wave Height, **ET**: Erosion Threshold, **SV**: Settling Velocity, **BC**: Boundary Concentration, **DL**: Dyke Location.

### 4.2.4. MODEL VALIDATION

To assess the reliability of the model in simulating cross-shore profile morphological evolution under both natural conditions and with anthropogenic influences (the enclosure of the upper intertidal flat), we compare the simulated results with in-situ measured profiles. The model is not designed to predict precise future bed elevations in this study; rather, it serves as a numerical lab to examine the morphological response to various combinations of environmental forcings. In the model validation section, we focus solely on the shape of the profile rather than on its specific elevation. This shape reflects the geometric characteristics of the tidal

flat profile under different processes, thereby demonstrating that our simulation effectively captures these processes.

#### 4.2.4.1. VALIDATION OF THE PROFILE SHAPE UNDER NATURAL EVOLUTION

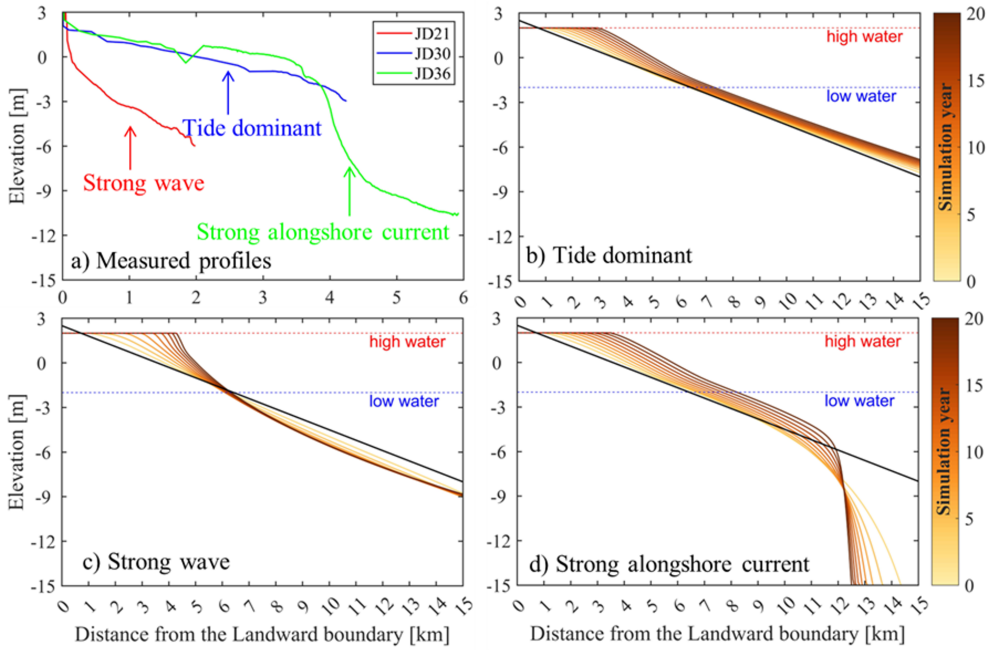


Figure 4.3: Validation of the simulated profile shape in the absence of human intervention against the measured profiles along the Jiangsu Coast, China. a) Measured profile shape along the Jiangsu Coast: JD21 represents a profile influenced by strong waves, JD30 represents an accretional profile with weak waves and alongshore currents, JD 6 represents a profile influenced by strong alongshore currents. b)–d) Simulated 20-year profile evolution under scenario S0, WH and AV respectively.

Figure 4.3 presents the validation results of the simulated profile shapes under natural conditions. We selected three representative profiles along the Jiangsu coast to validate the model: JD21, a profile subjected to intense wave action; JD30, a profile that exhibits continuous accretion under tidal influence; and JD36, a profile influenced by strong alongshore currents (a detailed description of these profiles can be referred to Kuai et al., 2021 ). Accordingly, we selected three sets of model results for comparison with the measured profiles: scenario WH, representing conditions with high significant wave heights; scenario S0, dominated by tidal influence; and scenario AV, characterized by high alongshore current velocities. The comparison results indicate that the model correctly simulates convex profile shapes under tide-

dominance influence, concave profile shapes under stronger wave action, and deep tidal channels in the seaside of the profile under strong alongshore currents. This demonstrates the model's capability to effectively reproduce tidal flat profile morphologies under various forcing conditions.

#### 4.2.4.2. VALIDATION OF TIDAL FLAT RESTORATION PROCESSES AFTER UPPER PART ENCLOSURE

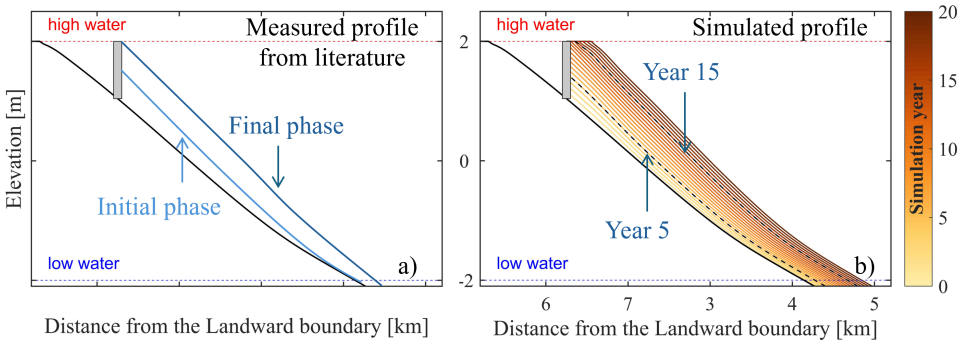


Figure 4.4: Validation of simulated post-reclamation profile evolution against previous studies. a) Distinct phases in the restoration of tidal flat profiles after upper part enclosure, concluded from Jiang and Feng, 1991. b) Simulated tidal flat profiles after upper part enclosure, starting from a convex equilibrium profile (Scenario ID: BC).

Based on historical observational data (Jiang and Feng, 1991), we conclude that the evolution of a tidal flat profile on an accreting tidal flat exhibits distinct characteristics at different stages following upper tidal flat reclamation (Figure 4.4). In the initial phase after construction, the tidal flat near the dyke responds quickly, with rapid sediment accumulation and an overall steepening of the slope. Over time, as sediment accumulation at the dyke base reaches the high tide level, the tidal flat profile gradually returns to its pre-construction shape with abundant sediment supply. This process is well replicated in our model, where significant sediment accumulation is observed near the dyke base within five years post-enclosure of the upper tidal flat. Approximately 15 years later, the profile gradually restores to its pre-construction shape and continues to extend seaward. Therefore, our model can effectively reflect the morphological evolution of tidal flat profiles following human engineering interventions.

### 4.2.5. MODEL RESULTS PROCESSING

#### 4.2.5.1. PROFILE ELEVATION EVOLUTION

At the end of each phase of model simulation, we record the annual elevation changes and the final morphological profiles of tidal flats under various scenarios. By comparing the equilibrium profiles of tidal flats under different combinations of natural hydrodynamic and sediment characteristics, we analyse the influence of these factors on the geometric shape and intertidal slope of tidal flats. Subsequently, by comparing tidal flat profiles before and after reclamation, we assess the recovery capacity of engineered tidal flats under different environmental conditions and identify the natural factors conducive to restoring tidal flats to their pre-reclamation state. Additionally, we track the annual distribution changes in bed shear stress (including its various components) on the tidal flat to analyse the processes of morphological adjustment following reclamation.



#### 4.2.5.2. SEDIMENT ACCOMMODATION AREA

To facilitate the comparison of the morphological characteristics of tidal flat profiles after a period of evolution, we define the sediment accommodation area as a metric. For a one-dimensional profile, this area is the cross-sectional area bounded by the high water level and the bed surface (see shaded areas in Figure 4.5), representing the maximum amount of sediment that can be accommodated on the profile. This parameter encapsulates multiple pieces of information: it reflects the extent of the intertidal zone and the location of tidal channels, while its rate of change provides insights into the evolution rate of the tidal flat profile.

To compare the morphological changes across different regions of the tidal flat, we divide the entire tidal flat domain into three sections: the intertidal zone, lower flat zone, and tidal channel zone (if a tidal channel exists). The intertidal zone refers to the area between the high and low water levels, while the lower flat zone spans from the low water level to the landward boundary of the tidal channel (see Figure 4.5 green shades). For different stages of tidal channel formation and development, it is challenging to establish a unified standard for determining the landward boundary of the tidal channel. In this study, we define the region that is eroded down to the erosion-resistant layer as the tidal channel.

The size of the areas in different regions provides significant insights into the

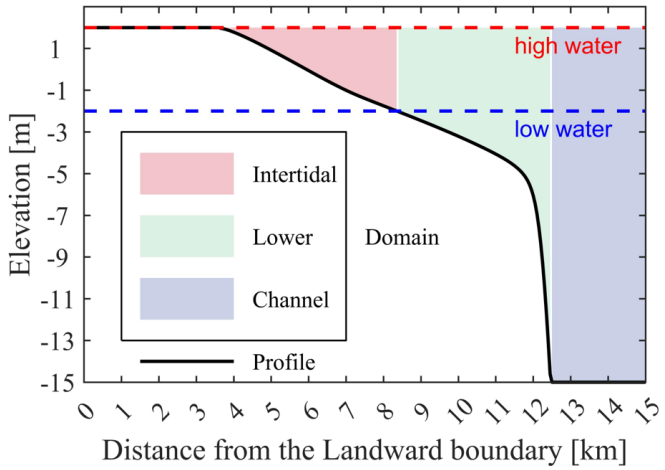


Figure 4.5: A schematic diagram of the sediment accommodation area. The bold black solid line represents the shape of the tidal flat profile. In the diagram, the red, green, and blue shaded areas correspond to the intertidal zone, lower flat zone, and tidal channel zone, respectively. These three areas together form the entire domain's accommodation area.



tidal flat's evolution. The area of the intertidal zone reflects changes in the intertidal slope. With a fixed tidal range, a smaller intertidal area typically indicates a narrower intertidal width and a steeper intertidal slope. Changes in the area of the lower flat zone determine whether the tidal flat profile is accreting seaward or eroding landward. The variation in the tidal channel area represents the extent to which the tidal channel has migrated landward. A larger area indicates that the tidal channel is closer to the land, thus limiting the available space for further tidal flat development. At the same time, the rate of change in the area of each section also reflects the speed of tidal flat evolution or post-engineering recovery. This indicator helps us identify more suitable natural environments for tidal flat restoration.

## 4.3. MODEL RESULTS

### 4.3.1. PROFILE EVOLUTION UNDER NATURAL CONDITIONS

IN the first phase of the model simulation, we obtained the profile morphology after 20 years of natural evolution starting from a linear profile (Figure 4.6). Based on the benchmark scenario S0, we varied the combinations of hydrodynamic forces, sediment erosion and deposition characteristics, and boundary sediment supply to

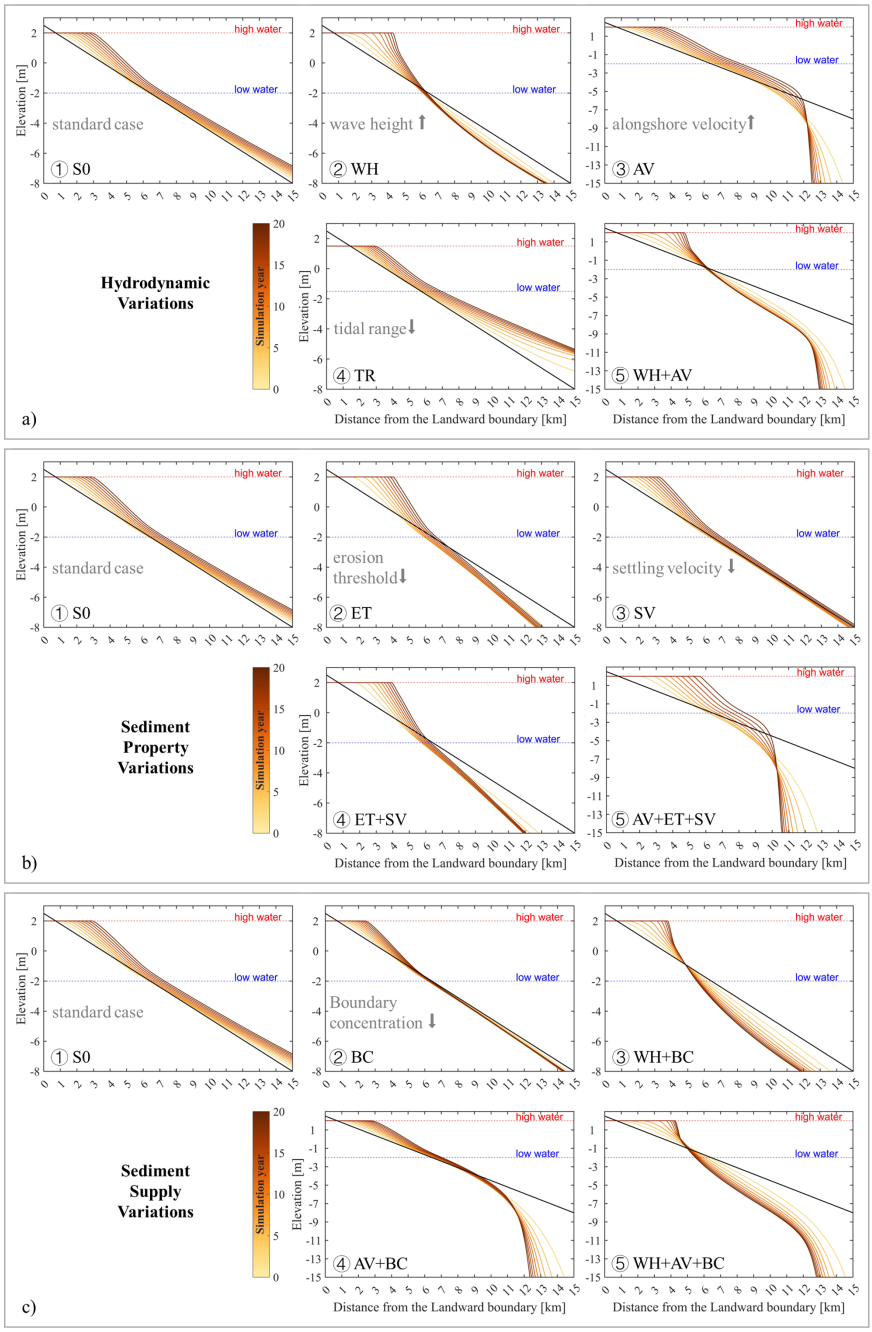


Figure 4.6: Evolution of a tidal flat profile from a linear shape to its morphology after 20 years under natural conditions. a) Impact of different hydrodynamic combinations, including tidal range, significant wave height, and alongshore current velocity. b) Impact of different sediment characteristics, including critical threshold for sediment entrainment and settling velocity. c) Impact of sufficient and insufficient external sediment supply. Different combinations of boundary conditions are summarized in Table 4.2.

compare the stable profile shapes and development rates under natural conditions.

First, we focus on the impact of hydrodynamics on tidal flat profile morphology (Figure 4.6a). In the figure, we observe that under sufficient sediment supply and weak wave and alongshore current conditions (scenario S0), the tide-dominated profile gradually develops a convex shape, ultimately maintaining this form while accreting seaward. When the tidal range decreases (scenario TR), the sedimentation thickness at the seaward boundary increases, and the entire tidal flat becomes flatter. Although the tidal range is reduced to 3/4 of that in scenario S0, the intertidal width does not significantly decrease. This model behaviour aligns with findings from previous studies (Liu et al., 2011; Pritchard and Hogg, 2003). When wave action intensifies (scenario WH), the upper part of the tidal flat continues to accrete, but the deeper regions are eroded, eventually maintaining a constant concave shape. In this case, the tidal flat slope becomes steeper, and the intertidal zone narrows significantly. This phenomenon has also been validated in previous studies (Kirby, 2000; Le Hir et al., 2000). When the alongshore current is stronger (scenario AV), the upper part of the tidal flat resembles scenario S0, displaying a convex shape. However, the intertidal flat slope becomes milder. Near the seaward boundary, the bed surface is eroded, eventually forming a stable tidal channel parallel to the shoreline, and its location becomes fixed. A similar pattern of alongshore tidal channel formation has been documented in other studies (Xing et al., 2022; Hughes, 2012). When both wave and alongshore current effects are strong (scenario WH+AV), the upper part of the profile adopts a concave shape dominated by waves, while the seaward section forms a stable deep tidal channel controlled by alongshore currents.

Next, we examine the morphological characteristics of profiles under different sediment properties (Figure 4.6b). In the muddy environment (i.e. the sediment is mainly consisted by clay and silt), as the critical threshold for sediment entrainment (scenario ET) and settling velocity (scenario SV) decrease, the overall profile becomes steeper, and the intertidal zone narrows. During the initial stages of profile evolution, the geometry rapidly adjusts to a stable shape, resulting in noticeable erosion at the seaward boundary. Once the profile reaches equilibrium shape, it maintains its shape while gradually accreting seaward, with sedimentation also beginning to occur at the seaward boundary. The intertidal zone retains a slightly convex shape. Under conditions of strong alongshore currents (scenario AV+ET+SV),

sediment that is more easily entrained and less prone to settling causes the final position of the tidal channel to shift landward, further constraining the tidal flat's seaward development.

Finally, we investigated the impact of sediment supply on profile morphology (Figure 4.6c). As sediment supply decreases (scenario BC), both the overall profile and the intertidal zone exhibit steeper slopes, and the rate of seaward accretion of the stabilized profile significantly declines. Under strong wave action (scenario WH+BC), observations of the profile near the high water line and in deeper regions (compared to scenario WH) reveal a more pronounced landward erosion of the entire profile. Under strong alongshore currents (scenario AV+BC), the position of the tidal channel also slightly shifts landward.



Based on the observations and comparisons of the aforementioned simulation results, in the simulated variable variation range, the following conclusions can be drawn:

1. In the DET-ESTMORF model, tidal flat profiles exhibit different morphological characteristics under various combinations of natural environmental factors but ultimately converge to a stable shape. This stable shape either accretes seaward or remains stationary in a state of equilibrium.

2. The final shape of a tidal flat is primarily determined by hydrodynamic conditions. Stable tidal flat shape can be categorized into three types: convex profiles, concave profiles, and profiles with offshore tidal channels. These types correspond to tide-dominance, strong waves, and strong alongshore current, respectively.

3. Sediment properties influence the overall slope of the profile but do not alter its shape (convex or concave) characteristics. Under constant hydrodynamic forcings and sediment supply, bed sediment with lower thresholds for entrainment and slower settling velocities results in steeper tidal flat profiles and narrower intertidal zones in a muddy coast.

4. Sediment supply does not change the shape (convex or concave) of the profile but affects its slope and development state. Under constant hydrodynamic forcing, the sediment supply plays a critical role in shaping tidal flat profiles

and their migration dynamics. Ample sediment supply promotes the development of flatter profiles and accelerates the seaward migration of the entire profile. In contrast, reduced sediment supply results in steeper profiles, slows down seaward migration, and may even lead to landward retreat.

5. Stronger alongshore currents, reduced external sediment supply, and sediment characteristics that are more easily entrained and less likely to settle can collectively drive the shore-parallel channels to develop further landward. This process restricts the tidal flat area landward of the channel, significantly impacting the overall geomorphological dynamics of the system.



### 4.3.2. PROFILE EVOLUTION AFTER A RECLAMATION

BASED on the morphological characteristics of profiles under natural evolution, we identify two typical types of tidal flat profile evolution for investigating post-reclamation recovery: accretional and erosional profiles. To remain consistent with the tidal flat profiles observed along the Jiangsu coast, we further classified the accreting-type profiles into two subcategories: those without channels and those with channels. For simplicity, these are referred to as Accretional Profile (accretion without channel), Channelized Profile (accretion with channel), and Erosional Profile, respectively (see Figure 4.7). Simulations in phase 2 are performed for three different conditions: profile evolution without human intervention and profile recovery following dyke construction at positions 1 m above and 1 m below mean sea level. The objective is to assess whether the profiles can recover their natural shapes following reclamation projects and whether the intertidal zone can regain its original width.

When a tidal flat is naturally accreting (Figure 4.7a,d,g), it implies a sufficient external sediment supply relative to the local hydrodynamic conditions. As shown in Figure 4.8, placing a dyke on such a tidal flat introduces a significant hydrodynamic gradient in the cross-shore direction, particularly in terms of bed shear stress ($\tau_{90}$). This gradient leads to rapid initial accretion at the dyke's toe as the system adjusts to reduce the steep gradient. The closer the dyke is positioned to the lower part of the tidal flat, the larger this initial gradient becomes, resulting in greater accretion at the toe and a steeper overall profile. As the profile continues to evolve, the hydrodynamic gradient gradually diminishes, and the accretion rates across the pro-

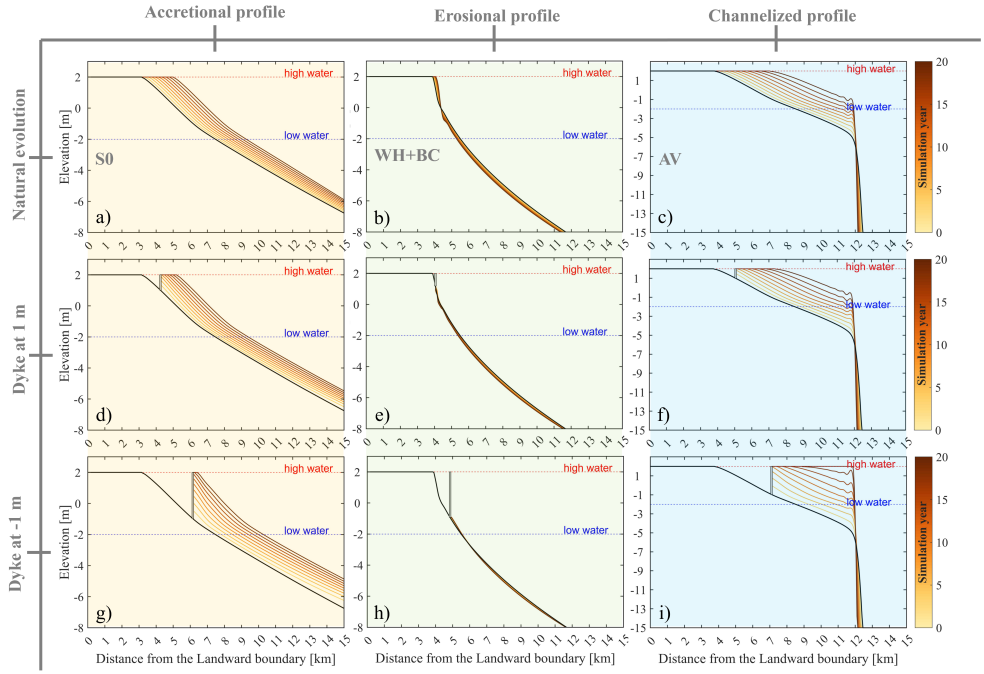


Figure 4.7: Morphological evolution of tidal flat profiles after 20 years under natural conditions and following dyke construction (initial profiles derived from 20 years of natural evolution). The comparison includes three typical profile types: accreting convex, eroding concave, and channelized profiles. The dyke positions (indicated by grey box) are set at +1 m and -1 m relative to the mean sea level (0 m).

file converge. Eventually, the profile returns to its natural shape, with the intertidal zone regaining a slope similar to that under natural conditions.

For an eroding profile(Figure 4.7b,e,h), the sediment supply is insufficient. Similar to the previous scenario, the placement of a dyke alters the hydrodynamic gradient. While the profile attempts to compensate for this gradient change through accretion at the dyke toe, the limited sediment availability results in only minimal accretion at this location. As a consequence, the intertidal zone width cannot fully recover, leading to a permanently steeper and narrower intertidal profile.

For an accreting tidal flat profile featuring an offshore channel (Figure 4.7c, f, i), the evolution of the upper part largely resembles that without a channel. However, the offshore channel limits the seaward expansion of the tidal flat. In the model simulations, the location of the channel is fixed for each scenario. Dyke construction appears to accelerate the infilling of the area between the dyke and the tidal chan-

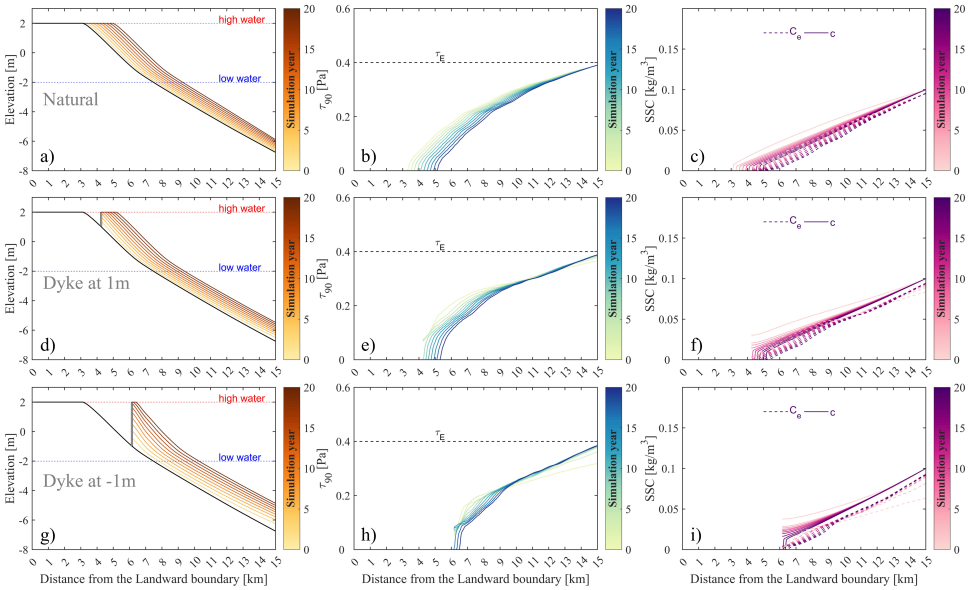


Figure 4.8: Morphological evolution of accreting profiles under natural conditions and post-dyke construction, along with the cross-shore distribution of BSS and SSC. $\tau_E$, $c_e$, and $c$ denote equilibrium BSS, local equilibrium SSC and simulated local SSC, respectively.

nel, leading to a faster disappearance of the intertidal zone. In reality, this behaviour may differ, as shore-parallel channels can migrate seaward with the development of the tidal flat. This model behaviour is further analysed in Section 4.5.2.1.

Based on the comparison of the three types of tidal flats, the following key conclusions can be drawn:

1. For an accreting tidal flat with sufficient sediment supply, under constant external conditions, the profile can recover to its natural state after enclosure, and the width of the intertidal zone can also be restored.

2. For an eroding tidal flat with insufficient sediment supply, enclosure may result in minor accretion at the base of the dyke. However, the tidal flat profile is unable to revert to its natural state, and the width of the intertidal zone permanently diminishes.

3. The model shows the presence of offshore channels limits the seaward development of the tidal flat. However, the model cannot reproduce the migration

of the channel in a single scenario. We still need further analysis on the influence of the channels.

### 4.3.3. VARIATION OF SEDIMENT ACCOMMODATION AREA UNDER VARIOUS ENVIRONMENTS

AFTER understanding the conditions under which the tidal flat can restore its natural form after reclamation, we further explore the scenarios that are more favourable for the restoration of the tidal flat. Therefore, we statistically analysed the changes in the sediment accommodation area across different parts of the tidal flat throughout the 40-year simulation period (see Figure 4.9). This metric was used to assess the rate and extent of the tidal flat's recovery. Unless otherwise specified, all references to "area" in this section refer to the sediment accommodation area.

The accreting profile is the most conducive to tidal flat morphological recovery. As shown in Figure 4.9a, the intertidal area quickly adjusts from a linear slope in the early stages of the simulation and remains constant. After the construction of the dyke, the intertidal area is rapidly reduced due to human intervention. However, it gradually recovers to an area similar to that in the natural evolution scenario, indicating that the profile at this point is nearly indistinguishable from the naturally evolved one. As the tidal flat continues to accrete seaward, the area of the lower flat zone within the model range gradually decreases. Comparing the scenarios with and without reclamation, we find that reclamation seems to accelerate the seaward accretion of the intertidal zone. We will explain this model behaviour in Section 4.4.3. In Figure 4.9c, we observe that, despite reduced sediment supply, as long as the tidal flat remains accreting, the intertidal zone can still recover to its previous shape, though the recovery time is longer when sediment supply is reduced. Additionally, we notice that with reduced sediment supply, the area of the intertidal zone decreases, meaning the intertidal zone becomes steeper and narrower, with less available width. In Figure 4.9f, we find that a reduction in tidal range also leads to a decrease in intertidal area, but this is due to a direct reduction in vertical height (for calculating the area) and does not imply a proportional reduction in the intertidal width. In fact, as seen in Figure 4.6, a smaller tidal range results in a gentler intertidal zone. Regarding recovery speed, tidal range changes do not cause significant variations in recovery time. Finally, in Figure 4.9h, we observe that smaller

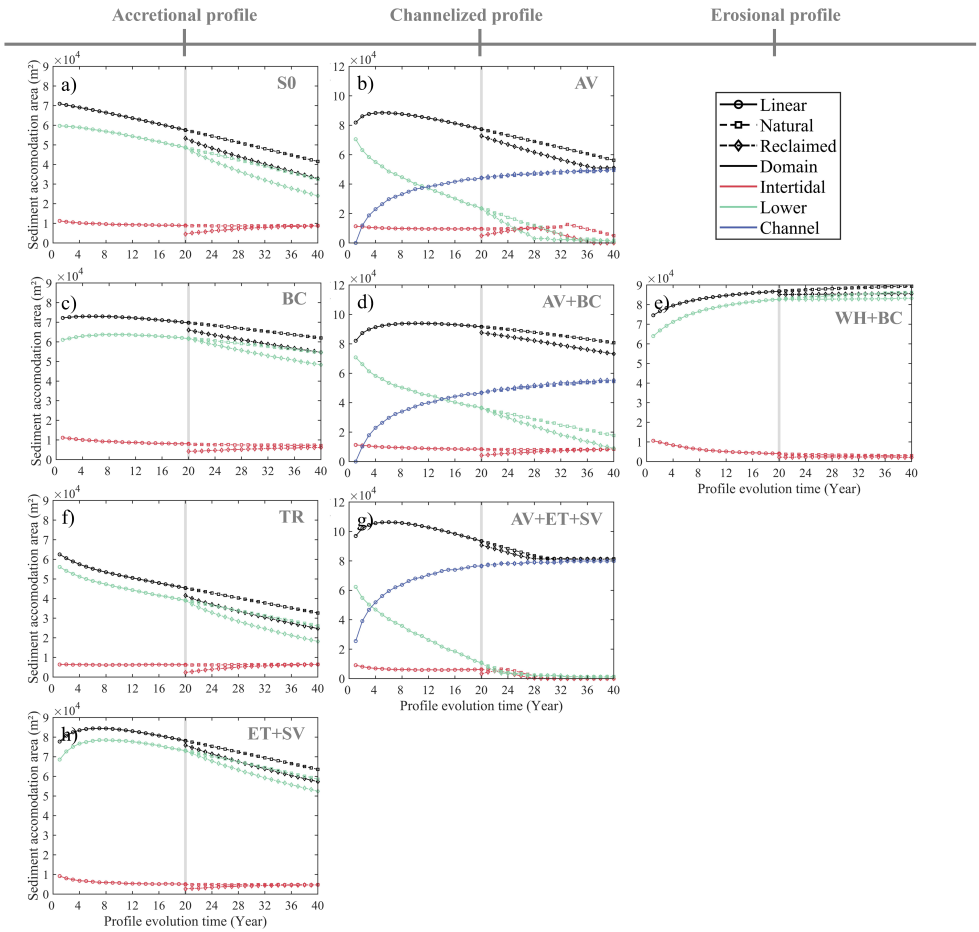


Figure 4.9: Changes in sediment accommodation area across different regions over a 40-year simulation period. The first 20 years represent the stage of natural development from a linear profile (marked as Linear). The grey vertical line at year 20 indicates the time of reclamation. The subsequent period from year 20 to 40 is divided into two scenarios: reclamation (marked as Reclaimed) and natural development (marked as Natural).

sediment initiation thresholds and settling velocities result in a smaller intertidal area, leading to a steeper and narrower intertidal zone. While the recovery time is reduced, the width of the reclaimed area at the same elevation is also shortened.

For accretional profiles with tidal channels, in addition to focusing on the rate of intertidal zone shape restoration, we also examine the space available for seaward development of the entire intertidal zone. As shown in Figure 4.9b, after the ini-

tial formation of the tidal channel, its area rapidly expands, with the expansion rate gradually slowing down. Eventually the channel stabilizes when the entire landward side of the channel is filled with sediment (see Figure 4.7i). The intertidal zone area remains constant at first, but eventually decreases to zero once it is filled up. After reclamation, the area of the intertidal zone experiences a sharp decrease, but then recovers more quickly to its natural state compared to profiles without tidal channels (compare the left and middle column in Figure 4.9). However, the changes in the tidal channel area are almost unaffected by reclamation. Because after the tidal channel forms, most of the discharge from the alongshore current is concentrated within the channel, receiving minimal impact from the changes in the areas of the shallower part. As shown in Figure 4.9d, reducing the boundary sediment supply decreases the restoration rate of the tidal flat but also slows down the rate at which the landward side of the tidal channel is filled. This allows the restored tidal flat to persist for a longer time. As shown in Figure 4.9g, sediments that are more easily mobilized but harder to settle accelerate the filling of the landward side of the tidal channel, leaving very little time for the tidal flat to develop.



For eroded-type profiles (Figure 4.9e), the intertidal area is smaller as compared to the accretional ones, and it cannot restore to its natural area after reclamation. Therefore, we do not recommend undertaking reclamation projects in such cases.

In this section, by comparing the temporal variations in the sediment accommodation area of different regions, we reached the following conclusions:

1. For accreting tidal flats, a higher sediment supply can not only create a larger intertidal area, but also be more beneficial for the rapid recovery of the tidal flat profile after reclamation.

2. For accretional tidal flat profiles with tidal channels, model results show a faster post-reclamation intertidal area restoration as compared to the ones without channels. However, the model settings cannot reproduce the migration of channels, eventually the flat above the channel are all filled up.

3. When sediments are more easily mobilized or difficult to settle, the restoration of intertidal flats after reclamation is faster. However, the intertidal flat area tends to be smaller.

4. Reclamation is not recommended for eroded-type tidal flats.

## 4.4. SENSITIVITY ANALYSIS

### 4.4.1. THE EROSION RESISTANT LAYER

#### 4.4.1.1. THE NECESSITY OF THE EROSION RESISTANT LAYER

In our model, we set up an erosion resistant layer to prevent the offshore tidal channel from continuously narrowing and becoming infinitely deeper. To demonstrate the necessity of this layer, we compared the model results with (Figure 4.11) and without (Figure 4.10) the layer.



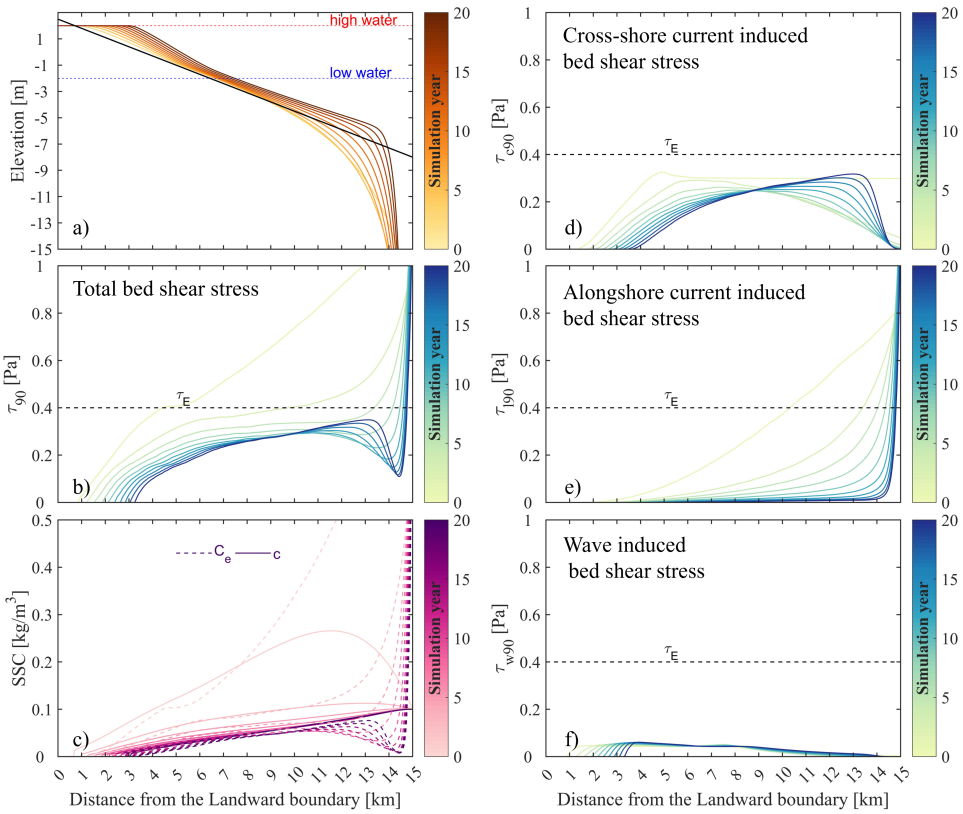


Figure 4.10: Simulated results of Scenario AV (however the erosion resistant layer is not implemented in this simulation). a)-f) temporal variation of profile elevation, 90$^{th}$ percentile total BSS, tidal averaged SSC, and 90$^{th}$ percentile cross-shore current, alongshore current and wave induced BSS.

As it can be seen in Figure 4.10, without the erosion-resistant layer in the model, the tidal channel on the seaward side continuously narrows and deepens. Eventu-

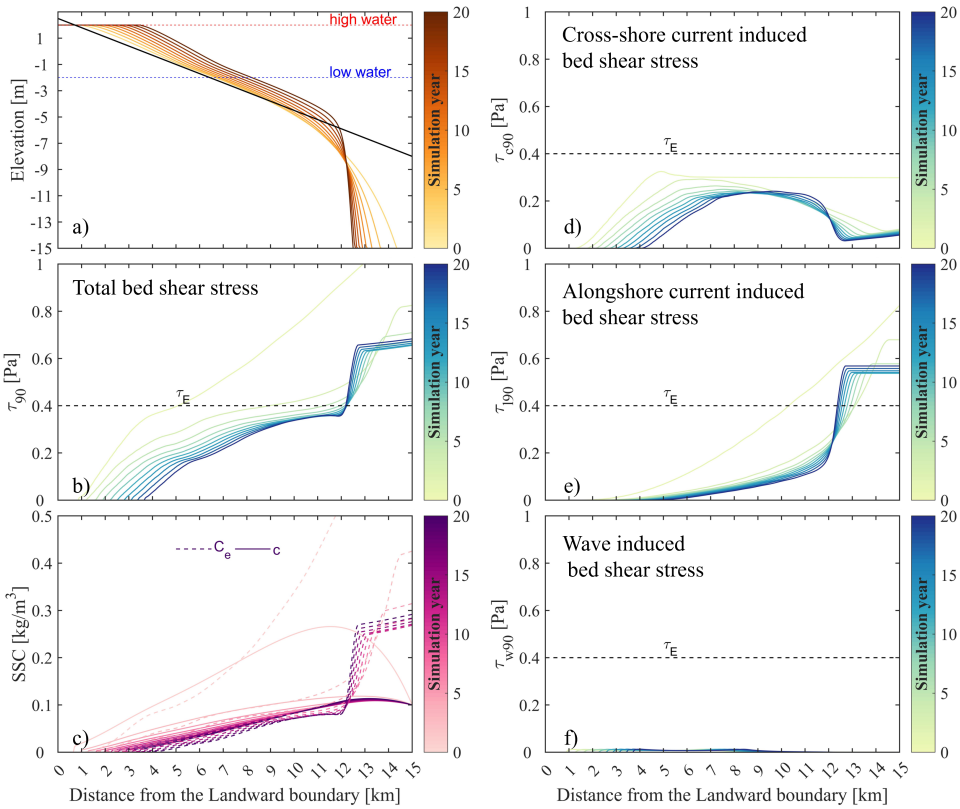


Figure 4.11: Simulated results of Scenario AV (with the implementation of erosion resistant layer). a)-f) temporal variation of profile elevation, 90$^{th}$ percentile total BSS, tidal averaged SSC, and 90$^{th}$ percentile cross-shore current, alongshore current and wave induced BSS.

ally, it only exists at a single grid cell at the seaward end, reaching an unrealistic depth. There is a negative feedback between the mean alongshore current velocity and the cross-sectional area of the tidal channel (Figure 4.12). The deepening of the tidal channel increases the overall cross-sectional area, which in turn reduces the profile-averaged alongshore current velocity. The continuous reduction in alongshore current velocity inhibits the further deepening of the tidal channel. This mechanism appears to prevent the offshore channel from becoming unrealistically deep.

However, there is another positive feedback among the alongshore velocity in the channel, discharge in the channel and the channel depth (Figure 4.12). As the

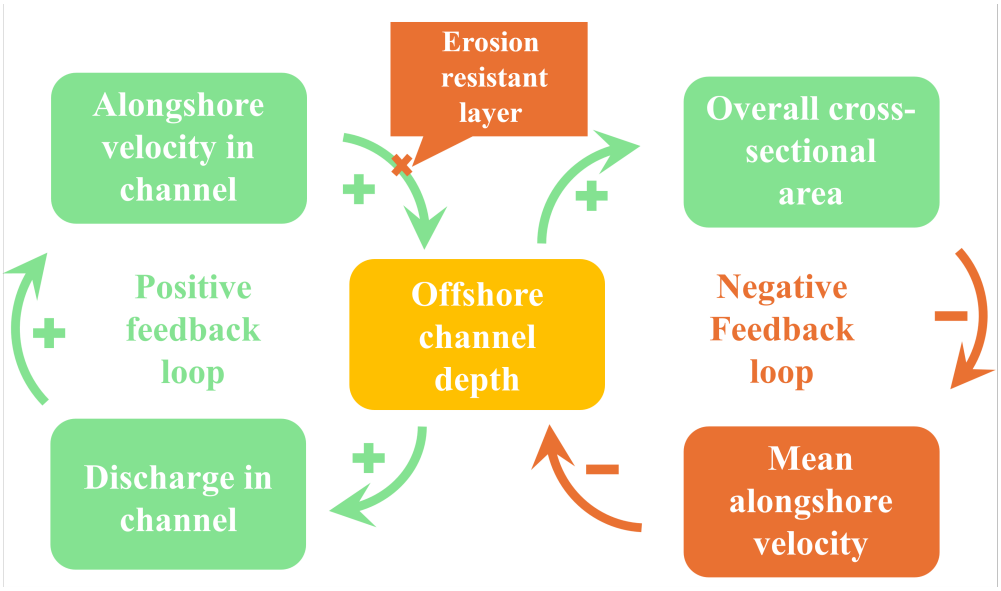


Figure 4.12: Schematic diagram for understanding the model behavior: the positive and negative feedback mechanisms of tidal channel depth variation during the simulation.



tidal channel deepens and its cross-sectional area increases, it draws a greater proportion of alongshore flow, concentrating the discharge within the channel. This intensified discharge results in higher alongshore velocities within the channel, which further accelerates its deepening. Consequently, the deeper sections of the channel become increasingly localized and pronounced. This phenomenon is reflected in the results shown in Figure 4.10, where alongshore-induced BSS becomes progressively concentrated in the seaward-most grid cells (Figure 4.10e), with its magnitude escalating to exaggerated levels. This represents an inherent limitation in the current model configuration, which we addressed by incorporating an erosion resistant layer approach.

When the erosion resistant layer is introduced into the model (Figure 4.11), it effectively disrupts the aforementioned positive feedback loop (illustrated in Figure 4.12). Once the seaward portion of the profile erodes down to this layer, further deepening is inhibited, regardless of the increased flow velocity. This breaks the cycle of intensifying alongshore currents and subsequent erosion. At this stage, the flow remains concentrated in the deeper seaward regions, but it stabilizes within a fixed range (Figure 4.11e), ultimately defining the tidal channel as observed in the

final model output.

#### 4.4.1.2. THE SENSITIVITY OF THE EROSION RESISTANT LAYER

Although we incorporated an erosion resistant layer in the model, its elevation was set to a constant value across all scenarios, assuming a uniform erosion resistance depth for all tidal flat profiles. However, the specific value of this parameter can influence the precise position of the tidal channel. To evaluate its impact, a sensitivity analysis was conducted (Figure 4.13).

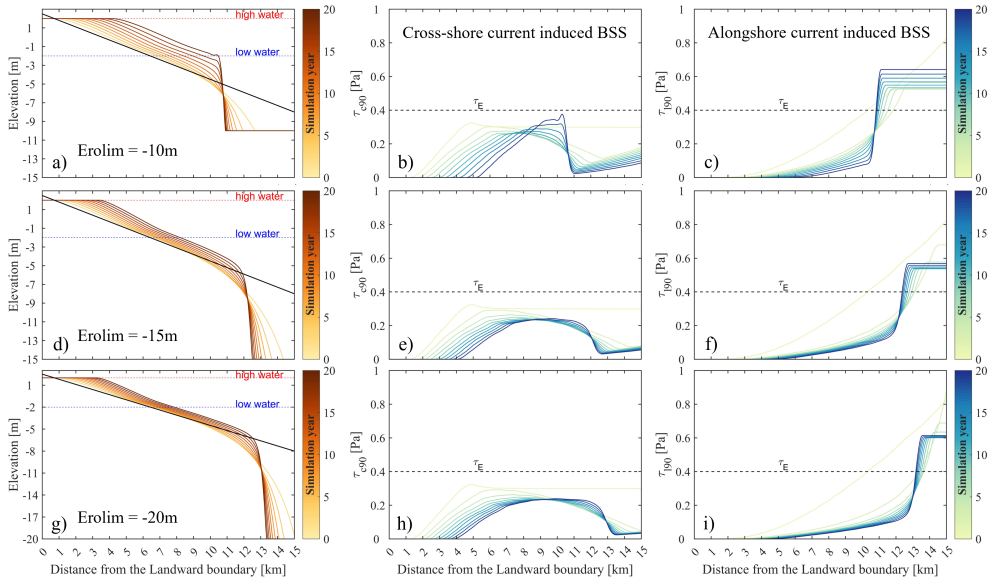


Figure 4.13: Comparison of simulation results under different erosion resistant layer elevations. The three columns represent (from left to right): The profile shape, The cross-shore current induced BSS, The alongshore current induced BSS.

As shown in Figure 4.13, the erosion-resistant depth parameter effectively sets a limit on how deeply the tidal channel can develop. Within the defined computational domain, when further downward development of the channel is restricted, the channel shifts landward to maintain a sufficient cross-sectional area. Consequently, the results indicate that a deeper erosion-resistant layer corresponds to a narrower channel width, and the tidal channel appears more seaward in the model.

If this model is to be applied for reproducing the evolution of real-world tidal flat profiles, ensuring that it accurately captures the actual location of tidal channels requires careful calibration of the erosion-resistant depth parameter. This pa-

rameter is therefore a critical factor that must be finely tuned for reliable model performance.

#### 4.4.1.3. COMPARISON WITH THE REAL WORLD

In this study, we adopted highly simplified boundary conditions for the model setup. The tidal flat within the model was assumed to consist of homogeneous sediment, with uniform erosion threshold in both the horizontal and vertical directions. Additionally, the elevation of the erosion-resistant layer across the tidal flat was fixed, which determined the final location and depth of tidal channels in the model. The elevation of the erosion-resistant layer represents, to some extent, the overall erosion resistance of the whole tidal flat, reflecting the degree of consolidation in the deeper layers underneath the flat surface. Under this setup, the model can capture the influence of hydrodynamics (particularly alongshore currents) and the sediment entrainment and deposition characteristics on the formation and location of tidal channels.



In the real world, tidal flats are composed of multi-component sediments with non-uniform horizontal and vertical distributions (Kuai et al., 2021; Gunaratna et al., 2019; Shi et al., 2018). Existing research indicates that the clay and silt content in bed sediments significantly influences their erosion characteristics (Yao et al., 2022; Van Ledden et al., 2004). For cohesive sediments, a widely accepted pattern is that erosion resistance increases with depth due to longer consolidation time and reduced water content (Amos et al., 2010; Bale et al., 2007; Winterwerp and Van Kesteren, 2004). However, this pattern can also be affected by other factors such as organic content and the presence of gas (Grabowski et al., 2011; Jepsen et al., 2000). Therefore, to more accurately simulate the location and depth of tidal channels, it is essential to incorporate the composition of bed sediments into the model setup. This allows for a more precise representation of the variation in erosion resistance with depth.

### 4.4.2. THE ALONGSHORE TIDE TYPE

In the model, we adopted a standing wave representation for the tidal alongshore current, where the alongshore velocity and the tidal level are 90° out of phase. However, most alongshore currents in real-world scenarios are progressive waves or a combination of both. To assess the influence of tidal wave types on the final

morphology of tidal flat profiles, we conducted a sensitivity analysis (Figure 4.14).

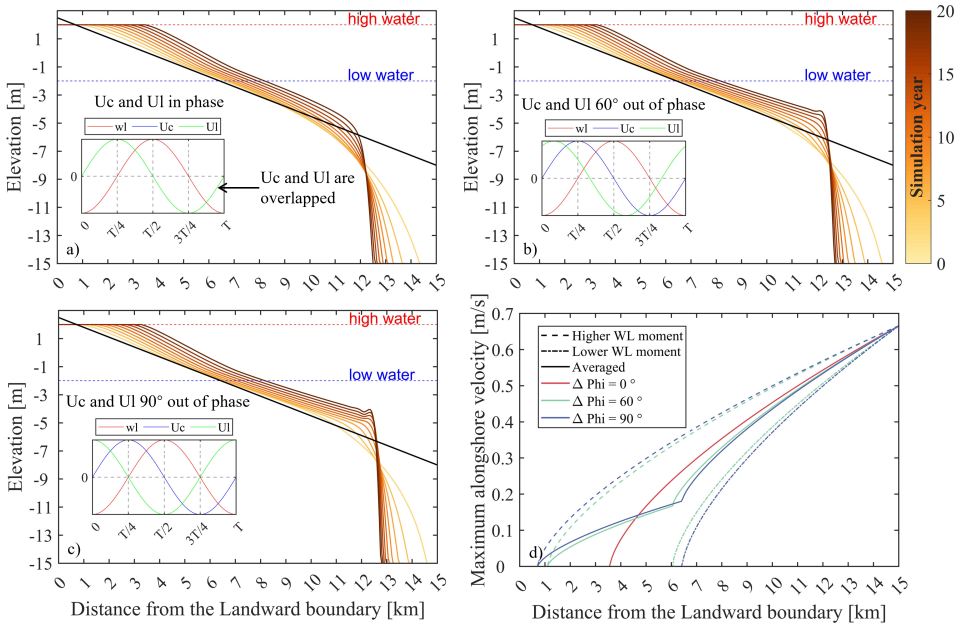


Figure 4.14: Comparison of tidal flat profile simulation results under natural conditions with varying phase differences between alongshore and cross-shore currents. From a) to c), the alongshore current transitions from a standing wave to a progressive wave. d) initial cross-shore distribution of the maximum alongshore velocity for different cross-shore and alongshore current phase differences.

As shown in Figure 4.14, as the alongshore current shifts from a standing wave to a progressive wave (with the alongshore current phase relative to the cross-shore one changing from 0° to 90°), the offshore tidal channel gradually moving seawards. This is initialized by initial cross-shore distribution of the alongshore current induced bed shear stress. Figure 4.14d illustrates the initial distribution pattern of alongshore velocity at its peak moment for all three scenarios. The maximum alongshore velocity occurs twice within a tidal cycle: once at a higher water level (indicated by dashed lines in the figure) and once at a lower water level (indicated by dash-dotted lines). The average of these two values (solid line) is used to represent the distribution of the maximum alongshore velocity over the entire tidal cycle. Based on the initial alongshore velocity distribution, it can be observed that in the deeper sections of the tidal flat profile, the alongshore velocity decreases as the tidal wave pattern transitions from a standing wave to a progressive wave. Conse-

quently, in the standing wave mode, the shear stress generated by the alongshore current in deeper waters is greater, leading to the formation of tidal channels closer to the shore.

### 4.4.3. THE TOPOGRAPHY

IN the DET-ESTMORF model, placing a dyke in the middle of the profile is similar to adjusting the profile shape and shifting the entire computational domain landward by a certain distance, while keeping the external driving conditions unchanged. In this sense, we simulate the natural evolution of tidal flat profiles under different initial topographies by modifying the slope and elevation of the initial linear profile (Figure 4.15). This approach serves as an analogy for the evolution of tidal flats after reclamation.



Under different initial tidal flat slopes and elevations, we find that the final shape of the intertidal zone and the location of the tidal channel do not change. Under the same external driving forces and sediment supply, the model drives the profile towards the similar equilibrium state, ultimately converging to the same shape. A flatter initial profile simply intensifies the extent of seaward extension but does not alter the profile shape. Similarly, lowering the initial profile elevation only slows down the seaward extension rate without changing the final profile shape.

In the model, the terrain evolution after constructing the dyke is essentially a change in the initial topography of the profile. The terrain after dyke construction is effectively shifted downward by a certain distance (similar to the "lower elevation" case shown in Figure 4.15), but at the same time, the computational domain becomes shorter. This shortening of the computational domain effectively shifts the seaward boundary landward, which is equivalent to a sudden increase in sediment supply within the computational domain. Consequently, we observed that the profile evolution after dyke construction significantly accelerated, even leading to a phenomenon where the tidal flat profile extended seaward more quickly than in the natural condition. If the seaward boundary of the model were set to infinity, this effect would be eliminated.

Through this sensitivity analysis, we concluded that the final shape of the profile is primarily driven by external driving forces and sediment characteristics/supply, rather than by its initial configuration. This finding suggests, as designers,our ability

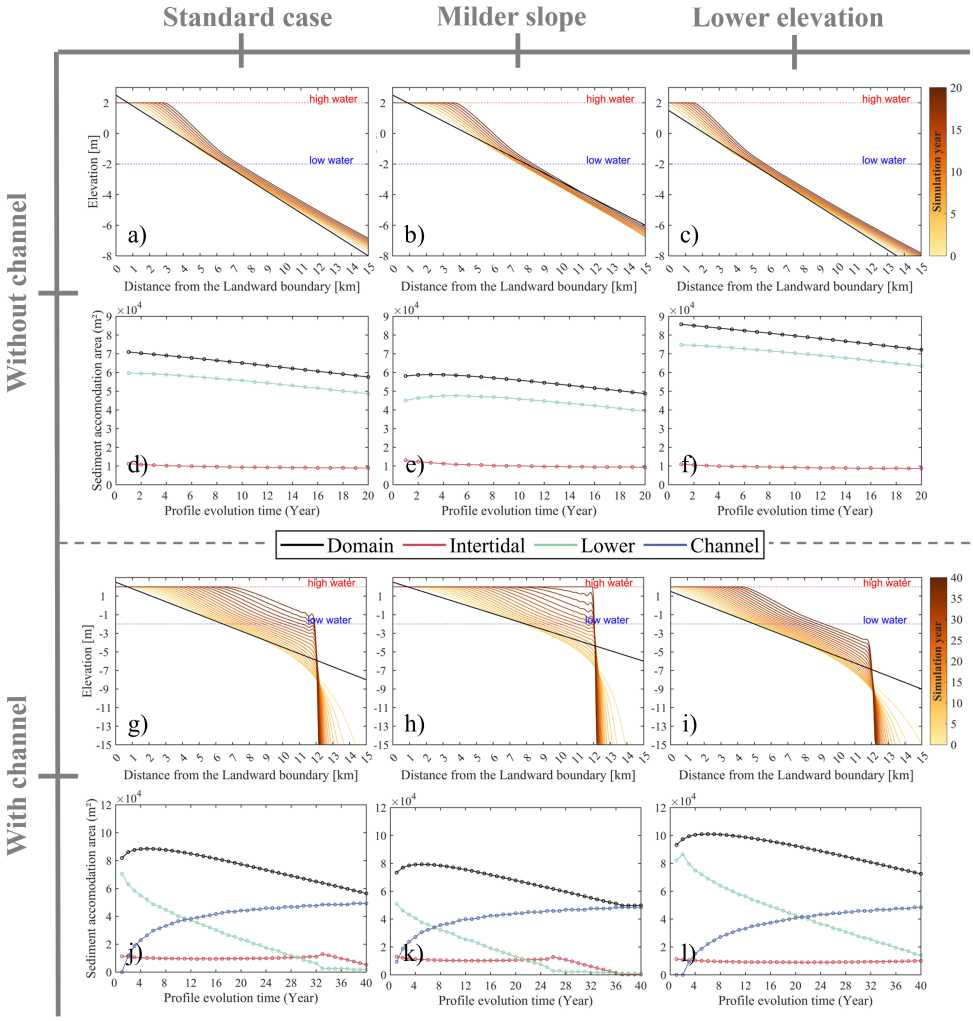


Figure 4.15: Influence of initial profile slope and elevation on the final tidal flat profile morphology. The top and bottom panels represent scenarios without and with tidal channels, respectively. Line charts illustrate the temporal evolution of sediment accommodation area across different profile sections.

to mitigate potential impacts is limited primarily to the selection of reclamation sites. As coastal administrators, it is essential to closely monitor and manage the adjacent natural environment to preserve the integrity of the tidal flats.

## 4.5. DISCUSSION

### 4.5.1. RELIABILITY OF THE MODEL RESULTS

#### 4.5.1.1. THE CONTINUITY OF THE MODEL RESULTS

FOR the simulation of the entire 40-year morphological evolution, we divided it into two independent 20-year periods. The tidal flat profiles in the first and second 20 years under natural conditions appear to follow two different patterns (Figures 4.16a and 4.16b), which raised concerns about the continuity of the model results between the two stages. Therefore, we separately ran the model from a linear profile for a full 40 years (Figure 4.16c) to ensure the continuity of the results and compared it with the results from the separate 20-year runs.



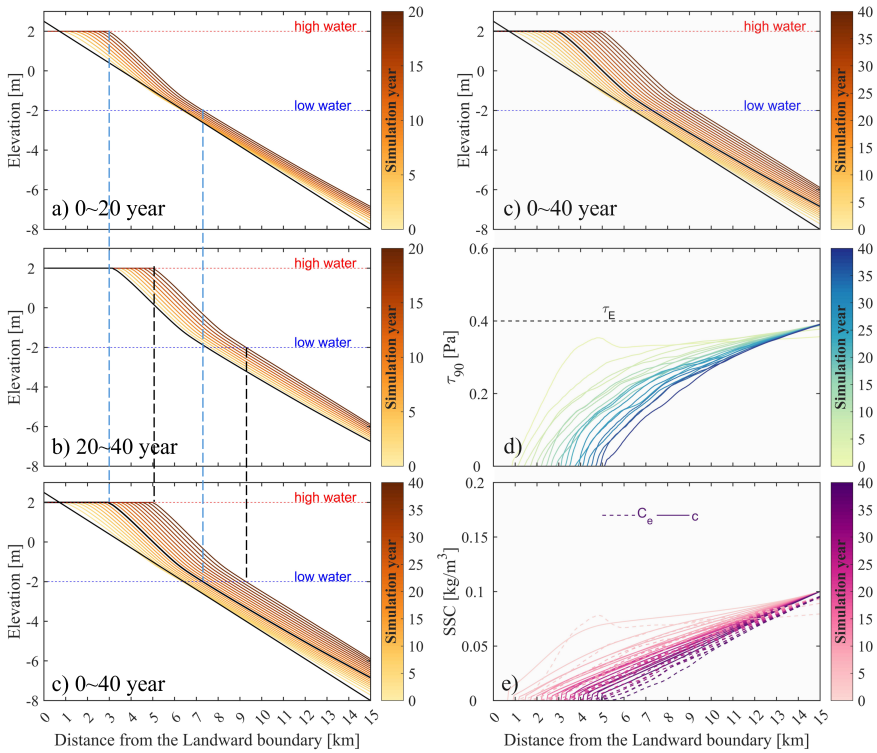


Figure 4.16: Temporal variation of the profile under natural conditions. a) 20-year profile evolution starting from a linear profile. b) 20-year profile evolution starting from the last step of a). c) 40-year profile evolution starting from a linear profile. d) and e) corresponding 90th percentile total BSS and SSC to c).

Through the comparison of the results, we found that the terrain at year 20 and year 40 in the independent simulations was identical to the results obtained from the continuous 40-year simulation. This confirms that the continuity of our model results in the process of morphological evolution is reliable. In fact, during the initial phase of the model run, the primary process was the adjustment of the profile shape to reach equilibrium. Specifically, as shown in Figures 4.16d and 4.16e, the cross-shore distribution of BSS and SSC gradually becomes parallel. This phase was mostly completed during the first 20 years of the simulation. Once the profile shape reached equilibrium, the entire profile maintained the same form and extended seaward. This characteristic is mainly reflected in the simulation during the latter 20 years.



#### 4.5.1.2. THE EFFECT OF MODEL SCHEMATIZATION

In this study our objective is to capture general tidal flat morphology responding patterns to various hydrodynamic forcing and sediment properties, rather than to predict precise morphological changes at specific sites. To this end, the DET-ESTMORF model is employed in a highly schematized manner.

The model is one-dimensional and does not account for alongshore sediment transport or other two-dimensional phenomena. Our results (see Figures 4.10 and 4.11) indicate that alongshore currents are significantly weaker on the intertidal flat than in the deep subtidal channels. Although these currents contribute to overall bed shear stress, they do not dominate the sediment transport on the intertidal zone. Given that the alongshore gradient is minimal over short distances, a one-dimensional model is sufficient to capture the system's dominant behaviour. While two-dimensional processes, such as tidal network formation, can affect detailed profile geometry and cross-shore sediment transport (Coco et al., 2013), they do not alter the primary conclusions drawn from our 1D model, which serves as a benchmark for future 2D investigations.

In addition, tidal forcing is represented solely by a single harmonic constituent ($M_2$ tide), and a uniform sediment composition is assumed. This approach treats the tidal flat profile as a unified system, and can adequately present the characteristic tidal induced BSS and erodibility of the system. We derive the conclusions by comparing the variations between systems not intra-system. Although a more detailed tidal signal and sediment composition representation might improve the

accuracy of tidal flat elevation simulations, it would not fundamentally change the main conclusions.

Overall, these simplifications facilitate a systematic investigation of the primary mechanisms driving tidal flat evolution and provide a foundation for future research incorporating higher-dimensional processes.

### 4.5.2. FURTHER INTERPRETATION OF THE MODEL RESULTS

#### 4.5.2.1. THE CONSTANT ALONGSHORE DISCHARGE



IN scenarios involving alongshore currents, we found that the model fails to reproduce the migration of tidal channel positions as the tidal flat progrades seaward. When calculating alongshore currents, the model assumes that the tidally averaged alongshore discharge remains constant within the model domain. This assumption holds for an open coastal environment with minimal topographic changes. However, as the tidal flat profile continues to prograde seaward, the alongshore discharge also shifts seaward, causing the alongshore current within the model domain to gradually decrease, ultimately altering the channel position. Currently, this model setup resembles a semi-enclosed estuarine cross-section rather than an open coast profile. On fringing tidal flats located in estuaries, study has shown that the position of deep estuarine channels can constrain the development space of adjacent tidal flats, thereby influencing the tidal flat profile (Hanssen et al., 2024). In contrast, on open coasts without the strict geometric constraints of estuaries, tidal channels and tidal flats typically migrate together (Pianca et al., 2014).

Although the alongshore flow discharge is held constant within a single scenario, resulting in no observed migration of the tidal channel position, a comparison of tidal channel positions under varying fixed alongshore flow discharges (as shown in Figure 4.17) reveals differences in the final offshore distances of stabilized tidal channels. Lower discharges lead to channels forming farther seaward. Figure 4.17c demonstrates that when the alongshore flow discharge is reduced mid-simulation, the final profile evolves toward a new equilibrium state, with the tidal channel also migrating seaward. Therefore, based solely on the modelling results in Section 4.3.3, we cannot conclude that shore-parallel tidal channels in open coasts necessarily constrain the development space of tidal flats on their landward side. From the current simulation results, it remains unclear whether the migration rates

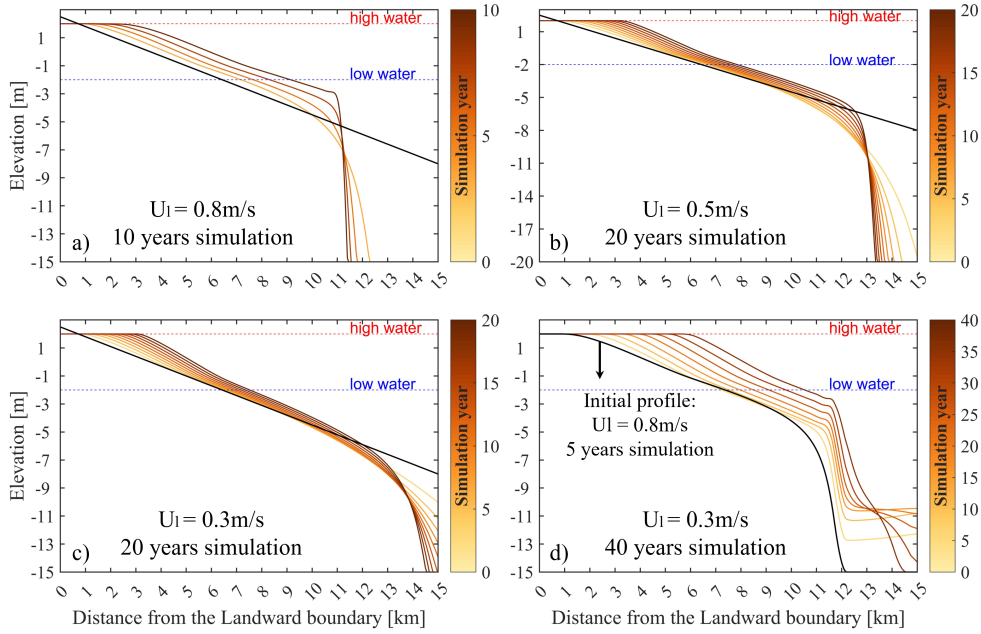


Figure 4.17: Simulated tidal flat profiles under different alongshore current velocities (discharges). a-c) Profiles evolved from an initially linear shape under mean alongshore current velocities of 0.8 m/s, 0.5 m/s, and 0.3 m/s, respectively, with profiles plotted every two years. d) Starting with a profile obtained after 5 years of simulation under a velocity of 0.8 m/s, the evolution was simulated for 40 years with a reduced velocity of 0.3 m/s, with profiles plotted every five years.

of tidal flats and tidal channels are equal under sufficient sediment supply. This question requires further investigation.

#### 4.5.2.2. THE VARIATION IN BOUNDARY CONDITIONS

In the model, the boundary conditions for each simulation remain constant over time, allowing the tidal flat profiles to eventually achieve an approximately stable configuration, characterized by consistent intertidal width and slope. However, in real-world environments, such idealized conditions rarely exist. Hydrodynamic forces and sediment supply are continuously changing over time, with sediment supply being particularly variable. Consequently, in reality, geomorphic features are constantly evolving toward new equilibrium states in response to these dynamic conditions (Zhou et al., 2017).

By comparing the profiles from different scenarios, we can qualitatively infer the likely direction of geomorphic evolution under varying boundary conditions. For

instance, both estuaries and coasts are facing declining sediment supply. The results from Scenario BC suggest that reduced sediment supply leads to steeper tidal flat profiles, narrower intertidal zones, slower seaward development, and, if the reduction is severe enough, even landward erosion. Numerous field measurements have shown that intertidal zones become steeper and narrower after reclamation over a certain period (Wu et al., 2024; Chen et al., 2016; Wang et al., 2012a; Yang et al., 2011). This is largely attributed to the fact that sediment supply in these regions was already diminishing.

#### 4.5.2.3. TIDAL FLAT ENVIRONMENTS SUITABLE FOR RECLAMATION



First of all, environments suitable for reclamation require tidal flats with the potential for continuous accretion, which is supported by sufficient sediment supply under local hydrodynamic conditions. This ensures that the width of the intertidal zone can recover relatively quickly after reclamation projects. Additionally, flatter tidal flats are preferable, as they allow for larger reclaimed areas at the same dyke elevation. According to model results, such environments are typically characterized by mild wave activity, smaller tidal ranges, and sediments that are less easily mobilized and more prone to deposition. Furthermore, the presence of shore-parallel tidal channels too close to the shoreline is undesirable, as it limits the extent of the tidal flat available for reclamation. To avoid this, alongshore currents should be as weak as possible, and bed sediments should remain relatively stable.

## 4.6. FUTURE STUDY

This study lays the groundwork for understanding tidal flat evolution and recovery following reclamation projects, but several aspects require further investigation to enhance the robustness and applicability of the findings. Future research can focus on the following areas:

### 4.6.1. EXPANDING THE RANGE OF MODEL PARAMETERS

The current study employs a limited set of parameter combinations and value ranges, which constrains the applicability of some conclusions to the specific conditions tested. For instance, the influence of sediment settling velocity on profile slope remains restricted within the tested ranges. Future research should explore a broader

spectrum of parameter combinations and variations to improve the generalizability of the conclusions.

### 4.6.2. REFINING BOUNDARY CONDITIONS

The boundary conditions in the current model are highly simplified and static over time. This approach does not account for the impacts of reclamation on hydrodynamic conditions, such as tidal range and tidal asymmetry. Additionally, the model assumes homogeneous sediment composition, neglecting changes in sediment sorting and associated variations in bed resistance to erosion, which could influence profile morphology and channel locations. Adjustments are also needed to more realistically represent alongshore flow discharges, preventing the model from resembling estuarine-fringing tidal flats rather than open-coast environments. Addressing these limitations in future studies will provide more nuanced insights.



### 4.6.3. INTEGRATING REAL-WORLD DATA

To validate the model results and improve its predictive capability for real-world applications, comprehensive datasets recording tidal flat evolution before and after reclamation are essential. Although direct observational data are limited, remote sensing techniques could be employed to analyse changes in intertidal zone positions and widths over time by tracking shifts in high- and low-water line locations.

### 4.6.4. INVOLVING BIOLOGICAL INFLUENCES

In current study, we only consider the bare tidal flat area. However, in reality, the presence of salt marshes and various benthic organisms introduces more complex ecological and geomorphic processes. These biological factors can significantly affect sediment dynamics, erosion, and accretion patterns, as well as the overall development of tidal flat morphology. We shall take these factors into account step by step in the future.

## 4.7. CONCLUSIONS

IN order to investigate the recovery of tidal flat profiles after reclamation, as well as the natural environmental factors that facilitate the restoration of the inter-

tidal zone morphology favourable for reclamation, a series of simulations were conducted using the DET-ESTMORF model. These simulations reversed the morphological changes before and after reclamation, as well as the profile evolution under different hydrodynamic conditions, sediment characteristics, and sediment supply combinations. By comparing the profile shapes before and after reclamation and the changes in sediment accommodation area across different sections, the following conclusions were drawn:

1. Under natural conditions, the tidal flat profile shape is solely determined by the dominant hydrodynamics, which manifest as an upward convex shape under strong tidal action, a downward concave shape under strong wave action, and a tidal channel form under alongshore current action. Tidal range, sediment characteristics, and sediment supply can alter the slope and location of the intertidal zone but do not change its convex or concave shape.

2. For naturally accreting tidal flats with sufficient sediment supply, the intertidal zone will gradually recover to its natural form and width after reclamation; for naturally eroding tidal flats, due to sediment shortages, the intertidal zone permanently narrows after reclamation and cannot recover. For naturally accreting tidal flats with tidal channels parallel to the shoreline, the intertidal zone can recover to its natural shape after reclamation; however, whether the channel will migrate seaward with the same speed of the flats or eventually restrict the extension of tidal flats needs further investigation.

3. Suitable tidal flat environments for reclamation should possess the ability to continuously accrete, have relatively gentle slopes, and avoid cross-shore constraints imposed by shore-parallel tidal channels. These characteristics typically align with the following natural conditions: ample sediment supply, weak wave forcing, bed sediments that are difficult to mobilize but easily settle, and as small alongshore currents as possible. These conditions are conducive to ensuring the effective restoration and stability of the tidal flat after reclamation.

# 5

# SYNTHESIS

THe preceding chapters have examined the morphological evolution of Jiangsu coastal tidal flats under both natural conditions and anthropogenic influences. Chapter 2 provided a detailed analysis of the spatial distribution of tidal flat morphology and sediment characteristics based on unique field data. This allowed for the identification of key morphological patterns and the formulation of initial hypotheses regarding their underlying mechanisms. Chapter 3 further investigated these mechanisms through numerical simulations, testing hypotheses related to hydrodynamics and sediment transport processes. Building upon this, Chapter 4 explored the response of tidal flats to coastal reclamation activities, with a particular focus on upper flat enclosure reclamation. Numerical modelling was employed to assess the impact of human interventions on tidal flat evolution and to evaluate the resilience of tidal flats under varying environmental conditions.



This chapter is structured into three sections. The first section revisits the research questions outlined in Chapter 1 and summarizes the key findings from the preceding chapters, highlighting the fundamental physical processes governing tidal flat evolution and their response to anthropogenic activities. The second section integrates these findings into a broader understanding of tidal flat dynamics, providing a comprehensive reflection on the study. Finally, the third section presents an outlook on future research directions, identifying critical knowledge gaps and potential methodological advancements that could further enhance our understanding of tidal flat evolution in the context of ongoing environmental and human-induced changes.

## 5.1. ANSWERS TO RESEARCH QUESTIONS

THIS section summarizes the key findings by addressing the core research questions formulated in Chapter 1.

(1) **What are the slopes of cross-shore intertidal flat profiles and the surficial sediment grain size distributions patterns along the Jiangsu Coast?**

The tidal flat morphology and surface sediments along the Jiangsu Coast exhibits distinct cross-shore and alongshore variations. In the cross-shore direction, sediment generally fines landward within the intertidal zone, a trend commonly observed in tide-dominated muddy environments. In the alongshore direction,

clear differences exist between the eroding northern coast and the accreting southern coast. The northern coast is characterized by steeper, concave-up profiles under erosional conditions, whereas the southern coast exhibits milder slopes with convex-up profiles, indicative of sediment accretion. Additionally, milder intertidal beach slope corresponding to coarser bed surface sediment is observed along the southern Jiangsu Coast, differing from trends commonly reported in other tidal environments, e.g. mud flats in the South San Francisco Bay (Bearman et al., 2010) and on the eastern coast of the Ariaka Bay, Japan (Yamada and Kobayashi, 2004). In the northern eroding region, alternating patterns of fine and coarse sediments emerge, likely influenced by variations in local clay content. These findings suggest that while many morphological and sediment distribution patterns along the Jiangsu Coast align with those documented in other tide-dominated muddy flats, certain regional deviations highlight unique environmental and hydrodynamic influences that merit further investigation.



(2) **What physical mechanisms are driving the formation of these observed patterns?**

The observed spatial patterns in tidal flat morphology and sediment distribution along the Jiangsu Coast are shaped by a combination of hydrodynamic forcing, and sediment provenance. The progressive flattening of tidal flats from north to south aligns with the regional shoreline evolution trend, where the northern coast is subject to erosion while the southern coast experiences accretion. In muddy environments, accreting flats typically develop milder slopes (Friedrichs, 2011), a trend that is also evident along the Jiangsu Coast. However, this alongshore variation in morphology is not solely governed by the gradient in hydrodynamic forcing; sediment provenance plays a crucial role, particularly in the transition zone between erosion and sedimentation, where local sediment properties become the dominant factor influencing tidal flat evolution.

The alongshore coarsening of surface sediments toward the south deviates from conventional expectations based on hydrodynamic sorting. As mentioned in the answer to the first question, in many tidal environments, finer sediments are typically associated with milder slopes. However, along the Jiangsu Coast, this pattern is reversed. This suggests that sediment grain size distribution is not controlled

by transport processes alone but instead is influenced by differences in sediment provenance. Variability in sediment supply along the coast appears to be a key factor driving these unexpected trends.

Anthropogenic activities, particularly large-scale reclamation projects, can also significantly alter the coastal system (Zhong and Hu, 2021; Flemming and Nyandwi, 1994). However, their specific impacts on tidal flat morphology and sediment characteristics cannot be fully assessed using a single-period dataset, as the data were collected too soon after the implementation of major reclamation projects. A longer-term investigation is necessary to disentangle the effects of natural processes from human interventions and to evaluate the full extent of their influence on tidal flat evolution.



(3) **What is the resilience of tidal flats in response to anthropogenic interventions under different natural environmental conditions?**

The resilience of tidal flats following anthropogenic interventions is governed by the dominant hydrodynamic forces, sediment supply, as well as pre-existing morphological characteristics. Under natural conditions, tidal flat profiles develop distinct shapes based on prevailing hydrodynamic conditions: convex profiles form under strong tidal forcing, concave profiles emerge with increased wave dynamics, and tidal channels develop under the influence of alongshore currents. While factors such as sediment characteristics, and sediment availability influence the steepness of intertidal slopes, they do not fundamentally alter these primary geometric shapes.

The capacity of a tidal flat to recover after reclamation is largely dependent on its natural morphological state. In naturally accreting environments where sediment supply is abundant, the intertidal zone tends to gradually restore both its original shape and width after reclamation. Conversely, in naturally eroding regions where sediment availability is limited, reclamation results in a permanent narrower intertidal zone, preventing full recovery. In cases where tidal channels run parallel to the shoreline within accreting systems, the intertidal zone may regain its original shape post-reclamation. However, whether these channels migrate seaward along with tidal flat progradation or eventually constrain further expansion depends on larger-scale morphological development and requires further investigation.

For tidal flat reclamation to be sustainable, the selected environments should exhibit long-term accretion potential, relatively mild slopes, and, where tidal channels are present, sufficient space between channels and shoreline to avoid interference with tidal flat evolution. Favourable conditions for post-reclamation recovery typically include a stable sediment supply, weak wave forcing, bed sediments that resist mobilization but facilitate deposition, and minimal alongshore current influence. These factors collectively enhance the resilience of tidal flats, ensuring their ability to recover and maintain stability following human interventions.

## 5.2. BROADER REFLECTIONS

### 5.2.1. THE DEBATE ON THE SEDIMENT SOURCE OF THE RADIAL SAND RIDGES



THE radial sand ridges (RSRs) represent a key morphological feature along the Jiangsu Coast due to their remarkable size and distinctive radial orientation. These extensive sand bodies provide habitat for a variety of species and supply sediment that promotes shoreline extension. The origin of the sediments forming the RSRs has long been a topic of debate. Various geological and geochemical studies have suggested multiple potential sources, with particular focus on the contributions of the Old Yellow River (OYR) and the Paleo-Yangtze River (PYR). Some studies suggest that the OYR was the dominant sediment supplier for the entire RSR system (Zhang, 1991; Ren and Shi, 1986). Others argue that the OYR only provided fine sediments to the northern RSRs (Li et al., 2001; Wang and Zhang, 1998). Some even propose that the PYR is widely considered the sole sediment source. (Wang et al., 2012b; Fu and Zhu, 1986; Yang, 1985). These conflicting interpretations largely stem from the inherent limitations of geological approaches, which rely on localized measurements and lack a broader dynamic perspective on sediment transport and morphological evolution.

Our numerical experiments indicate that the alongshore sediment grain size distribution cannot be solely explained by hydrodynamic forcing alone, implying that sediment provenance plays a dominant role. Additionally, the analysis of clay-to-silt ratios from sediment samples, as presented in Chapter 2, reveals that the sediments on the central Jiangsu tidal flat originate from multiple sources. These findings indirectly support the argument that the RSRs are not derived from a single

sediment source but instead result from a complex interplay of contributions from both the Old Yellow River and the Yangtze River. This underscores the necessity of adopting a more integrated approach that combines sediment provenance analysis with dynamic sediment transport modelling to better understand the formation and evolution of the RSR system.

### 5.2.2. THE RELATIVE IMPORTANCE OF HYDRODYNAMIC FORCINGS AND LOCAL SEDIMENT COMPOSITIONS IN DECIDING THE SHORELINE STATE

THE evolution of shorelines is governed not only by hydrodynamic forces but also by the inherent properties of the sediments present within the system. While hydrodynamic conditions dictate the potential for sediment transport, the actual rate and pattern of sediment redistribution are strongly influenced by local sediment provenance, including its resistance to erosion, cohesion, and settling velocity. These factors introduce spatial variability that can significantly modify the way sediments respond to hydrodynamic forcing, leading to deviations from predictions without considering variations of sediment properties, which has been proven by other modelling studies as well (e.g. Jiang et al., 2024; Xu et al., 2016).

A comprehensive understanding of shoreline evolution requires moving beyond highly simplified assumptions of uniform sediment characteristics. Instead, spatial heterogeneity in sediment properties must be integrated into predictive models, as the combination of hydrodynamics and sediment provenance plays a crucial role in determining erosion and deposition patterns. By considering both external forcing mechanisms and local sedimentological controls, we can improve the accuracy of shoreline evolution models and develop more effective strategies for coastal management and protection.

### 5.2.3. INTEGRATED CONSIDERATIONS FOR SUSTAINABLE RECLAMATION

THE suitability of tidal flats for reclamation is not solely determined by their local morphological characteristics but also by broader environmental and anthropogenic influences that shape their long-term evolution. While environments conducive to tidal flat restoration generally exhibit continuous sediment accretion, sufficient sediment supply, and moderate hydrodynamic conditions, these factors do not exist in isolation. Human activities beyond the immediate coastline, such as

dam construction in rivers and large-scale coastal engineering projects, have profound downstream effects on tidal flat development (Kirwan and Megonigal, 2013; Yang et al., 2011; Blum and Roberts, 2009). These interventions collectively modify hydrodynamic gradients, alter sediment transport pathways, and ultimately reshape the coastal environment.

For sustainable reclamation planning, it is crucial to recognize that individual engineering projects do not act in isolation. The cumulative effects of upstream and coastal modifications must be considered holistically to assess their combined impact on tidal flat dynamics. For instance, while model results suggest that environments with mild wave activity, appropriate tidal ranges, and stable sediment beds are favourable for post-reclamation restoration, these conditions can be significantly influenced by sediment supply changes resulting from upstream damming (e.g. Yang et al., 2011). Similarly, the presence of shore-parallel tidal channels too close to the shoreline can limit tidal flat expansion, a factor that may be exacerbated by anthropogenic alterations to alongshore sediment transport (e.g. Xing et al., 2022).



Therefore, sustainable coastal management requires a shift from localized impact assessments to an integrated framework that accounts for interactions across the entire sedimentary system. By considering the interdependence of riverine, estuarine, and coastal processes, we can develop more resilient reclamation strategies that align with long-term environmental stability and sustainable coastal development goals.

### 5.2.4. FROM UNDERSTAND THE SYSTEM TO UTILIZE THE SYSTEM EFFECTIVELY

EFFECTIVE management and utilization of tidal flat resources require a deep understanding of their natural dynamics. While short-term reclamation projects can offer immediate economic benefits, the long-term impacts—such as increased vulnerability to natural disasters and ecosystem degradation—can result in economic losses that outweigh these initial gains (Chee et al., 2023; Xu et al., 2021; Zhang et al., 2021; Zhu et al., 2016). Therefore, to manage these resources efficiently, it is essential to preserve the natural evolution of tidal flats as much as possible.

Understanding the system means recognizing that tidal flats evolve and recover differently depending on local environmental conditions. Utilizing the system ef-

fectively means to ensure that development projects align with the natural characteristics of the tidal flats, minimizing disruptions and enhancing long-term sustainability. By applying the knowledge developed in this thesis, we can identify locations where sustainable engineering and reclamation are best feasible.

## 5.3. OUTLOOKS

### 5.3.1. RECOMMENDATION FOR FUTURE DATA COLLECTION AND ANALYSIS

A comprehensive understanding of tidal flat evolution requires multi-method observational approaches to capture both spatial and temporal variations. Our current study, based on a single large-scale field survey (Zhang, 2012), has enabled us to analyse the spatial distribution of tidal flat morphology and sediment characteristics. However, without repeated measurements, it is challenging to assess dynamic temporal changes in tidal flat geomorphology. For integrated coastal management planning, it is imperative to understand how these spatial features vary over time and to validate numerical model for future prediction. This necessitates tracking and recording the temporal changes in Jiangsu's tidal flat resources. There are several established long-term cross-sectional monitoring stations (e.g. Gong et al., 2017; Wang et al., 2012a) on the Jiangsu Coast. However, these stations are concentrated in the central region, capturing only local tidal flat evolution and failing to reflect the evolution patterns of tidal flats under different environmental conditions along the entire Jiangsu coastline.

While it is impractical to monitor every cross-section (as marked in Chapter 2) on an annual or seasonal basis due to resource constraints, a strategic approach can be adopted. By combining existing information on alongshore distribution of hydrodynamics, sediment supply, shoreline accretion and erosion status, vegetation cover, and the locations of human interventions (Zhang, 2012), several representative cross-sections—selected in a manner similar to the four characteristic profiles outlined in Chapter 3—can be continuously observed. These observations should focus on parameters such as local hydrodynamic information, vegetation distribution, tidal flat profile, as well as bed sediment grain size distribution. In addition, (variations in) alongshore processes are also important to the evolution of coastal tidal flats. However, it is challenging to assess their influence based solely on these

isolated transects. Remote sensing can bridge this gap by providing valuable data on the evolution of intertidal zone area, the distribution of human activities, vegetation extent, and coastal land-use zoning (Xu et al., 2024; Sun et al., 2023; Xu et al., 2022). Furthermore, monitoring should capture both annual trends and seasonal variations, including the changes following extreme events like storm surges. By integrating these diverse data, we can achieve a more systematic understanding of the spatiotemporal evolution of Jiangsu's tidal flats and identify the dominant physical processes and mechanisms across different regions and timescales. Moreover, by combining analyses of large-scale hydrodynamic and sediment supply dynamics with assessments of ecological and anthropogenic influences, we can develop more scientifically robust and comprehensive coastal management strategies.

For engineered tidal flats, additional data collection is necessary to improve our understanding of their morphological adaptation in response to human interventions. This includes detailed observations of morphological evolution as well as sediment grain size distribution before and after reclamation, which are crucial for validating numerical model results and improving predictive capabilities for practical applications. Given the challenges associated with obtaining historical post-reclamation profile data, remote sensing techniques, such as satellite imagery, can serve as a valuable tool to reconstruct past changes in intertidal morphology as well as the sediment characteristics (Zhao et al., 2023; Wang et al., 2018). By tracking shifts in high- and low-water lines over time, remote sensing provides an effective means of assessing the width and location of tidal flats and filling data gaps in long-term monitoring records. These datasets can robustly support our simulation results regarding both the short- and long-term responses of tidal flats to reclamation projects under varying environmental conditions. They also offer quantitative benchmarks for validating model outputs, such as post-reclamation recovery rates, thereby enhancing the reliability of the model's predictive capabilities for tidal flat evolution.



### 5.3.2. IMPROVEMENT IN THE MODEL SETTING

The DET-ESTMORF model employed in this study captures highly simplified scenarios, omitting several secondary processes that influence detailed tidal flat evolution. In particular, it does not account for hydrodynamic responses to

anthropogenic activities (Chu et al., 2022; Suh et al., 2014), sediment sorting effects (Zhou et al., 2021; Zhou et al., 2015), interactions between sand and mud fractions as well as the spatial heterogeneity of bed surface erosion resistance (Colina Alonso et al., 2023; Van Ledden et al., 2004). Nevertheless, our simplified model incorporates the critical physical processes and reflects the overall relationship between hydrodynamic forcing, sediment characteristics, sediment supply and the tidal flat morphology, thereby capturing the general evolution trend of tidal flat profiles. Due to the omission of these aforementioned processes, the current model cannot quantitatively simulate the detailed evolution of tidal flat profiles or analyse the specific roles of these processes and the perturbations induced by human activities. These limitations constrain the model's ability to fully represent the complex dynamics of tidal flat development, particularly under the influence of large-scale reclamation projects.



Apart from expanding the range of model parameters—such as sediment settling velocity and erosion thresholds—to enhance the generalizability of the findings beyond the specific conditions tested in Chapter 4, there are several further improvements to the model possible. These improvements focus on refining both the physical parameterization and boundary conditions.

Firstly, incorporating multiple sediment fractions would allow for a representation of sediment sorting, variations in bed resistance to erosion, and channel formation and migration. Collectively, involving these processes can lead to a more robust understanding of long-term morphological evolution. Besides, current static hydrodynamic boundary conditions failed to account for the feedback between reclamation and hydrodynamic processes, such as modifications to tidal range and tidal asymmetry. Future studies should integrate more detailed hydrodynamic models to generate dynamic boundary conditions that better reflect the real-world impacts of coastal engineering interventions. A promising approach is to couple idealized conceptual models with process-based numerical models - such as Delft3D (Deltares, 2014) – to simulate the temporal variations in hydrodynamic forcing resulting from human activities. By allowing the boundary conditions of the idealized model to evolve dynamically rather than remain fixed, this coupling would provide a more comprehensive assessment of the interactions between anthropogenic interventions and natural tidal flat development. Addressing these improvements will

significantly enhance the predictive capability of the model, ultimately supporting more effective coastal management strategies.

Beyond the physical processes and human activities governing tidal flat evolution, biological factors play a crucial role in modulating sediment dynamics and morphological development (Zhou et al., 2022). While this study focuses on bare tidal flats, natural intertidal systems often include salt marshes and benthic organisms, which influence sediment stabilization, accretion patterns, and hydrodynamic conditions (Paarlberg et al., 2005). The presence of vegetation, for instance, can enhance sediment retention and mitigate wave-induced erosion (Jiang et al., 2025), while bioturbation by benthic fauna can alter sediment composition and erodibility (Joensuu et al., 2018). Incorporating these ecological interactions into future research will provide a more holistic understanding of tidal flat evolution, bridging the gap between geomorphological and ecological processes.



### 5.3.3. EXPANDING THE TEMPORAL PERSPECTIVE

Tidal flat evolution operates across multiple timescales, ranging from short-term variations driven by extreme weather events (Xie et al., 2021; Bartholdy and Aagaard, 2001) to long-term changes influenced by sea-level rise and climate change (Guo et al., 2022; Kirwan and Megonigal, 2013). Understanding these temporal dynamics is essential for predicting future tidal flat responses and improving coastal management strategies.

On shorter timescales, extreme events such as storms and typhoons can induce abrupt morphological changes, significantly altering tidal flat profiles within days or weeks (Gong et al., 2019a). However, these systems also exhibit natural recovery processes, gradually re-establishing equilibrium post-disturbance (de Vet et al., 2020). Future research should focus on quantifying the mechanisms and timescales of these recovery processes, as well as identifying the conditions under which human interventions might either hinder or facilitate natural restoration.

Over longer timescales, climate change and sea-level rise will fundamentally reshape tidal flat morphodynamics (van der Wegen et al., 2017). Reclamation projects, by restricting the landward migration of tidal flats, can disrupt their natural adaptation to these changing conditions, potentially leading to coastal squeeze and loss of intertidal habitats (Guo et al., 2022). Future studies must integrate climate change

considerations into coastal engineering planning, assessing how reclamation affects tidal flat resilience under rising sea levels.

# List of References


Alexander, C. R., Nittrouer, C. A., Demaster, D. J., Yong-Ahn Park, & Soo-Chul Park. (1991). Macrotidal mudflats of the southwestern Korean coast: a model for interpretation of intertidal deposits. *Journal of Sedimentary Petrology*, *61*(5), 805–824.

Allen, J. R. (2000). Morphodynamics of Holocene salt marshes: A review sketch from the Atlantic and Southern North sea coasts of Europe. *Quaternary Science Reviews*, *19*(12), 1155–1231.

Amos, C. L. (1995). Siliciclastic Tidal Flats. *Developments in Sedimentology*, *53*, 273–306.

Amos, C. L., Umgiesser, G., Ferrarin, C., Thompson, C. E., Whitehouse, R. J., Sutherland, T. F., & Bergamasco, A. (2010). The erosion rates of cohesive sediments in Venice lagoon, Italy. *Continental Shelf Research*, *30*(8), 859–870.

Andersen, T. J., & Pejrup, M. (2001). Suspended sediment transport on a temperate, microtidal mudflat, the Danish Wadden Sea. *Marine Geology*, *173*(1-4), 69–85.

Archer, A. W. (1995). Modeling of cyclic tidal rhythmites based on a range of diurnal to semidiurnal tidal-station data. *Marine Geology*, *123*(1-2), 1–10.

Bale, A. J., Stephens, J. A., & Harris, C. B. (2007). Critical erosion profiles in macrotidal estuary sediments: Implications for the stability of intertidal mud and the slope of mud banks. *Continental Shelf Research*, *27*(18), 2303–2312.

Bao, J. (2016). *Jiangsu coastal salt making geography and changes of human-land relationship during the 15-20th centuries*. Fudan University Press (in Chinese).

Bao, J., & Gao, S. (2016). Traditional coastal management practices and land use changes during the 16–20th centuries, Jiangsu Province, China. *Ocean & Coastal Management*, *124*, 10–21.

Bartholdy, J., & Aagaard, T. (2001). Storm surge effects on a back-barrier tidal flat of the Danish Wadden Sea. *Geo-Marine Letters*, *20*(3), 133–141.

Bearman, J. A., Friedrichs, C. T., Jaffe, B. E., & Foxgrover, A. C. (2010). Spatial Trends in Tidal Flat Shape and Associated Environmental Parameters in South San Francisco Bay. *Journal of Coastal Research*, *262*(2), 342–349.

Bianchi, T. S., Mayer, L. M., Amaral, J. H., Arndt, S., Galy, V., Kemp, D. B., Kuehl, S. A., Murray, N. J., & Regnier, P. (2024). Anthropogenic impacts on mud and organic carbon cycling. *Nature Geoscience*, *17*, 287–297.

Blum, M. D., & Roberts, H. H. (2009). Drowning of the Mississippi Delta due to insufficient sediment supply and global sea-levelrise. *Nature Geoscience*, *2*(7), 488–491.

Brown, A. G., Tooth, S., Bullard, J. E., Thomas, D. S., Chiverrell, R. C., Plater, A. J., Murton, J., Thorndycraft, V. R., Tarolli, P., Rose, J., Wainwright, J., Downs, P., & Aalto, R. (2017). The geomorphology of the Anthropocene: emergence, status and implications. *Earth Surface Processes and Landforms*, *42*(1), 71–90.

Bujan, N., Cox, R., & Masselink, G. (2019). From fine sand to boulders: Examining the relationship between beach-face slope and sediment size. *Marine Geology*, *417*, 106012.

Byun, D. S., Wang, X. H., & Holloway, P. E. (2004). Tidal characteristic adjustment due to dyke and seawall construction in the Mokpo Coastal Zone, Korea. *Estuarine, Coastal and Shelf Science*, *59*(2), 185–196.

Carling, P., Williams, J., Croudace, I., & Amos, C. (2009). Formation of mud ridge and runnels in the intertidal zone of the Severn Estuary, UK. *Continental Shelf Research*, *29*(16), 1913–1926.

Chee, S. Y., Tan, M. L., Tew, Y. L., Sim, Y. K., Yee, J. C., & Chong, A. K. M. (2023). Between the devil and the deep blue sea: Trends, drivers, and impacts of coastal reclamation in Malaysia and way forward. *Science of the Total Environment*, *858*, 159889.

Chen, L., Zhou, Z., Xu, M., Xu, F., Tao, J., & Zhang, C. (2018). Exploring the influence of land reclamation on sediment grain size distribution on tidal flats: A numerical study. *Coastal Engineering Proceedings*, (36), 85–85.

Chen, P., Sun, Z., Zhou, X., Xia, Y., Li, L., He, Z., Wang, R., & Xie, H. (2021). Impacts of coastal reclamation on tidal and sediment dynamics in the Rui'an coast of China. *Ocean Dynamics*, *71*(3), 323–341.

Chen, Y., Dong, J., Xiao, X., Zhang, M., Tian, B., Zhou, Y., Li, B., & Ma, Z. (2016). Land claim and loss of tidal flats in the Yangtze Estuary. *Scientific Reports*, *6*, 1–10.

Chen, Y., Xie, D., Zhang, C., & Qian, X. (2013). Estimation of long-term wave statistics in the East China Sea. *Journal of Coastal Research*, *65*, 177–182.

Choi, S. M., Seo, J. Y., & Ha, H. K. (2023). Contribution of local erosion enhanced by winds to sediment transport in intertidal flat. *Marine Geology*, *465*, 107171.

Choi, Y. R. (2019). Profitable tidal flats, governable fishing communities: Assembling tidal flat fisheries in post-crisis South Korea. *Political Geography*, *72*, 20–30.

Christensen, E. D., Jensen, J. H., & Mayer, S. (2001). Sediment transport under breaking waves. In *Coastal engineering 2000* (pp. 2467–2480).

Christoffersen, J. B. (1982). *Current depth refraction of dissipative water waves.* (tech. rep.). Institute of Hydrodynamics and Hydraulic Engineering, Technical University of Denmark.

Christoffersen, J. B., & Jonsson, I. G. (1985). Bed friction and dissipation in a combined current and wave motion. *Ocean Engineering*, *12*(5), 387–423.

Chu, N., Yao, P., Ou, S., Wang, H., Yang, H., & Yang, Q. (2022). Response of tidal dynamics to successive land reclamation in the Lingding Bay over the last century. *Coastal Engineering*, *173*, 104095.

Coco, G., Zhou, Z., van Maanen, B., Olabarrieta, M., Tinoco, R., & Townend, I. (2013). Morphodynamics of tidal networks: Advances and challenges. *Marine Geology*, *346*, 1–16.

Colina Alonso, A., van Maren, D. S., van Weerdenburg, R. J., Huismans, Y., & Wang, Z. B. (2023). Morphodynamic Modeling of Tidal Basins: The Role of Sand-Mud Interaction. *Journal of Geophysical Research: Earth Surface*, *128*(9), 1–22.

Davies, J. (1964). A morphogenic approach to world shoreline. *Zeitschrift für Geomorphologie*, *8*, 27–42.

Davis, R. A., & Hayes, M. O. (1984). What is a wave-dominiated coast? *Marine Geology*, *60*, 313–329.

de Vet, P. L., van Prooijen, B. C., Colosimo, I., Steiner, N., Ysebaert, T., Herman, P. M., & Wang, Z. B. (2020). Variations in storm-induced bed level dynamics across intertidal flats. *Scientific Reports*, *10*(1), 1–15.

Dean, R. G. (1991). Equilibrium beach profiles: characteristics and applications. *Journal of Coastal Research*, *7*(1), 53–84.

Deegan, L. A., Johnson, D. S., Warren, R. S., Peterson, B. J., Fleeger, J. W., Fagherazzi, S., & Wollheim, W. M. (2012). Coastal eutrophication as a driver of salt marsh loss. *Nature*, *490*(7420), 388–392.

Deltares. (2014). *Delft3D 4 - hydrodynamic and morphodynamic modelling suite*. Deltares.

Elfrink, B., & Baldock, T. (2002). Hydrodynamics and sediment transport in the swash zone: A review and perspectives. *Coastal Engineering*, *45*(3-4), 149–167.

Engelund, F., & Hansen, E. (1967). *A monograph on sediment transport in alluvial streams*.

Fan, D., Wang, Y., & Liu, M. (2013). Classifications, sedimentary features and facies associations of tidal flats. *Journal of Palaeogeography*, *2*(1), 66–80.

Firoozfar, A., Neshaei, M., & Dykes, A. (2014). Beach Profiles and Sediments, a Case of Caspian Sea. *International Journal of Marine Science*, *4*(43), 1–9.

Fivash, G. S., Temmerman, S., Kleinhans, M. G., Heuner, M., van der Heide, T., & Bouma, T. J. (2023). Early indicators of tidal ecosystem shifts in estuaries. *Nature communications*, *14*(1), 1911.

Flemming, B. W., & Nyandwi, N. (1994). Land reclamation as a cause of fine-grained sediment depletion in backbarrier tidal flats (Southern North Sea). *Netherlands Journal of Aquatic Ecology*, *28*(3-4), 299–307.

Foley, S. F., Gronenborn, D., Andreae, M. O., Kadereit, J. W., Esper, J., Scholz, D., Pöschl, U., Jacob, D. E., Schöne, B. R., Schreg, R., Vött, A., Jordan, D., Lelieveld, J., Weller, C. G., Alt, K. W., Gaudzinski-Windheuser, S., Bruhn, K. C., Tost, H., Sirocko, F., & Crutzen, P. J. (2013). The Palaeoanthropocene - The beginnings of anthropogenic environmental change. *Anthropocene*, *3*, 83–88.

Folk, R., & Ward, W. (1957). Brazos River bar (Texas); a study in the significance of grain size parameters. *Journal of sedimentary research*, *27*(1), 3–26.

Francis P. Shepard. (1954). Nomenclature Based on Sand-silt-clay Ratios. *Journal of Sedimentary Research*, *Vol. 24*(3), 151–158.

Friedrichs, C. T. (2011). Tidal Flat Morphodynamics: A Synthesis. In *Treatise on estuarine and coastal science* (pp. 137–170). Academic Press.

Fu, M. Z., & Zhu, D. K. (1986). The sediment sources of the offshore submarine sand ridge field of the coast of Jiangsu province (in Chinese with an English abstract). *Journal of Nanjing University (Natural Sciences Edition)*, *22*(3), 536–544.

Galappatti, G., Vreugdenhil, C. B., Armanini, A., & Di Silvio, G. (1986). A Depth-Integrated Model for Suspended Sediment Transport. *Journal of Hydraulic Research*, *24*(5), 437–442.

Gao, G. D., Wang, X. H., & Bao, X. W. (2014). Land reclamation and its impact on tidal dynamics in Jiaozhou Bay, Qingdao, China. *Estuarine, Coastal and Shelf Science*, *151*, 285–294.

Gao, S. (2009). Modeling the preservation potential of tidal flat sedimentary records, Jiangsu coast, eastern China. *Continental Shelf Research*, *29*(16), 1927–1936.

Gao, S. (2019). Geomorphology and sedimentology of tidal flats. In *Coastal wetlands* (pp. 359–381). Elsevier B.V.

Gao, S., & Collins, M. (1994). Tidal inlet stability in response to hydrodynamic and sediment dynamic conditions. *Coastal Engineering*, *23*(1-2), 61–80.

Gong, J. C., Li, B. H., Hu, J. W., Ding, X. J., Liu, C. Y., & Yang, G. P. (2023). Tidal effects on carbon dioxide emission dynamics in intertidal wetland sediments. *Environmental Research*, *238*, 117110.

Gong, Z., Huang, S., Xu, B., Zhu, S., Zhang, Y., & Zhou, Z. (2019a). Evolution of tidal flat in response to storm surges: a case study from the central Jiangsu Coast (in Chinese with an English abstract). *Advances in Water Science*, *30*(2), 243–254.

Gong, Z., Jin, C., Zhang, C., Zhou, Z., Zhang, Q., & Li, H. (2017). Temporal and spatial morphological variations along a cross-shore intertidal profile, jiangsu, china. *Continental Shelf Research*, *144*, 1–9.

Gong, Z., Wang, Z., Stive, M. J. F., Zhang, C., & Chu, A. (2012). Process-Based Morphodynamic Modeling of a Schematized Mudflat Dominated by a Long-Shore Tidal Current at the Central Jiangsu Coast, China. *Journal of Coastal Research*, *285*(6), 1381–1392.

Gong, Z., Zhang, Y., Zhao, K., Zhou, Z., & Zhang, C. (2019b). Advances in coastal storm impacts on morphological evolution of mud tidal flat-creek system

(in Chinese with an English abstract). *Advances in Science and Technology of Water esources*, *39*(4), 75–84.

Grabowski, R. C., Droppo, I. G., & Wharton, G. (2011). Erodibility of cohesive sediment: The importance of sediment properties. *Earth-Science Reviews*, *105*(3-4), 101–120.

Green, M. O., & Coco, G. (2007). Sediment transport on an estuarine intertidal flat: Measurements and conceptual model of waves, rainfall and exchanges with a tidal creek. *Estuarine, Coastal and Shelf Science*, *72*(4), 553–569.

Gugliotta, M., Saito, Y., Nguyen, V. L., Ta, T. K. O., & Tamura, T. (2019). Sediment distribution and depositional processes along the fluvial to marine transition zone of the Mekong River delta, Vietnam. *Sedimentology*, *66*(1), 146–164.

Gunaratna, T., Suzuki, T., & Yanagishima, S. (2019). Cross-shore grain size and sorting patterns for the bed profile variation at a dissipative beach: Hasaki Coast, Japan. *Marine Geology*, *407*, 111–120.

Guo, L., Zhu, C., Xu, F., Xie, W., Van Der Wegen, M., Townend, I., Wang, Z. B., & He, Q. (2022). Reclamation of tidal flats within tidal basins alters centennial morphodynamic adaptation to sea-level rise. *Journal of Geophysical Research: Earth Surface*, *127*(6), e2021JF006556.

Hanssen, J. L. J., van Prooijen, B. C., Volp, N. D., de Vet, P. L. M., & Herman, P. M. J. (2022). Where and why do creeks evolve on fringing and bare tidal flats? *Geomorphology*, *403*, 108182.

Hanssen, J. L., van Prooijen, B. C., & van Maren, D. S. (2024). The shape of fringing tidal flats in engineered estuaries. *Frontiers in Marine Science*, *11*, 1–15.

Horn, S., Schwemmer, P., Mercker, M., Enners, L., Asmus, R., Garthe, S., & Asmus, H. (2020). Species composition of foraging birds in association with benthic fauna in four intertidal habitats of the Wadden Sea. *Estuarine, Coastal and Shelf Science*, *233*, 106537.

Hu, Z., Wang, Z. B., Zitman, T. J., Stive, M. J., & Bouma, T. J. (2015). Predicting long-term and short-term tidal flat morphodynamics using a dynamic equilibrium theory. *Journal of Geophysical Research : Earth Surface*, *120*(9), 1803–1823.

Hughes, Z. J. (2012). Tidal channels on tidal flats and marshes. *Principles of tidal sedimentology*, 269–300.

Jepsen, R., McNeil, J., & Lick, W. (2000). Effects of gas generation on the density and erosion of sediments from the Grand River. *Journal of Great Lakes Research*, *26*(2), 209–219.

Jiang, C. H., Zhou, Z., Townend, I. H., Guo, L. C., Wei, Y. Z., Luo, F., & Zhang, C. K. (2024). Modelling the impact of sediment composition on long-term estuarine morphodynamics. *Coastal Engineering*, *193*, 104595.

Jiang, G., & Feng, H. (1991). The effect of dike on development of tidal flat profiles (in Chinese with an English abstract). In the Chinese Society of Oceanology and Limnology (Ed.), *Proceedings of the fourth chinese oceanological and limnological science conference* (pp. 26–33). Science Press.

Jiang, W., Huang, Z., Dai, Z., Luo, J., Zeng, W., & Liang, X. (2025). Attenuation of Hydro - Sediment Dynamics Progradation Over Mangrove Wetland. *Journal of Geophysical Research: Oceans*, *130*(2), 1–20.

Joensuu, M., Pilditch, C. A., Harris, R., Hietanen, S., Pettersson, H., & Norkko, A. (2018). Sediment properties, biota, and local habitat structure explain variation in the erodibility of coastal sediments. *Limnology and Oceanography*, *63*(1), 173–186.

Karunarathna, H., Horrillo-Caraballo, J., Kuriyama, Y., Mase, H., Ranasinghe, R., & Reeve, D. E. (2016). Linkages between sediment composition, wave climate and beach profile variability at multiple timescales. *Marine Geology*, *381*, 194–208.

Kim, B. O. (2003). Tidal modulation of storm waves on a macrotidal flat in the Yellow Sea. *Estuarine, Coastal and Shelf Science*, *57*(3), 411–420.

King, C. (1972). *Beaches and Coasts* (second ed.). Edward Arnold.

Kirby, R. (2000). Practical implications of tidal flat shape. *Continental Shelf Research*, *20*(10-11), 1061–1077.

Kirwan, M. L., & Megonigal, J. P. (2013). Tidal wetland stability in the face of human impacts and sea-level rise. *Nature*, *504*(7478), 53–60.

Klein, G. d. (1985). Intertidal flats and intertidal sand bodies. In *Coastal sedimentary environments* (pp. 187–224). Springer.

Kleinhans, M. G., Schuurman, F., Bakx, W., & Markies, H. (2009). Meandering channel dynamics in highly cohesive sediment on an intertidal mud flat in the Westerschelde estuary, the Netherlands. *Geomorphology*, *105*(3-4), 261–276.

Kuai, Y., Tao, J., Zhou, Z., Aarninkhof, S., & Wang, Z. B. (2021). Sediment Characteristics and Intertidal Beach Slopes along the Jiangsu Coast, China. *Journal of Marine Science and Engineering*, *9*(3), 347.

Le Hir, P., Roberts, W., Cazaillet, O., Christie, M., Bassoullet, P., & Bacher, C. (2000). Characterization of intertidal flat hydrodynamics. *Continental Shelf Research*, *20*(12-13), 1433–1459.

Lee, S.-C., & Mehta, A. J. (1997). Problems in Characterizing Dynamics of Mud Shore Profiles. *Journal of Hydraulic Engineering*, *123*(4), 351–361.

Lesser, G., Roelvink, J., van Kester, J., & Stelling, G. (2004). Development and validation of a three-dimensional morphological model. *Coastal Engineering*, *51*(8-9), 883–915.

Li, C. X., Zhang, J. Q., Fan, D. D., & Deng, B. (2001). Holocene regression and the tidal radial sand ridge system formation in the Jiangsu coastal zone, east China. *Marine Geology*, *173*(1-4), 97–120.

Li, J., Chen, X., Townend, I., Shi, B., Du, J., Gao, J., Chuai, X., Gong, Z., & Wang, Y. P. (2021). A comparison study on the sediment flocculation process between a bare tidal flat and a clam aquaculture mudflat: The important role of sediment concentration and biological processes. *Marine Geology*, *434*.

Liu, C., Zhang, Z., Zhang, X., Ren, H., Liu, B., Bao, Z., & Xiaoxiang, Z. (2019). Coastal development history and tidal flat ecosystem conservation along the coast of Jiangsu Province, China. *Journal of Coastal Conservation*, *23*(4), 857–867.

Liu, J., Kong, X., Saito, Y., Liu, J. P., Yang, Z., & Wen, C. (2013). Subaqueous deltaic formation of the Old Yellow River (AD 1128–1855) on the western South Yellow Sea. *Marine Geology*, *344*, 19–33.

Liu, X. J., Gao, S., & Wang, Y. P. (2011). Modeling profile shape evolution for accreting tidal flats composed of mud and sand: A case study of the central Jiangsu coast, China. *Continental Shelf Research*, *31*(16), 1750–1760.

Maan, D. C., Van Prooijen, B. C., Wang, Z. B., & De Vriend, H. J. (2015). Do intertidal flats ever reach equilibrium? *Journal of Geophysical Research: Earth Surface*, *120*(11), 2406–2436.

Mariotti, G., & Fagherazzi, S. (2012). Channels-tidal flat sediment exchange : The channel spillover mechanism. *Journal of Geophysical Research: Oceans*, *117*, 1–18.

Martín-Antón, M., Negro, V., del Campo, J. M., López-Gutiérrez, J. S., & Esteban, M. D. (2016). Review of coastal land reclamation situation in the world. *Journal of Coastal Research*, *75*, 667–671.

Medina, R., Losada, M., Losada, I., & Vidal, C. (1994). Temporal and spatial relationship between sediment grain size and beach profile. *Marine Geology*, *118*(3-4), 195–206.

Miao, D., & Xue, Z. (2021). The current developments and impact of land reclamation control in China. *Marine Policy*, *134*, 104782.

Milliman, J. D., Huang-ting, S., Zuo-sheng, Y., & H. Mead, R. (1985). Transport and deposition of river sediment in the Changjiang estuary and adjacent continental shelf. *Continental Shelf Research*, *4*(1-2), 37–45.

Muller, J. R., Chan, Y., Piersma, T., Chen, Y., Aarninkhof, S. G., Hassell, C. J., Tao, J., Gong, Z., Wang, Z. B., & van Maren, D. S. (2020a). Building for Nature: Preserving Threatened Bird Habitat in Port Design. *Water*, *12*(8).

Muller, J. R., Chen, Y., Aarninkhof, S. G., Chan, Y., Piersma, T., van Maren, D. S., Tao, J., Wang, Z. B., & Gong, Z. (2020b). Ecological impact of land reclamation on Jiangsu coast (China): A novel ecotope assessment for Tongzhou Bay. *Water Science and Engineering*, *13*(1), 57–64.

Murray, N. J., Phinn, S. R., DeWitt, M., Ferrari, R., Johnston, R., Lyons, M. B., Clinton, N., Thau, D., & Fuller, R. A. (2019). The global distribution and trajectory of tidal flats. *Nature*, *565*(7738), 222–225.

Newton, A., Icely, J., Cristina, S., Perillo, G. M., Turner, R. E., Ashan, D., Cragg, S., Luo, Y., Tu, C., Li, Y., Zhang, H., Ramesh, R., Forbes, D. L., Solidoro, C., Béjaoui, B., Gao, S., Pastres, R., Kelsey, H., Taillie, D., … Kuenzer, C. (2020). Anthropogenic, Direct Pressures on Coastal Wetlands. *Frontiers in Ecology and Evolution*, *8*, 1–29.

Ouyang, X., & Lee, S. Y. (2020). Improved estimates on global carbon stock and carbon pools in tidal wetlands. *Nature Communications*, *11*(1), 1–7.

Paarlberg, A. J., Knaapen, M. A., De Vries, M. B., Hulscher, S. J., & Wang, Z. B. (2005). Biological influences on morphology and bed composition of an intertidal flat. *Estuarine, Coastal and Shelf Science*, *64*(4), 577–590.

Partheniades, E. (1965). Erosion and Deposition of Cohesive Soils. *Journal of the Hydraulics Division*, *91*(1), 105–139.

Pianca, C., Holman, R., & Siegle, E. (2014). Mobility of meso-scale morphology on a microtidal ebb delta measured using remote sensing. *Marine Geology, 357*, 334–343.

Pritchard, D., & Hogg, A. J. (2003). Cross-shore sediment transport and the equilibrium morphology of mudflats under tidal currents. *Journal of Geophysical Research: Oceans, 108*(10), 1–15.

Pritchard, D., Hogg, A., & Roberts, W. (2002). Morphological modelling of intertidal mudflats: the role of cross-shore tidal currents. *Continental Shelf Research, 22*(11-13), 1887–1895.

Prodger, S., Russell, P., & Davidson, M. (2017). Grain-size distributions on high-energy sandy beaches and their relation to wave dissipation. *Sedimentology, 64*(5), 1289–1302.

Pu, J., Chen, Y., Su, M., Mei, J., Yang, X., Yu, Z., & Yao, P. (2022). Residual sediment transport in the fine-grained jiangsu coast under changing climate: The role of wind-driven currents. *Water, 14*(19), 3113.

Reed, D., van Wesenbeeck, B., Herman, P. M., & Meselhe, E. (2018). Tidal flat-wetland systems as flood defenses: Understanding biogeomorphic controls. *Estuarine, Coastal and Shelf Science, 213*, 269–282.

Ren, M. E. (1986a). *Comprehesive Investigation of the Coastal Zone and Tidal Land Resources of Jiangsu Province*. China Ocean Press.

Ren, M. E. (1986b). *Modern sedimentation in the coastal and nearshore zones of China*. Springer US.

Ren, M., Zhang, R., & Yang, J. (1984). Sedimentation on tidal mud flat of Wanggang area, Jiangsu Province, China (in Chinese with an English abstract). *Marine Science Bulletin, 3*(1), 40–54.

Ren, M. E., & Shi, Y. (1986). Sediment discharge of the Yellow River and its effect on sedimentation of the Bohai and Yellow Sea. *Scientia Geographica Sinica, 6*(1), 1–12.

Roberts, W., Le Hir, P., & Whitehouse, R. (2000). Investigation using simple mathematical models of the effect of tidal currents and waves on the profile shape of intertidal mudflats. *Continental Shelf Research, 20*(10-11), 1079–1097.

Roelvink, D., Walstra, D.-J., Roelvink, J. A., & Walstra, D.-J. (2004). Keeping It Simple By Using Complex Models. *Advances in Hydro-Science and Engineering*, *6*, 1–11.

Rosli, F. A., Lee, K. E., Goh, C. T., Mokhtar, M., Latif, M. T., Goh, T. L., & Simon, N. (2017). The use of constructed wetlands in sequestrating carbon: An overview. *Nature Environment and Pollution Technology*, *16*(3), 813–819.

Schoutens, K., Heuner, M., Minden, V., Schulte Ostermann, T., Silinski, A., Belliard, J. P., & Temmerman, S. (2019). How effective are tidal marshes as nature-based shoreline protection throughout seasons? *Limnology and Oceanography*, *64*(4), 1750–1762.

Sengupta, D., Chen, R., & Meadows, M. E. (2018). Building beyond land: An overview of coastal land reclamation in 16 global megacities. *Applied Geography*, *90*, 229–238.

Sengupta, D., Choi, Y. R., Tian, B., Brown, S., Meadows, M., Hackney, C. R., Banerjee, A., Li, Y., Chen, R., & Zhou, Y. (2023). Mapping 21st Century Global Coastal Land Reclamation. *Earth's Future*, *11*(2), 1–13.

Shi, B., Wang, Y. P., Wang, L. H., Li, P., Gao, J., Xing, F., & Chen, J. D. (2018). Great differences in the critical erosion threshold between surface and subsurface sediments: A field investigation of an intertidal mudflat, Jiangsu, China. *Estuarine, Coastal and Shelf Science*, *206*, 76–86.

Soulsby, R. L. (1995). Bed shear stress due to combined waves and currents. *Advances in Coastal Morphodynamics*, 4–23.

Soulsby, R. L. (1997). *Dynamics of marine sands: a manual for practical applications*. Thomas Telford.

Stark, J., Van Oyen, T., Meire, P., & Temmerman, S. (2015). Observations of tidal and storm surge attenuation in a large tidal marsh. *Limnology and Oceanography*, *60*(4), 1371–1381.

Studds, C. E., Kendall, B. E., Murray, N. J., Wilson, H. B., Rogers, D. I., Clemens, R. S., Gosbell, K., Hassell, C. J., Jessop, R., Melville, D. S., Milton, D. A., Minton, C. D., Possingham, H. P., Riegen, A. C., Straw, P., Woehler, E. J., & Fuller, R. A. (2017). Rapid population decline in migratory shorebirds relying on Yellow Sea tidal mudflats as stopover sites. *Nature Communications*, *8*, 1–7.

Su, M., Yao, P., Wang, Z. B., Zhang, C. K., & Stive, M. J. (2017a). Exploratory morphodynamic hindcast of the evolution of the abandoned Yellow River delta, 1578–1855 CE. *Marine Geology*, *383*, 99–119.

Su, M., Yao, P., Wang, Z. B., Zhang, C. K., & Stive, M. J. (2017b). Exploratory morphodynamic modeling of the evolution of the Jiangsu coast, China, since 1855: Contributions of old Yellow River-derived sediment. *Marine Geology*, *390*, 306–320.

Suh, S. W., Lee, H. Y., & Kim, H. J. (2014). Spatio-temporal variability of tidal asymmetry due to multiple coastal constructions along the west coast of Korea. *Estuarine, Coastal and Shelf Science*, *151*, 336–346.

Sun, C., Li, J., Liu, Y., Zhao, S., Zheng, J., & Zhang, S. (2023). Tracking annual changes in the distribution and composition of saltmarsh vegetation on the Jiangsu coast of China using Landsat time series–based phenological parameters. *Remote Sensing of Environment*, *284*, 113370.

Tang, R. (1997). *History of salt industry in China (part of the local)*. People's Press.

Tao, J., Yang, T., Xu, F., & Yao, J. (2012). Effect of large scale tidal flat reclamation on hydrodynamic circulation in jiangsu coastal areas. *Asian and Pacific Coasts, 2011*, 662–669.

Tao, J., Wang, Z. B., Zhou, Z., Xu, F., Zhang, C., & Stive, M. J. (2019). A Morphodynamic Modeling Study on the Formation of the Large-Scale Radial Sand Ridges in the Southern Yellow Sea. *Journal of Geophysical Research: Earth Surface*, *124*(7), 1742–1761.

Teuchies, J., Vandenbruwaene, W., Carpentier, R., Bervoets, L., Temmerman, S., Wang, C., Maris, T., Cox, T. J., Van Braeckel, A., & Meire, P. (2013). Estuaries as Filters: The Role of Tidal Marshes in Trace Metal Removal. *PLoS ONE*, *8*(8), e70381.

Tian, B., Zhou, Y., Zhang, L., & Yuan, L. (2008). Analyzing the habitat suitability for migratory birds at the Chongming Dongtan Nature Reserve in Shanghai, China. *Estuarine, Coastal and Shelf Science*, *80*(2), 296–302.

Tong, S. S., Deroin, J. P., & Pham, T. L. (2020). An optimal waterline approach for studying tidal flat morphological changes using remote sensing data: A case of the northern coast of Vietnam. *Estuarine, Coastal and Shelf Science*, *236*, 106613.

van Dijk, W. M., Cox, J. R., Leuven, J. R., Cleveringa, J., Taal, M., Hiatt, M. R., Sonke, W., Verbeek, K., Speckmann, B., & Kleinhans, M. G. (2021). The vulnerability of tidal flats and multi-channel estuaries to dredging and disposal. *Anthropocene Coasts*, *4*(1), 36–60.

van der Spek, A. J., & Elias, E. P. (2021). Half a century of morphological change in the Haringvliet and Grevelingen ebb-tidal deltas (SW Netherlands) - Impacts of large-scale engineering 1964–2015. *Marine Geology*, *432*, 106404.

van der Wegen, M., Jaffe, B., Foxgrover, A., & Roelvink, D. (2017). Mudflat Morphodynamics and the Impact of Sea Level Rise in South San Francisco Bay. *Estuaries and Coasts*, *40*(1), 37–49.

Van Ledden, M., Van Kesteren, W. G., & Winterwerp, J. C. (2004). A conceptual framework for the erosion behaviour of sand-mud mixtures. *Continental Shelf Research*, *24*(1), 1–11.

Van Rijn, L. (1993). *Principles of Sediment Transport in Rivers, Estuaries and Coastal Seas, Part1*. Aqua publications, Amsterdam.

Wang, A., Wu, X., Bi, N., Ralston, D. K., Wang, C., & Wang, H. (2022). Combined effects of waves and tides on bottom sediment resuspension in the southern Yellow Sea. *Marine Geology*, *452*, 106892.

Wang, F., Liu, J., Qin, G., Zhang, J., Zhou, J., Wu, J., Zhang, L., Thapa, P., Sanders, C. J., Santos, I. R., Li, X., Lin, G., Weng, Q., Tang, J., Jiao, N., & Ren, H. (2023). Coastal blue carbon in China as a nature-based solution toward carbon neutrality. *Innovation*, *4*(5), 100481.

Wang, L., Hu, S., Yu, G., Ma, M., & Liao, M. (2017). Comparative study on magnetic minerals of tidal flat deposits from different sediment sources in Jiangsu coast, Eastern China. *Studia Geophysica et Geodaetica*, *61*(4), 754–771.

Wang, X., Xiao, X., Zou, Z., Chen, B., Ma, J., Dong, J., Doughty, R. B., Zhong, Q., Qin, Y., Dai, S., Li, X., Zhao, B., & Li, B. (2018). Tracking annual changes of coastal tidal flats in China during 1986–2016 through analyses of Landsat images with Google Earth Engine. *Remote Sensing of Environment*, *238*, 110987.

Wang, X., & Ke, X. (1997). Grain-size characteristics of the extant tidal flat sediments along the Jiangsu coast, China. *Sedimentary Geology*, *112*, 105–122.

Wang, Y., Zhu, D., You, K., Pan, S., Zhu, X., Zou, X., & Zhang, Y. (1999). Evolution of radiative sand ridge field of the South Yellow Sea and its sedimentary characteristics. *Science in China Series D: Earth Sciences*, *42*, 97–112.

Wang, Y., & Zhu, D. K. (1994). Tidal flats in China. In *Oceanology of china seas* (pp. 445–456). Springer, Dordrecht.

Wang, Y. P. (2006). High-resolution data collection for analysis of sediment dynamic processes associated with combined current-wave action over intertidal flats. *Chinese Science Bulletin*, *51*, 866–877.

Wang, Y. P., & Zhang, R. S. (1998). Geomorphology responses on dynamics pattern of Jiangsu offshore sandbanks, Eastern China (in Chinese with an English abstract). *J, Marine Sciences*, *3*, 43–46.

Wang, Y., Gao, S., Jia, J., Thompson, C. E., Gao, J., & Yang, Y. (2012a). Sediment transport over an accretional intertidal flat with influences of reclamation, Jiangsu coast, China. *Marine Geology*, *291*, 147–161.

Wang, Y., & David, G. A. (1987). The characteristics of the China coastline. *Continental Shelf Research*, *7*(4), 329–349.

Wang, Y., Zhang, Y., Zou, X., Zhu, D., & Piper, D. (2012b). The sand ridge field of the South Yellow Sea: Origin by river–sea interaction. *Marine Geology*, *291*, 132–146.

Wang, Y., Liu, Y., Jin, S., Sun, C., & Wei, X. (2019a). Evolution of the topography of tidal flats and sandbanks along the Jiangsu coast from 1973 to 2016 observed from satellites. *ISPRS Journal of Photogrammetry and Remote Sensing*, *150*, 27–43.

Wang, Y., Wang, Y. P., Yu, Q., Du, Z., Wang, Z. B., & Gao, S. (2019b). Sand-Mud Tidal Flat Morphodynamics Influenced by Alongshore Tidal Currents. *Journal of Geophysical Research: Oceans*, 1–19.

Wang, Z. B., Vriend, H. J. D., Stive, M. J., & Townend, I. H. (2008). On the parameter setting of semi-empirical long-term morphological models for estuaries and tidal lagoons. *Proceedings of River, Coastal and Estuarine Morphodynamics: RCEM*, 103–111.

Waycott, M., Duarte, C. M., Carruthers, T. J., Orth, R. J., Dennison, W. C., Olyarnik, S., Calladine, A., Fourqurean, J. W., Heck, K. L., Hughes, A. R., Kendrick, G. A., Kenworthy, W. J., Short, F. T., & Williams, S. L. (2009). Accelerating loss of

seagrasses across the globe threatens coastal ecosystems. *Proceedings of the National Academy of Sciences of the United States of America*, *106*(30), 12377–12381.

Whitehouse, R., Soulsby, R., Roberts, W., & Mitchener, H. (2000a). *Dynamics of estuarine muds*. Thomas Telford.

Whitehouse, R. J., Bassoullet, P., Dyer, K. R., Mitchener, H. J., & Roberts, W. (2000b). The influence of bedforms on flow and sediment transport over intertidal mudflats. *Continental Shelf Research*, *20*(10-11), 1099–1124.

Winterwerp, H., & Van Kesteren, W. (2004). *Introduction to the Physics of Cohesive Sediment in the Marine Environment*. Elsevier.

Work, P., & Dean, R. (1992). Effect of varying sediment size on equilibrium beach profiles. *Coastal Sediments*, 890–904.

Wu, W., Yang, Z., Tian, B., Huang, Y., Zhou, Y., & Zhang, T. (2018). Impacts of coastal reclamation on wetlands: Loss, resilience, and sustainable management. *Estuarine, Coastal and Shelf Science*, *210*, 153–161.

Wu, W., Zhang, M., Chen, C., Chen, Z., Yang, H., & Su, H. (2024). Coastal reclamation shaped narrower and steeper tidal flats in Fujian, China: Evidence from time-series satellite data. *Ocean and Coastal Management*, *247*, 106933.

Xie, W., Wang, X., Guo, L., He, Q., Dou, S., & Yu, X. (2021). Impacts of a storm on the erosion process of a tidal wetland in the Yellow River Delta. *CATENA*, *205*, 105461.

Xing, F., Wang, Y. P., & Jia, J. (2022). Hydrodynamics and sediment transport patterns on intertidal flats along middle Jiangsu coast. *Anthropocene Coasts*, *5*(1), 12.

Xing, F., Wang, Y. P., & Wang, H. V. (2012). Tidal hydrodynamics and fine-grained sediment transport on the radial sand ridge system in the southern Yellow Sea. *Marine Geology*, *291*, 192–210.

Xing, G., Wang, H., Yang, Z., & Bi, N. (2016). Spatial and temporal variation in erosion and accumulation of the subaqueous Yellow River Delta (1976–2004). *Journal of Coastal Research*, *74*, 32–47.

Xu, C., & Liu, W. (2022). The Spatiotemporal Characteristics and Interactions between Urban Expansion and Tidal Flat Dynamics: A Case Study of Three Highly Urbanized Coastal Counties in the Southeastern United States. *Earth*, *3*(2), 557–576.

Xu, F., Tao, J., Zhou, Z., Coco, G., & Zhang, C. (2016). Mechanisms underlying the regional morphological differences between the northern and southern radial sand ridges along the Jiangsu Coast, China. *Marine Geology, 371*, 1–17.

Xu, H., Shi, F., Song, X., & Bai, Y. (2024). Quantifying spatiotemporal variations in tidal flats and coastal land use in Jiangsu Radial Sandbars through remote sensing. *Regional Studies in Marine Science, 74*, 103539.

Xu, L., Ding, S., Nitivattananon, V., & Tang, J. (2021). Long-term dynamic of land reclamation and its impact on coastal flooding: A case study in Xiamen, China. *Land, 10*(8), 1–18.

Xu, N., Wang, Y., Huang, C., Jiang, S., Jia, M., & Ma, Y. (2022). Monitoring coastal reclamation changes across Jiangsu Province during 1984–2019 using landsat data. *Marine Policy, 136*, 104887.

Yamada, F., & Kobayashi, N. (2004). Annual Variations of Tide Level and Mudflat Profile. *Journal of Waterway, Port, Coastal, and Ocean Engineering, 130*(3), 119–126.

Yang, B., Wang, Y., & Zhu, D. (1997). The tidal flat resource of China (in Chinese). *Journal of Natural Resources, 12*(4), 307–316.

Yang, B., Feng, W., & Zhang, Y. (2014). Wave characteristics at the south part of the radial sand ridges of the Southern Yellow Sea. *China Ocean Engineering, 28*(3), 317–330.

Yang, C. S. (1985). On the origin of Jianggang radial sand ridges in Yellow Sea (in Chinese with an English abstract). *Mar. Geol. Quat. Geol, 5*(3), 35–44.

Yang, S. L., Milliman, J. D., Li, P., & Xu, K. (2011). 50,000 dams later: Erosion of the Yangtze River and its delta. *Global and Planetary Change, 75*(1-2), 14–20.

Yang, S. Y., Li, C. X., Jung, H. S., & Lee, H. J. (2002). Discrimination of geochemical compositions between the Changjiang and the Huanghe sediments and its application for the identification of sediment source in the Jiangsu coastal plain, China. *Marine Geology, 186*(3-4), 229–241.

Yao, P. (2016). *Tidal and sediment dynamics in a fine-grained coastal region: A case study of the Jiangsu coast* [Doctoral dissertation, Technology University of Delft].

Yao, P., Su, M., Wang, Z. B., van Rijn, L. C., Stive, M. J., Xu, C., & Chen, Y. (2022). Erosion Behavior of Sand-Silt Mixtures: Revisiting the Erosion Threshold. *Water Resources Research*, *58*(9), 1–24.

Yao, P., Su, M., Wang, Z., van Rijn, L. C., Zhang, C., & Stive, M. J. (2018). Modelling tidal-induced sediment transport in a sand-silt mixed environment from days to years: Application to the Jiangsu coastal water, China. *Coastal Engineering*, *141*(135), 86–106.

Yu, X., & Yang, W. (2010). NUMERICAL STUDY OF NEARSHORE WAVES ALONG THE COAST OF JIANGSU, CHINA. *Asian and Pacific Coasts 2009*, 193–200.

Zhang, C., Yang, Y., Tao, J., Chen, Y., Yao, P., & Su, M. (2013). Suspended sediment fluxes in the radial sand ridge field of South Yellow Sea. *Journal of Coastal Research*, *65*, 624–629.

Zhang, C., Zhang, D., Zhang, J., & Wang, Z. (1999). Tidal current-induced formation-storm-induced change-tidal current-induced recovery - Interpretation of depositional dynamics of formation and evolution of radial sand ridges on the Yellow Sea seafloor. *Science in China, Series D: Earth Sciences*, *42*(1), 1–12.

Zhang, C. (2012). *The Comprehensive Survey and Evaluation Report on Coastal Zone of Jiangsu Province* (tech. rep.). Beijing, China, Science Press.

Zhang, G. (1991). Formation and evolution of sand ridges in the south Huanghai Sea (in Chinese with an English abstract). *Shelf. Mar. Geol. Quat. Geol.*, *11*, 25–35.

Zhang, H., Shen, Y., & Tang, J. (2023). Wave and storm surge evolutions in the Pearl River Estuary with large-scale land reclamation impacts. *Ocean Engineering*, *273*, 113977.

Zhang, M., Dai, Z., Bouma, T. J., Bricker, J., Townend, I., Wen, J., Zhao, T., & Cai, H. (2021). Tidal-flat reclamation aggravates potential risk from storm impacts. *Coastal Engineering*, *166*, 103868.

Zhang, R. (1992). Suspended sediment transport processes on tidal mud flat in Jiangsu Province, China. *Estuarine, Coastal and Shelf Science*, *35*(3), 225–233.

Zhang, R. (1984). Land-forming history of the Huanghe River delta and coastal plain of north Jiangsu (in Chinese with an English abstract). *Acta geographica sinica Beijing*, *39*(2), 173–184.

Zhang, R. (1986). Characteristics of Tidal Current and Sedimentation of Suspended Load on Tidal Mud Flat in Jiangsu Province (in Chinese). *Oceanologia et Limnologia Sinica*, *17*(3), 235–245.

Zhang, R., Lu, L., & Wang, Y. (2002). The mechanism and trend of coastal erosion of Jiangsu Province in China (in Chinese with an English abstract). *Geographical Research*, *21*(4), 469–478.

Zhao, Y., Zhang, D., Deng, H., & Cutler, M. E. (2023). Mudflat surface sediment type mapping by remote sensing considering the effect of the chlorophyll-a content. *Estuarine, Coastal and Shelf Science, 284*, 108276.

Zhong, Z., & Hu, Z. (2021). The Impact of Reclamation on Tidal Flat Morphological Equilibrium. *Frontiers in Marine Science*, *8*, 1–11.

Zhou, L., Liu, J., Saito, Y., Diao, S., Gao, M., Qiu, J., Xu, C., He, L., & Ye, S. (2020). Sediment budget of the Yellow River delta during 1959–2012, estimated from morphological changes and accumulation rates. *Marine Geology*, *430*, 106363.

Zhou, L., Liu, J., Saito, Y., Zhang, Z., Chu, H., & Hu, G. (2014). Coastal erosion as a major sediment supplier to continental shelves: example from the abandoned Old Huanghe (Yellow River) delta. *Continental Shelf Research*, *82*, 43–59.

Zhou, Z., Coco, G., Townend, I., Olabarrieta, M., van der Wegen, M., Gong, Z., D'Alpaos, A., Gao, S., Jaffe, B. E., Gelfenbaum, G., He, Q., Wang, Y., Lanzoni, S., Wang, Z., Winterwerp, H., & Zhang, C. (2017). Is "Morphodynamic Equilibrium" an oxymoron? *Earth-Science Reviews*, *165*, 257–267.

Zhou, Z., Coco, G., van der Wegen, M., Gong, Z., Zhang, C., & Townend, I. (2015). Modeling sorting dynamics of cohesive and non-cohesive sediments on intertidal flats under the effect of tides and wind waves. *Continental Shelf Research*, *104*, 76–91.

Zhou, Z., Liang, M., Chen, L., Xu, M., Chen, X., Geng, L., Li, H., Serrano, D., Zhang, H., Gong, Z., & Zhang, C. (2022). Processes, feedbacks, and morphodynamic evolution of tidal flat–marsh systems: Progress and challenges. *Water Science and Engineering*, *15*(2), 89–102.

Zhou, Z., Liu, Q., Fan, D., Coco, G., Gong, Z., Möller, I., Xu, F., Townend, I., & Zhang, C. (2021). Simulating the role of tides and sediment characteristics on tidal

flat sorting and bedding dynamics. *Earth Surface Processes and Landforms*, *46*(11), 2163–2176.

Zhu, Q., van Prooijen, B. C., Maan, D. C., Wang, Z. B., Yao, P., Daggers, T., & Yang, S. L. (2019). The heterogeneity of mudflat erodibility. *Geomorphology*, *345*, 106834.

Zhu, Q., Wang, Y. P., Ni, W., Gao, J., Li, M., Yang, L., Gong, X., & Gao, S. (2016). Effects of intertidal reclamation on tides and potential environmental risks: a numerical study for the southern Yellow Sea. *Environmental Earth Sciences*, *75*(23), 1–17.

Zhu, Y., & Chen, Q. (2005). On the origin of the Radial Sand Ridges in the Southern Yellow Sea: Results from the modeling of the paleoradial tidal current fields off the Paleo-Yangtze River Estuary and Northern Jiangsu Coast. *Journal of Coastal Research*, *21*(6), 1245–1256.

Some portions of the English text in this dissertation were refined with the assistance of an AI-based language editing tool (ChatGPT by OpenAI) to improve clarity and readability. This tool was used exclusively for language polishing. All academic content, including research ideas, figures, analysis, interpretations, and conclusions, was conceived and written entirely by the author without the use of AI-generated content.

# ACKNOWLEDGEMENTS

As my PhD journey draws to a close, I find myself looking back on these eight long years. It has truly been a remarkable and often difficult path. The fact that I was able to persevere through it all is largely thanks to the many people who have appeared along the way. Their companionship, support, and encouragement have constantly reignited my motivation and helped me overcome obstacle after obstacle, leading me to where I stand today.

Coming to TU Delft for my PhD was the first time I had ever lived and studied so far from home. Immersing myself in an unfamiliar culture brought a mixture of excitement and apprehension. I am especially grateful to my two PhD supervisors, Prof. Zheng Bing Wang and Prof. Stefan Aarninkhof, for offering me not only academic guidance, but also advice on time management, personal well-being, and how to grow in independence. At times, I could not help but see in them the image of the two masters of Sun Wukong in the classic Chinese novel Journey to the West, mentors who not only taught him how to fight demons, but also how to discipline himself and ultimately reach enlightenment.

First and foremost, I would like to express my sincere thanks to Prof. Zheng Bing Wang, who gave me the opportunity to pursue a PhD at TU Delft. During my progress meetings, you always managed to pinpoint problems with precision and offer constructive suggestions at the right moments. You taught me how to form hypotheses from observed phenomena, how to analyse data from multiple perspectives, and how to interpret model results from a appropriate way. More importantly, you instilled in me a rigorous scientific attitude, encouraged me to "jump into the water," and helped me develop the habit of documenting the research process in detail. These are lessons and habits that will shape every step I take in the future. Despite your busy schedule, you have always shown concern for us in daily life. I still vividly remember my first day at TU Delft when I was unfamiliar with the office setting. You kindly crouched down to help fix the workstation for me, and I was truly touched. During Chinese New Year, you and other professors organized gath-

erings for us overseas students far from home. You also invited us to your home, where you and your wife warmly welcomed us, introduced your beautiful garden, and shared stories from your youth. All of this made me feel a deep sense of warmth and belonging, like being cared for by family.

I am equally grateful to my other supervisor, Prof. Stefan Aarninkhof. I remember our first encounter during the Coastal Dynamics course. You had not yet become my official supervisor, but I gathered the courage to ask you a question about 'plate tectonics' during the break. You answered patiently, and that was the first time I realized how approachable this tall Dutch professor was. After you became my supervisor, despite your are more 'a sandy guy' while my research concerned muddy areas, you always managed to quickly identify gaps in my research logic and provide clear, actionable directions. From our meetings, I gradually learned how to improve the efficiency of discussions and take ownership of my PhD process. Your excellent time management and wide professional network were also a form of mentorship. You taught me the importance of prioritizing major tasks, staying on schedule, and making time to connect with fellow PhD students to learn from their experiences. During the difficult COVID period, when I struggled with low motivation and stagnation, you and Prof. Wang actively helped me find a way out and create a more comfortable environment to return to my research. I also cherished the "little chats" before our meetings, and they brought warmth and humanity to our otherwise serious academic discussions.

I would also like to express my gratitude to the many individuals who have supported me throughout this journey by sharing data, technical knowledge, practical experience, and hardware resources. Your generous help has been instrumental in bringing me to the final stage of my PhD. I am deeply grateful to Jianfeng Tao from Hohai University, China, for generously providing valuable field survey data from the Jiangsu coast. These data laid a critical foundation for my subsequent research. Thanks also go to Peng Yao, Min Su, and Zhenshan Xu, also from Hohai University, for sharing their expertise and experience with Delft3D modeling. The many discussions we had helped me avoid numerous modeling pitfalls and solved several technical issues. Many thanks to Qinghua Ye from Deltares for your advice on setting up the 2D alongshore-uniform flow model, and to Anne Ton and Julia Hopkins from TU Delft for your useful tips and suggestions regarding the wave

module in Delft3D. I would also like to thank Zhan Hu and Zehua Zhong from Sun Yat-sen University, China, for sharing the DET-ESTMORF model and for our fruitful discussions throughout its application. Your help was essential in improving the model's stability and saved me a great deal of time in later stages of my research. I would like to thank the secretaries who have supported me over the years—Inge, Otti, and Marije—for helping me solve various administrative and workplace issues, and for coordinating my meetings with my supervisors so efficiently. My appreciation also goes to the colleagues at the Graduate School for carefully reviewing all required documents and ensuring the smooth progress of my PhD defense procedure. I would like to thank my doctoral defense committee members, Jill Slinger, Piet Hoekstra, Bram van Prooijen, Bas van Maren, and Zeng Zhou, for your time, interest, and constructive evaluation of my work.

To my office mates at TU Delft, thank you for the friendly and productive working atmosphere we created together. To Hassan, thank you for being such a strong and thoughtful person. I truly appreciated our conversations about culture and perspectives. Your support and empathy meant a lot to me. To Menno, thank you for moving into our office first, making it feel less lonely. I also appreciate all the things you shared with us, and the invitation to visit your fascinating physical experiments at Deltares. To Alperen, thank you for bringing new energy into our room. You are sincere and warm, and I really enjoyed our bouldering session together. I also would also like to thank my former office colleagues, Chunyan, Jianliang, Enrica, Antonia, Frederik, Bob, and Tommaso, for your friendly companionship and the many enjoyable conversations that kept the office a great place to work in.

I feel incredibly fortunate to have been part of the Coastal Engineering group at TU Delft, where I have met so many amazing people. I would like to thank Raylton, Dimitris, Marlies, Jos, Natascia, Mark, Isabel, Filipe, Ligaya, Deepika, Anna, Su, Vincent, Jakob, Bart, Kevin, Gijs, Daan, Sander, Stuart, Sierd, Judith, Marcel, Bram, Bas, and many others. Whether it was participating in the tidal flats meetings, our daily lunch chats, summer schools, or just casual coffee breaks, these moments have left me with countless cherished memories. Thanks to Roy and Marthe for sharing so many fun stories about tidal flat fieldwork. They gave me, as a modeller, a new perspective and a different kind of joy. Roy, I also appreciate how you took over from Wout as my informal Dutch teacher. Thanks to you, learning Dutch has once again

become one of my daily highlights.

I am especially grateful to my dear friends Zaiyang Zhou and Jianwei Sun. I still vividly remember our many discussions about research, cooking sessions, travel adventures, PUBG battles, BBQs, hotpot nights, and workout. You always made time for me when I needed it most—listening, offering advice, and helping me figure things out. I'm so lucky to have you as lifelong friends. I would also like to extend my big thanks to Valeria. Thank you for constantly encouraging me when I felt socially anxious, for helping me recognize my strengths when I was full of self-doubt, and for being there when I needed help most. I truly believe that kind people will always be met with kindness in return. A special thank you to Wout. Although we only shared an office for a short period, your presence made a lasting impact on me. You supported me with great kindness during a time of personal grief. You also took on the role of my Dutch teacher from time to time, teaching me humorous and useful expressions. Your kindness, patience, emotional stability, and genuine concern for others will surely take you far, wherever life leads you.

I'm also grateful for the many wonderful Chinese friends who made my life in the Netherlands so colorful: Sien Liu, Yang Zhou, Rong Zhang, Yuning Zhang, Lian Liu, Runxiang Li, Yujian Zhan, Yue Li, Weiming Xie, Jinxu Yi, Fucang Zhou, Jiamin Chen, Haisheng Yu, and so many others. From cooking competitions, dumpling and rice dumpling making, weekend dinners, to outdoor adventures, our time together brought immense joy to my life. Even during the pandemic, we stayed connected through our virtual gatherings, making sure no one felt alone. I also want to thank my badminton buddies: Nianlei Zhang, Zhonggang Li, Yingtao Sun, Shuai Wang, Yueqian Liu, Li Wang, Jie Liu, Yi Zheng, and many others. Your companionship helped me improve my skills and gradually turned badminton into a passion and strength of mine. It helped me find joy again during the low moments.

Lastly, I wish to extend my deepest and most heartfelt gratitude to my family. To my parents: thank you for your unconditional love, support, and understanding. You have always tried your best to ease my burdens and help me move forward, no matter the circumstances. To my uncle and aunt: thank you for your invaluable guidance in both life and career, and for always being emotionally steady listeners who could gently guide me through my most difficult moments. To my grandparents: I know you are no longer here to witness this day, but I believe that, wherever

you are, you would be proud of me. To Weiqiu: thank you for walking this journey with me. Your support and encouragement have not only accompanied me through all the highs and lows, but also helped me rediscover myself and grow along the way. I would also like to thank myself for not giving up, no matter how difficult the journey became.

To all of you, named and unnamed, thank you from the bottom of my heart. I wish you all the very best in the future.

Yu Kuai
June, 2025
Delft

# About the author

Yu Kuai was born on June 2nd, 1992, in Sheyang County, Jiangsu Province, China. He completed his primary, middle, and high school education in his hometown. In 2010, upon his admission to Hohai University, he began his studies in Harbor, Waterway, and Coastal Engineering, and graduated in 2014 as an outstanding graduate student. He then pursued graduate studies at the same university, where he investigated hydrodynamic and sediment transport patterns as well as morphological evolution in estuarine regions. During this period, he also began applying numerical modelling techniques. In 2017, he graduated from Hohai University as an outstanding graduate student once again. Then he moved to the Netherlands at the end of 2017 to begin his PhD research at the Delft University of Technology, where his research focused on the morphodynamic evolution of muddy tidal flats at the open coast. His work aims to advance our understanding of coastal geomorphology, sediment dynamics, and sustainable coastal management.

# List of Publications

## First Author

1. **Kuai, Y.**, Aarninkhof, S.G.J. and Wang, Z.B. (2023). Diagnostic modelling of the shoreline variation along the Jiangsu Coast, China. *Geomorphology*, 425, p.108581. https://doi.org/10.1016/j.geomorph.2023.108581. [Chapter 3]

2. **Kuai, Y.**, Tao, J., Zhou, Z., Aarninkhof, S.G.J. and Wang, Z.B. (2021). Sediment characteristics and intertidal beach slopes along the Jiangsu Coast, China. *Journal of Marine Science and Engineering*, 9(3), p.347. https://doi.org/10.3390/jmse9030347. [Chapter 2]

## Co-Author

1. Zhou, Z., **Kuai, Y.**, Ge, J., van Maren, D.S., Wang, Z., Huang, K., Ding, P. and Wang, Z.B. (2025). Modeling non-stationary wind-induced fluid motions with physics-informed neural networks for the shallow water equations in a polar coordinate system. *Water Resources Research*, 61(1), p.e2024WR037490. https://doi.org/10.1029/2024WR037490.

2. Zhou, Z., Ge, J., Van Maren, D.S., **Kuai, Y.**, Ding, P. and Wang, Z.B. (2024). Groyne-Induced Effects on Channel-Shoal Exchange and Saltwater Intrusion in Estuarine Environments. *Journal of Hydraulic Engineering*, 150(1), p.04023056. https://doi.org/10.1061/JHEND8.HYENG-13500.

3. Zhou, Z., Ge, J., Van Maren, D.S., Wang, Z.B., **Kuai, Y.** and Ding, P. (2021). Study of sediment transport in a tidal channel-shoal system: Lateral effects and slack-water dynamics. *Journal of Geophysical Research: Oceans*, 126(3), p.e2020JC016334. https://doi.org/10.1029/2020JC016334.

## Prepared

1. **Kuai, Y.**, Zhong, Z., Hu, Z., Zhou, Z., Aarninkhof, S.G.J. and Wang, Z.B., On tidal flat morphological restoration after coastal land reclamation. [Chapter 4]